1992

# Analytical and experimental studies of advanced laser cutting techniques

Ming-Jen Hsu
*Iowa State University*

Order Number 9302002

# Analytical and experimental studies of advanced laser cutting techniques

Hsu, Ming-Jen, Ph.D.

Iowa State University, 1992

U·M·I
300 N. Zeeb Rd.
Ann Arbor, MI 48106

# Analytical and experimental studies of advanced laser cutting techniques

by

Ming-Jen Hsu

A Dissertation Submitted to the
Graduate Faculty in Partial Fulfillment of the
Requirements for the Degree of
DOCTOR OF PHILOSOPHY

Department: Mechanical Engineering
Major: Mechanical Engineeering

Approved:

Signature was redacted for privacy.

In Charge of Major Work

Signature was redacted for privacy.

For the Major Department

Signature was redacted for privacy.

For the Graduate College

Iowa State University
Ames, Iowa

1992

# TABLE OF CONTENTS

# SYMBOLS AND ABBREVIATIONS

NOMENCLATURE:

a = focused laser beam diameter, m
A = absorptivity
b = heat transfer coefficient, $W/m^2 \cdot K$
c = speed of sound, m/sec
C = speed of light, m/sec
$C_p$ = specific heat, $J/kg \cdot K$
d = tube diameter, m
D = grooving (or cutting) depth, m
E = radius of laser beam, m
f = frequency, Hz
g = acceleration of gravity, $m/sec^2$
H = decomposition energy, J/kg
$\Delta H$ = heat of combustion, J/kg
I = power density, $W/m^2$
k = thermal conductivity, $W/m \cdot K$
$K_0$ = modified Bessel function of the 2nd kind and zeroth order
l = workpiece thickness, m
L = latent heat, J/kg
M = mass removed, kg
$\dot{M}$ = mass removal rate, kg/sec
P = laser power, watts (W)
q = heat rate, watts (W)
q' = q/l, heat rate per unit length, W/m
r = radius, m
R = half the kerf width, m

s = vR/2$\alpha$, normalized cutting speed
T = temperature, K
u = velocity, m/sec
v = cutting speed, m/sec
V = velocity, m/sec
$\forall$ = volume,$m^3$
$\dot{\forall}$ = volume gas flow rate, $m^3$/sec
w = 2R, kerf width, m
$\alpha$ = thermal diffusivity,$m^2$/sec
$\delta$ = thickness of liquid melt film, m
$\eta$ = combustion efficiency
$\theta$ = cutting front angle, degree
$\mu$ = viscosity, kg/m.sec
$\rho$ = density, kg/$m^3$
$\tau$ = shear stress, MPa
$\phi$ = side (off-axial) jet impinging angle, degree

SUBSCRIPTS:
co = coaxial
off = off-axial
rm = room
m = melting
mp = melting point
l = liquid
g = gas
s = solid
sh = shearing
e = ejection
ex = exhaust
o = outside
i = inside
f = fusion
v = vaporization

w = workpiece
a = ambient
n = nozzle

# GENERAL INTRODUCTION

Laser (acronym of *L*ight *A*mplified by *S*timulated *E*mission of *R*adiation) has become an important tool in modern technology. There is hardly a field untouched by the laser. Due to its unique properties - namely, high power density, monochromaticity, coherency and directionality - lasers have a variety of applications which include materials processing, medicine, research and development, communications and measurements to name a few. Among those applications in materials processing, laser machining outweighs welding and heat treatment and accounts for approximately three-quarters of the installations in the U.S. (Belforte, 1988). The attractive characteristics of laser machining include :

(1) narrow kerf width and material savings
(2) narrow heat-affected zone (HAZ) and low thermal distortion
(3) high precision/machining rate and superior surface finish
(4) non-contact process and no tool wear
(5) soft tooling and simple fixturing
(6) easy automation

According to Steen (1983), there are five different ways in which a laser can be used to cut different materials. They are:

(1) Vaporization cutting. The beam energy heats the substrate to above its boiling temperature and material leaves as vapor or ejecta.
(2) Fusion cutting. The beam energy melts the substrate and an inert gas-jet blows the melt out of the cutting region.
(3) Reactive fusion cutting. The beam energy heats the material to the combustion temperature and workpiece burns in a reactive gas-jet; as in (2). The gas-jet also clears the dross away.
(4) Controlled fracture. The beam energy sets up a thermal field in a brittle material such that it can initiate cracking and fracturing.
(5) Scribing. A blind cut is used as a stress raiser to allow mechanical snapping.

Gas-assisted laser cutting, which utilizes a coaxial gas-jet with the laser beam through a nozzle is, by far, the most common process in industrial practice (see Figure 1). The assist gas provides the following benefits:

(1) It protects the focusing optic from dross spattering
(2) It cools off the focusing optic
(3) It provides additional cutting energy from the chemical reaction between assist gas and the workpiece.
(4) It ejects liquid droplets (slags)

Figure 1 shows the standard laser cutting process. A laser beam is focused by a lens on the surface of the material to be machined. Assist gas (usually oxygen) is supplied to the heating zone through a coaxial nozzle. The incident radiation is absorbed by the surface layer of the workpiece which is heated and oxidized. For metallic materials, only a small portion (5-10 %) of the laser energy is absorbed at the beginning. Continued heating of the metal leads to oxide film/plasma formation and energy coupling becomes very efficient (Bunkin et al., 1980). The temperature of the workpiece rises to the melting point and liquid melt/oxides are blown out of the cutting zone by the gas-jet. The workpiece can be cut along a specified contour by moving either the worktable where the workpiece is stationed or the laser beam. The width of cut (kerf width) is usually slightly larger than the diameter of the focused laser beam and the thermal-damaged layer (heat affected zone, HAZ) is only a fraction of a millimeter along the cut edges.

Due to the several benefits listed previously, gas-assisted laser machining is becoming popular in manufacturing industries where conventional machining techniques are not satisfactory or economically viable. Typical laser machining users are prototype/small-batch production in the automotive industry; drilling/cutting of exotic materials such as superalloys in the aerospace industry and trimming/micromachining in the electronics industry. However, laser cutting is limited by the laser's inability to cut thick-sectioned materials (> 6 mm), its tendency to produce a tapered kerf and the general inefficient cutting of several materials for the following reasons:

(1) high reflectivity and thermal conductivity (Cu, Al, W, Mo)
(2) high melting and boiling points (W, Mo, most ceramics)
(3) existence of non-volatile, high viscous oxides that passivate the surface to further oxidation (stainless steels, superalloys, aluminum)

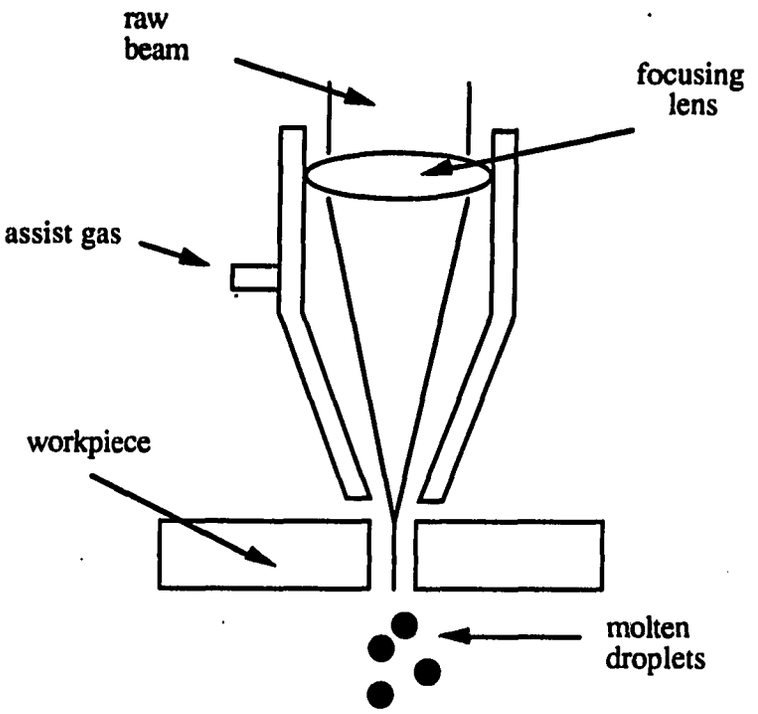


Figure 1. Schematic diagram of a gas-assisted laser cutting process

(4) difficulties in removing dross or slag (titanium, stainless steels, superalloys, aluminum)

(5) incomplete removal of all components of a composite material

It is therefore important that we understand the physical and chemical mechanisms associated with laser machining and apply this knowledge to further improvement in laser materials processing.

## Explanation of dissertation organization

In this study, experimental and theoretical investigations of gas-assisted laser machining were carried out and are described in five separate papers suitable for publication. The papers are preceded by a Literature Review and followed by a General Summary, and all references cited in chapters other than those within the papers are listed following the General Summary. In Paper I, a two-dimensional conductive heat transfer model dealing with the laser beam characteristics, combustion reaction and the material properties was developed for oxygen-assisted laser cutting of carbon steel. In Paper II, a new cutting technique, which employs two gas-jets (coaxial and off-axial) was developed to effectively laser machine stainless steels, and superalloys up to 6.35 mm (1/4 in.) plate thickness with dross-free edge quality. A dual gas-jet laser cutting technique coupled with a fluid dynamics model is also presented. The material removal mechanisms in conventional and dual gas-jet laser cutting were investigated in terms of gas shearing and momentum transfer to the erosion cutting front. The analysis of the energy, mass and momentum balance equations and the metallurgical characteristics of the combustion products together explain the effectiveness of this new laser cutting technique. In Paper III, conventional and axicon-lens focusing methods in the laser machining of egg shells were studied. The energy balance model accurately predicts the processing parameters and the experimental results indicate that laser machining of egg shells can improve the resulting cut quality and productivity. The dual gas-jet method developed in Paper II was further applied to cut 6.35 mm (1/4 in.) thick metal matrix composites (MMC) and the results are discussed in Paper IV. In Paper V, sulfur hexafluoride ($SF_6$) gas was used as an assist gas in the laser cutting of polymers. The effect on the surface finish of laser-cut polymers via dissociation and plasma formation of $SF_6$ molecules was investiagated.

# LITERATURE REVIEW

Laser machining is a complex process and the factors governing the process are many and include the following,

(1) Laser beam: power, wavelength, mode, polarization, diameter and position of the focal spot.

(2) Gas dynamics and flow characteristics of the assist gas: nozzle design, chemical composition, temperature, pressure, flow rate and velocity.

(3) Interaction between laser irradiation and the workpiece material: optical, thermal and chemical properties, plasma formation.

(4) Types of workpiece materials: metals, polymers, ceramics, and composites.

(5) Combustion reactions and products if a combustible assist gas is used: combustion heat, types of oxides (slags), viscosity, ejection velocity and temperature of slag.

(6) Heat transfer associated with the laser heat source and the combustion effect: conductive, convective and radiative heat transfer, latent heat of phase transformation.

(7) Fluid dynamics of the melt film and assist gas in the erosion cutting front: viscosity of melt, gas momentum transfer.

The first major development using a laser for cutting was reported by Houldcroft (1968) who added an oxygen jet to the focused laser beam to increase the cutting speeds through the exothermic reaction between the workpiece and oxygen. This oxygen-assisted laser cutting method was later discussed in great detail by Adams (1970) and is the most common method employed today in the laser cutting industry.

The lasers currently used for machining include $CO_2$ gas laser (wavelength 10.6 $\mu$m), Nd-YAG solid-state laser (wavelength 1.06 $\mu$m) and Excimer gas laser (wavelength 157 nm to 351 nm). As laser power increases the cutting speed and thickness increase. Figures 2 to 4 show the typical $CO_2$ laser cutting rate vs. material thickness at various laser powers for

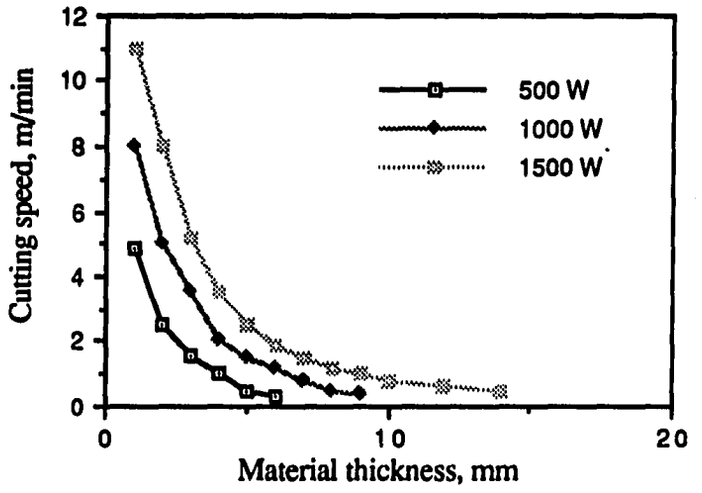


Figure 2. Cutting speed vs. material thickness for mild steel

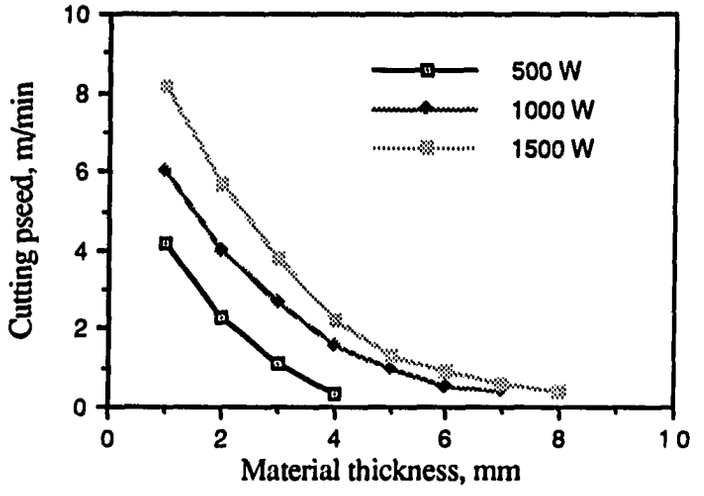


Figure 3. Cutting speed vs. material thickness for stainless steel

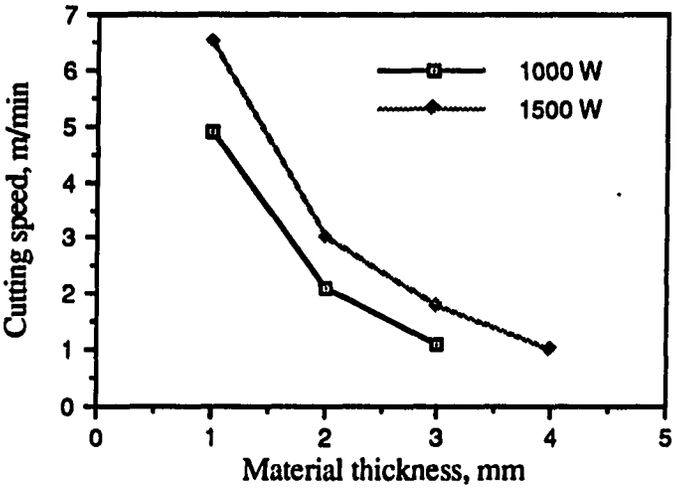


Figure 4. Cutting speed vs. material thickness for aluminum

steel, stainless steel, and aluminum (Powell, 1990). High power laser with short wavelength is preferred in cutting metallic materials because the reflectivity of metals increases with the laser wavelength (Sona, 1987). Belforte (1990) reported that high power lasers with a $TEM_{00}$ (Gaussian) energy distribution can cut metals better and faster than multi-mode laser beams, because the $TEM_{00}$ mode can be focused to a smaller spot thereby providing a higher energy density. Olsen (1982, 1988) observed variations in laser cutting with respect to polarization and concluded that the beam would be absorbed optimally if it were vibrated along the direction of the kerf. Rothe and Sepold (1987) suggested that the focus should be positioned one-third of the cutting thickness beneath the surface for thick plate laser cutting.

Forbes (1975) showed that nozzle design and flow characteristics affected the cutting performance at a given laser power. He also demonstrated a significant variation in metal surface finish with alteration in cutting rate. Steen (1983) explained that the low cutting speeds observed with polished samples were due to reflection of the laser irradiation. Ward's efforts (1986, 1987) concentrated on the flow dynamics in gas-assisted laser cutting. He reported that for diatomic gases supersonic flow develops if $P_n$ (gas pressure) > 1.89 $P_a$, where $P_n$ and $P_a$ are the absolute nozzle pressure and ambient pressure respectively. Formation of a strong normal shock (the Mach shock disk, MSD) from an underexpanded jet in laser cutting impairs cutting performance. New coaxial nozzle designs were described which eliminated MSD and stagnation bubble formation at normal operating pressures. Duley (1976, 1983) reported that

cutting speed increases with increasing oxygen gas flow rate reaching to a maximum, then decreases and becomes almost independent of gas supply. He interpreted this phenomenon in terms of Bakenko and Tychinskii's theory (1973) and explained this effect as follows.

(1) Increasing flow rate reduces the absorptivity of the laser power and consequently reduces the cutting speed for a given cut.

(2) Increasing the flow rate causes a cooling effect.

Steen and Kamalu (1983) pointed out that as gas pressure (flow rate) increases, supersonic flow develops. They believed that the supersonic gas-jet provides a high stagnation pressure above the cut slot and this increases the cutting velocity to its maximum. According to these workers further increase in the gas pressure (flow rate) causes the formation of a shock wave, which leads to gas density and pressure discontinuities. Increasing the gas density and pressure gradients across the flow field affects the focusing characteristics but improves the ejection efficiency of liquid droplets. Nielsen (1985) used a variety of assist gas mixtures at high reservoir in laser cutting. A supersonic flow was achieved for air at reservoir pressures above 190 kPa (28 psi) and it was found that a Mach shock disk may form at jet pressures above 350 kPa (50 psi). The convergent-divergent nozzle in conjunction with a supersonic jet was suggested as being a suitable method for producing a more favorable shock structure for laser cutting. Ketting and Olsen (1992) tilted the laser beam in the standard laser cutting method and used high pressure gas to allow the gas flow to enter the kerf more efficiently. Dross-free edge quality was achieved when cutting stainless steel and aluminum in thicknesses up to 3 mm. Masuda and Nakamura (1992) studied the aerodynamic characteristics of the gas-jet beneath different nozzle contours and demonstrated that a high surface pressure concentrated at the jet center could be produced when an annular nozzle with a high ratio of inner/outer diameters and large ejection angle was used.

Roessler and Gregson (1978) measured the reflectivity of steel subjected to $CO_2$ laser irradiation in air and concluded that the reflectivity decreased significantly when the laser intensity reached $10^7$ W/cm$^2$. They explained that surface damage from strong absorption of laser energy is due to plasma formation. Reflectivity and plasma formation in laser material interaction was discussed by Schawlow (1977). Beyer et al. (1987) studied plasma fluctuations during laser machining and noted that plasma formation frequencies were correlated to the dynamics of the melt pool.

In general, the reflectivity of metals subjected to laser irradiation increases as the wavelength increases and typically is above 90% in the infrared range of the electromagnetic spectrum at room temperature (Sona, 1987). As the surface heats up the reflectivity falls due to the change in the electronic structure of the workpiece (Ready, 1978), plasma formation of the vapor or gas breakdown (Schawlow, 1977), and surface oxidation (Duley, 1976). Saunders (1977) reported that pulsed laser cutting had advantages over CW for heat sensitive material since the evaporation cutting mode obtained with pulsed mode reduced the size of the heat-affected zone (HAZ). The laser cutting of polymers and process optimization were studied extensively by Van Cleave (1980, 1981, 1983) and Powell et al. (1987). The primary factors in the laser cutting of plastics are melt shearing, vaporization, and chemical degradation. Powell et al. (1987) adopted a simple energy balance method to predict the laser cutting speeds for various plastics within 10% accuracy. The hazardous fumes developed in the laser cutting of polymers were investigated by Doyle et al. (1985) and by Flaum and Karlsson (1987) as well as by Doyle and Kokosa (1987) for polymer composites. Ceramics such as alumina, quartz and silica with thicknesses from 0.6 mm to 4.0 mm were laser cut by Powell et al. (1987), who also concluded that the primary material removal mechanism was evaporation. Laser cutting of oxides and carbides was reported by Affolter and Schmid (1987) and Hamann and Rosen (1987). It was concluded that processing defects such as microcracks, recast layers, pores and HAZ could be controlled by pulse length, shape, frequency and nozzle design. Firestone and Veseley (1988) preheated the workpiece to minimize micro-cracking during the laser cutting of silicon nitride. Yamamoto and Yamamoto (1987) described the microstructural changes in laser-cut silicon nitride and the subsequent recovery of flexural strength through an annealing treatment. Tonshoff and Gonschior (1992) proposed several methods for reducing cracking damage during the laser cutting of ceramics which included a process simulation system to calculate temperature and stress gradients; cutting under water; preheating the workpiece; and process control by plasma detection. De Iorio et al. (1987) studied the cut edge quality of graphite fiber composite and concluded that differences in thermal properties between the matrix and reinforcement material were detrimental for laser cutting (Di Ilio, 1987). Utsunomiya et al. (1986) studied the laser machining of carbon fiber/aluminum and silicon fiber/aluminum composites and determined a threshold of laser power for drilling and cutting. Lee (1987) investigated the laser cutting performance of continuous fiber metal matrix composites and compared the results to those obtained by abrasive water-jet and diamond saw cutting. Laser

beam cutting is the fastest cutting method, but it tends to induce thermal cracking due to the high heat flux. This difficulty could possibly be overcome if a pulsed laser beam combined with an optimum level of power were employed.

Forbes (1975) estimated that in oxygen-assisted laser cutting of steel, 70% of the cutting energy is derived from combustion. Steen and Kamalu (1983) compared the laser cutting rate of steel with argon and oxygen assist gases and concluded that about 60% of the cutting energy is supplied by combustion. On the other hand, Ivarson et al. (1991) estimated that the oxidation process contributes 40% of the energy input to the cutting zone and that the laser provides the remaining 60%. Clarke and Steen (1978) improved the cutting speed as much as 70% by adding more energy to the laser interaction zone with an electric arc. Molian (1987) used a mixture gas of oxygen and acetylene to cut 19 mm thick steel without deteriorating the quality of the cut. The success was attributed to the combustion reaction and the use of optimal gas-flow parameters which included a low pressure/flow rate, a small nozzle diameter, and a multiple off-axis jet. Arata (1986) observed directly the mechanisms of laser gas cutting of mild steel by high speed filming. It was found that above a critical cutting speed, the periodic cutting phenomena at the upper portion of the cutting front disappeared and that a steady cutting stage was established. Under such circumstances, the surface finish was significantly improved due to the elevated temperature at the cutting front. A radiation pyrometer was employed to measure the surface temperature of the melt film. The temperature at the cutting front was found to increase as the cutting speed and distance from the top surface increased. For a material thickness of 2 mm, surface temperatures ranging from 1600 $^0$C to above 2000 $^0$C were observed.This temperature range was consistent with that given in the report by Ivarson et al. (1991) who measured a temperature of approximately 2000 K. Direct optical observation of the cutting zone revealed an intense radiation in the pale yellow band of the electromagnetic spectrum which indicated the existence of low temperatures. Schulz et al. (1987) neglected vaporization and used the energy balance and heat conduction equations to estimate the surface temperature of the melt film. In this theoretical treatment, the cutting power (sum of combustion power and absorbed laser power) and the combustion power were related to the surface temperature by solving the diffusion equation for the oxide layer within the melt. It was demonstrated that combustion reaction is strongly controlled by diffusion. In further experimental work, Arata (1986) improved the cut edge quality of 2 mm thick stainless steel by using "pile" and "tandem nozzle" cutting methods. Iron oxide (FeO) from pile cutting was found to dilute the

concentration of chromium oxide and allowed further oxidation to reach the less viscous single liquid-phase region. In tandem nozzle cutting, the dynamic force from the side gas-jet contributed effectively to the removal of the liquid melt along the cutting front. Nielsen (1985) further reduced the dross formation in the laser cutting of stainless steel by using a 60% $CO_2$ and 40% $O_2$ gas mixture which suppressed the $Cr_2O_3$ formation and helped in ejecting the molten material. This work was a development of earlier research by Steen (1977) who adopted a cross blowing gas-jet device beneath the cutting zone to improve the dross dragging force. Powell (1985) invented a multiple "drossjet" in which eight identical nozzles were arranged in a ring with each nozzle connected to a solenoid valve. This device was placed beneath the workpiece and a dross-free edge was obtained by blowing the gas-jet to the cutting zone. The solenoid valves opened and closed in sequence thereby allowing profile cutting to be carried out.

In an early theoretical development, Duley and Gonsalves (1972) used a moving point heat-source model to successful predict the performance of a laser when cutting thin stainless steel. Bunting and Cornfield (1975) investigated the effects of laser power density, cutting speed, kerf width, material thickness and thermal properties through a line heat-source model. By assuming uniform strength of the line heat-source, it was found that the power density could be correlated with the normalized cutting speed. The review paper by Babenko and Tychinskii (1973) described the fundamental theory of gas-jet laser cutting. In this paper the thermal source technique (in terms of absorbed laser power, combustion power and power removed by gas-jet) was applied to the heat conduction equation by using point and Gaussian heat-source models. The theory indicated that for cutting speed v, $(\alpha b)^{1/2} < v < (4\alpha/a)$;

$\psi = Q/(C_p \cdot T_s) < 1.9$ for steady-state cutting conditions

$\psi = Q/(C_p \cdot T_s) > 1.9$ for nonsteady-state cutting conditions

where, $\psi$ = a dimensionless thermochemical parameter

Q = the specific energy yield of the chemical reactions, J/kg

These authors concluded that under unstable cutting conditions, the kerf width varies and therefore the quality of cut is poor. The criterion can also be applied to a Gaussian heat-source model if U ($= v \cdot a / 4 \cdot \alpha$) is less than 0.8. At higher values of U, stable cutting conditions can be obtained even for $\psi > 1.9$. Estimated values of $\psi$ for metallic and organic materials were discussed by Babenko and Tychinskii (1973) for vaporization and gas-assisted laser cutting. Decker et al. (1983) used the energy balance method and neglected heat loss to predict the maximum cutting speed in the laser cutting of thin sheets. A quasi-

sublimation cutting process was assumed which implied that the temperature at the cutting front increases with cutting speed until the evaporation temperature is reached. When cutting thick sections, the temperature is lower due to the low cutting speed and in this case the proportion of evaporated material is minimal. It was concluded that the combustion reaction is limited to the oxidation process at the surface of the melt and is controlled by the diffusion rate of oxygen through the partially oxidized melt film.

The striations which form on the laser cut surface were studied by Adams (1970), Forbes (1975), and Arata et al. (1979) using high speed photography and were explained in terms of an intermittent flow of the molten product. However Shinada et al. (1980) suggested that intermittent plasma blockage of the incoming laser beam could also play a role. Lee et al. (1985) investigated the striation pattern and observed two distinct zones on the kerf edge. In the first zone, the regular striations near the kerf entrance were thought to be the result of oxygen-assisted laser beam heating. The second zone (the region of indistinct zones near the kerf bottom) was believed to be caused by a diffusive thermochemical reaction in the absence of direct contact with the laser beam. An increase in the depth of the first zone was shown to correspond with an increase in beam pulse-width. Adams (1970) had earlier reported that in the laser cutting of mild steel, the beam heated a small area on the erosion front and that the interface between the oxide melt and the solid material moved at about 4 to 6 times faster than the cutting speed. Stainless steel was observed to give a similar result except that in this case the advancing interface did not move as fast as for mild steel due to the higher viscosity of the oxide melt.

In a series of recent studies, Schuocker (1983, 1984, 1985, 1986, 1988) investigated the cutting mechanisms in gas-assisted laser machining and provided a mechanism for laser cutting which is shown diagrammatically in Figure 5. In this model the erosion cutting front takes place at a nearly vertical plane at the momentary end of the cut. A thin molten layer forms on the plane, which is subsequently heated by the absorbed laser radiation and by the exothermic chemical reaction. The removal of material from this layer is carried out by evaporation and by ejection of molten material, which is caused by the shear force and momentum transfer between the melt and the reaction gas flow. Using energy, momentum and mass balance methods for the melt film, the velocity of ejected droplets can be estimated.

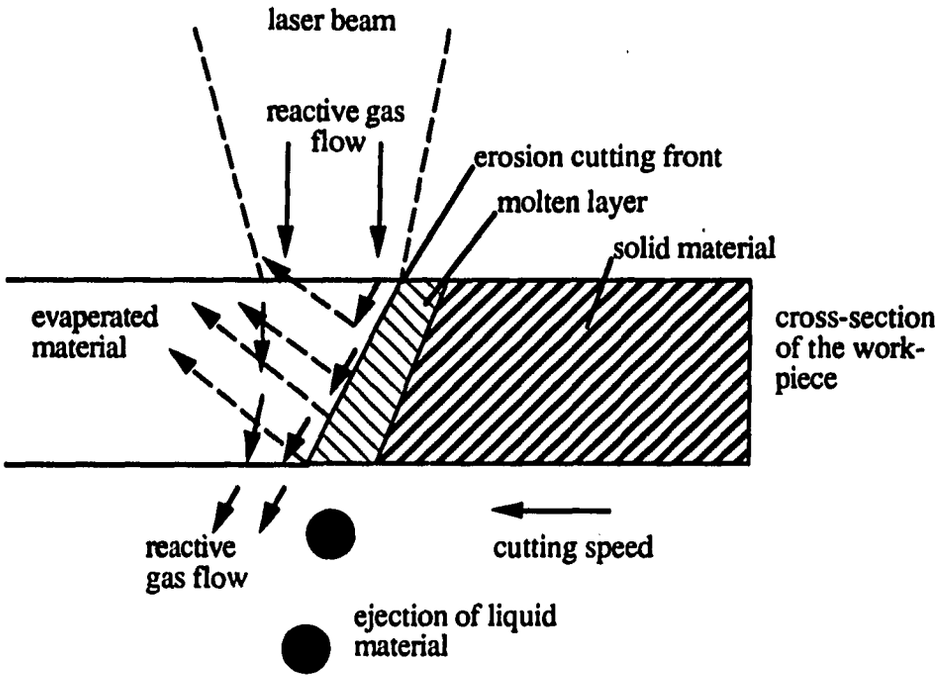


Figure 5. Mechanism of gas-assisted laser cutting

Conductive heat loss into the workpiece and the average thickness of melt film can also be determined. Calculated values of surface temperature and average thickness of the melt film were reported for various combinations of laser and material parameters. Cutting speeds due to evaporation and melting mechanisms were compared for different material thicknesses and laser powers. A small perturbation treatment under nonsteady-state condition was applied to the energy and mass balance equations to analyze the fluctuations of the surface temperature and melt film thickness under continuous wave (CW) or pulsing operations. The conclusions were that the striations in laser cutting may be smoothed out by suppressing the temperature variations through proper selection of pulsing frequency.

Vicanek et al. (1986, 1987) solved the boundary layer equations for the melt flow in gas-assisted laser cutting. The stationary solutions yielded the thickness and velocity of the melt flow for a given cutting speed, gas-jet formation, viscosity and density of the melt and gas respectively. The coefficient of the Blasius solution (which applies to the shear stress of the

gas- jet) was found to depend solely on the inclined cutting plane angle and was found to be nearly constant over the cutting front except at both edges. The pressure distribution along the cutting front was also calculated through a numerical technique and was found to depend on both the inclined cutting plane angle and the location at the cutting plane. These authors concluded that molten material is removed by friction forces between the gas-jet and the melt film as well as by the pressure gradient of the gas flow. It was estimated that in gas-assisted laser cutting both mechanisms contributed the same order of force magnitude in ejecting liquid melt. In further work, Petring et al. (1988) neglected material vaporization and obtained the following conduction heat loss equation,

$$P_{loss} = \frac{\pi k(T_m - T_\infty)\sqrt{wD}}{\tan^{-1}\left(\frac{16\alpha}{vD}\right)^{1/2}} \exp\left(-\frac{vw}{2\alpha}\right)$$

The conduction heat loss was calculated from the power or energy balance and the final equation was solved for D to determine the geometry of the cutting front.

A series of papers by Modest (1986, 1988, 1990, 1991) analyzed the conductive heat transfer and evaporative cutting phenomena in laser grooving using numerical methods. Multiple reflection and beam guiding effects were found to be important for high reflective materials or deep grooves with aspect ratios greater than one. This author concluded that to accurately predict groove depth, the evaporation mechanism and absorptivity of laser energy due to the beam guiding effect should be substantiated. Chryssolouris (1991) recently published a book which provided extensive and in-depth information on laser machining. He also demonstrated that an additional off-axial gas-jet could improve grooving depth up to 20 % on aluminum oxide when optimal process parameters were used (Chryssolouris, 1989). A theoretical analysis based on the control volume method of gas-jet momentum balance, conservation of mass and melting/conduction heat transfer was elaborated and the grooving depth was determined as

$$D = \frac{AP}{w\left[\rho vL + 2k(T_s - T_m)\int_0^{2\pi} \frac{d\theta}{\delta(\theta)}\right]}$$

Later, Chryssolouris (1990) combined two grooving laser beams by intersection for the three-dimensional laser machining of a composite material. An energy balance analysis in consideration of material ablation and heat conduction for the case of a CW/pulsed laser

beam was carried out and the calculated values of incremental grooving depth were reported. Furthermore, Chryssolouris (1991) used a closed-loop control concept through acoustic sensing for process control in the laser grooving, cutting and drilling of acrylic material. Resonant frequencies were obtainedby solving the wave equation of gas flow and were found to be related to grooving/cutting/hole depths as follows.

In laser grooving:

$$f = \frac{1.202 G_1 c}{\pi (G_0 + G_1 D)}$$

where:

$$G_0 = \frac{\pi}{4} w^2$$

$$G_1 = \frac{\pi}{4} w \cdot e$$

e is the gas-jet expansion coefficient

In laser cutting:

$$f = \frac{1.914 G_1 c}{\pi (G_0 + G_1 D)}$$

In laser drilling:

$$f = \frac{c}{4D}$$

Discrepancies between analytical and theoretical data were attributed to the assumed groove geometry and jet-flow. Ramanathan and Modest (1992) and Trubelja et al. (1992) discussed the laser machining of composite ceramics. A two-dimensional heat conduction model for cutting was described and comparisons were made with experimental material removal rates. Compared with diamond-cut composite, laser-cut samples were found to have 20% lower bending strength. However recovery of strength could be obtained after removing about 200 micron of the material from the laser-cut surface by grinding.

# PAPER I: THERMOCHEMICAL HEAT TRANSFER MODELING IN $CO_2$ LASER CUTTING OF CARBON STEEL

## ABSTRACT

A thermochemical heat transfer model for the oxygen-assisted laser cutting of carbon steel has been developed in terms of the laser mode pattern, the power density, the combustion reaction, the kerf width and the cutting speed. This model emphasizes the chemical combustion effect as well as the laser mode pattern which are usually neglected by most existing laser cutting models. The model indicates that approximately 55-70% of the cutting energy is supplied by the combustion reaction of the steel with oxygen which is consistent with the experimental data obtained by other investigators. Good agreement was obtained between the theoretical and experimental values on laser cutting of steel.

# 1. INTRODUCTION

Industrial laser applications in manufacturing are primarily in the areas of machining and welding, which account for more than 70% of the total laser processing category in the U.S. (Belforte, 1988). In general, laser cutting with a coaxial oxygen-jet significantly improves the cutting speed due to the combustion reaction between oxygen and the workpiece at the erosion cutting front (see Figure 1). Laser cutting is a complex process and mathematical models have been developed by many investigators to describe the cutting phenomena (Ready, 1971; Kamalu and Steen, 1983; Duley and Gonsalves, 1972; Schuocker, 1983, 1984, 1986; Modest, 1986, 1988, 1990, 1991; Chryssolouris, 1990, 1991). Most of the existing laser cutting models neglect the combustion reaction and/or the energy distribution of the laser beam and often result in limited practical applications. Forbes (1975) estimated that in oxygen-assisted laser cutting of steel, 70% of the cutting energy derived is from combustion. Kamalu and Steen (1983) concluded that 60% of the cutting energy is supplied by combustion. On the other hand, Ivarson et al. (1991) estimated that the oxidation process contributes 40% of the energy input to the cutting zone and that the laser provides the remaining 60%. Belforte (1990) reported that high power lasers with a $TEM_{00}$ (Gaussian) energy distribution can cut metals better and faster than a multi-mode laser beam.

Therefore, it is important to develop a theoretical model that describes the laser cutting process in terms of the combustion reaction and the energy distribution of the heat source. The basis of the present work originates from the effort by Bunting and Cornfield (1975), who ignored the combustion effect and assumed a uniform power density heat source in their model. In the present analysis, the effects of combustion and the laser beam mode are included.

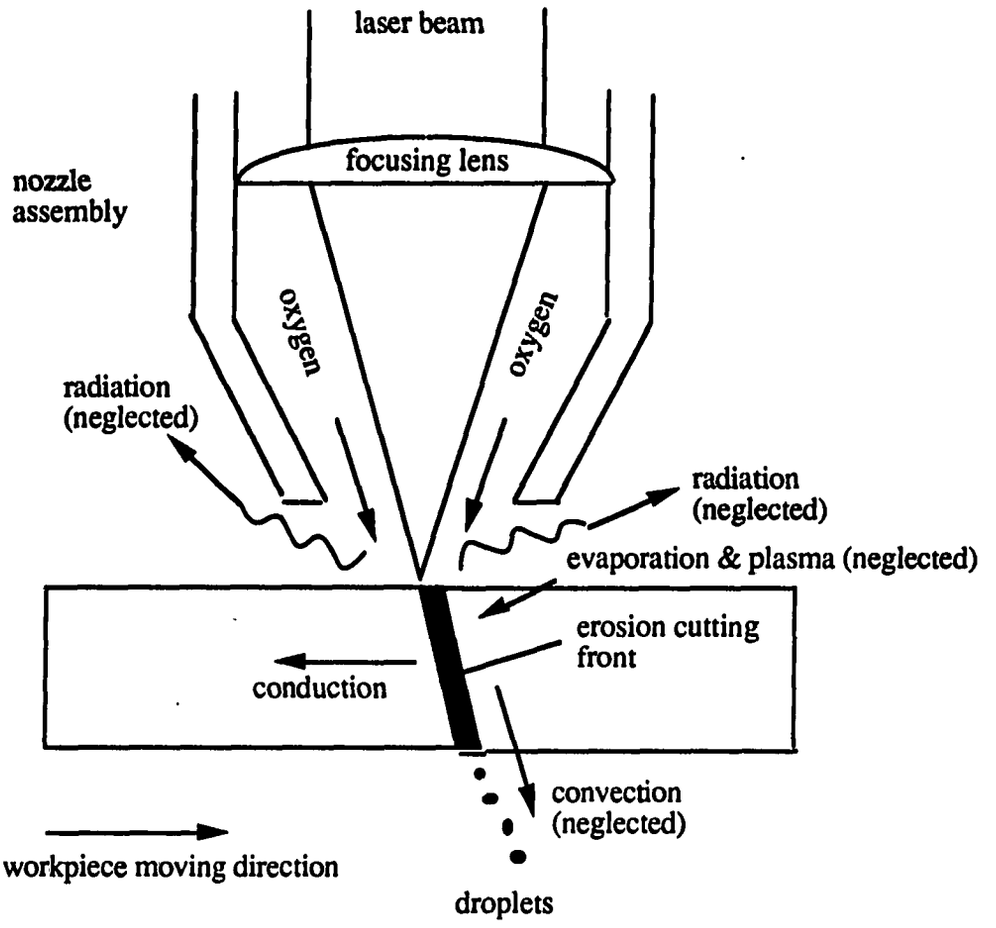


Figure 1. Schematic diagram of oxygen-assisted laser cutting and heat transfer modes

## 2. EXPERIMENTAL PROCEDURE

A continuous wave $CO_2$ laser (Spectra-Physics Model 820, maximum 2 kW output power) was used to cut AISI 1020 steel plates with oxygen as assist gas. The thickness of the workpiece was varied from 1.27 mm (0.05 in.) to 12.7 mm (0.5 in.). The laser was operated to 1500 watts power. The laser beam exhibited a near $TEM_{00}$ (Gaussian energy distribution) mode pattern. A nominal 127 mm (5 in.) zinc selenide (ZnSe) focusing lens was used to focus the laser beam to a spot size of 0.1 mm (0.004 in.). The focal point was set either on the surface of the workpiece in thin section cutting or at a distance equal to one-third the thickness from the surface in thick-section cutting (thickness > 6.3 mm). A convergent nozzle was used for the oxygen gas flow and the reservoir oxygen pressure was varied from 0.069 MPa to 0.276 MPa (10 to 40 psi). The steel plates were mounted on a computer numerically controlled worktable and cut with the laser beam. The maximum cutting speed was recorded as the speed at which cutting through the thickness of workpiece became impossible. The experimental setup is illustrated in Figure 1. Combustion products (such as droplets) were collected and analyzed by X-ray diffraction (XRD) to determine the compounds and compositions. The kerf width was measured directly using a thickness gage with an accuracy of 0.03 mm (0.001 in.).

# 3. THEORETICAL MODELING

## 3.1 Assumptions

The following assumptions are made to facilitate the theoretical modeling process.

1. A two-dimensional, moving-heat-source model for a slab is considered. The thermal gradient in the Z direction (material thickness) is small compared to those in other directions if the material is relatively thin (Babenko and Tychinskii, 1973; Arata and Miyamoto, 1974).
2. Heat losses due to convection and radiation are negligible (Vicanek and Simon, 1987; Ready, 1965).
3. Classical heat transfer theory is applicable to the laser heating process (Kamalu and Steen, 1983, Charschan, 1972).
4. Beam guiding and multiple reflection effects are ignored due to the high absorptivity in laser cutting of steel (Roessler and Gregson, 1978). The increased absorptivity may be explained by plasma formation inside the cutting kerf.
5. No vaporization and associated latent heat is involved during laser cutting. This assumption may only be valid in cutting thick-section materials as evaporation occurs only at the upper portion of the erosion cutting front.

## 3.2 Modeling

The governing differential equation for the two-dimensional steady state conduction heat transfer of a moving linear heat source at a velocity V in the x direction is given by:

$$\frac{\partial^2 T}{\partial x^2} + \frac{\partial^2 T}{\partial y^2} = \frac{v}{\alpha}\frac{\partial T}{\partial x} \qquad (1)$$

subject to following boundary conditions

(i) $\frac{\partial T}{\partial x} \to 0$ as $x \to \pm\infty$

(ii) $\frac{\partial T}{\partial y} \to 0$ as $y \to \pm\infty$

(iii) $-2\pi rk\frac{\partial T}{\partial r} \to q'$ as $r \to 0$ where $r = (x^2+y^2)^{1/2}$

The solution to the above equation was given by Carslaw and Jaegar (1959).

$$T(x,y) = T_{\infty} + \frac{q}{2\pi lk}\exp\left(\frac{vx}{2\alpha}\right)\left\{K_0\left[\frac{v(x^2+y^2)^{1/2}}{2\alpha}\right]\right\}$$
$$= T_{\infty} + \frac{q'}{2\pi k}\exp\left(\frac{vx}{2\alpha}\right)\left\{K_0\left[\frac{v(x^2+y^2)^{1/2}}{2\alpha}\right]\right\} \qquad (2)$$

For a fixed point (x,y), the temperature rise due to a polar coordinate linear heat source $q'(r,\theta)$ becomes

$$T(x,y) = T_{\infty} + \frac{q'}{2\pi k}\exp\left(\frac{v(x-r\cos\theta)}{2\alpha}\right)\left\{K_0\left[\frac{v((x-r\cos\theta)^2+(y-r\sin\theta)^2)^{1/2}}{2\alpha}\right]\right\} \qquad (3)$$

Consider now a focused laser beam as a moving heat source. Then, equation (3) can be formulated as

$$T(x,y) = T_{\infty} + \frac{1}{2\pi lk}\int I_{total}\,dr \int \exp\left(\frac{v(x-r\cos\theta)}{2\alpha}\right)\left\{K_0\left[\frac{v((x-r\cos\theta)^2+(y-r\sin\theta)^2)^{1/2}}{2\alpha}\right]\right\}d\theta \qquad (4)$$

where $I_{total}$ is the total power density, which includes absorbed laser radiation and that derived from the related combustion reaction. Typically, isotherms of a moving heat source in a two-dimensional case show an elliptical shape with the long axis in the moving direction (Babenko, 1973; Arata, 1974). By choosing $x = 0$ and $y = R$, the melting isotherm from equation (4) coincides with the half of the kerf width R. Then,

$$T_{mp} = T(0,R) = T_{\infty} + \frac{1}{2\pi lk}\int I_{total}\,dr \int \exp\left(\frac{v(-r\cos\theta)}{2\alpha}\right)\left\{K_0\left[\frac{v(R^2-2Rr\sin\theta+r^2)^{1/2}}{2\alpha}\right]\right\}d\theta \qquad (5)$$

For a Gaussian mode ($TEM_{00}$,TEM: transverse electromagnetic mode) $CO_2$ laser beam, the power density $I_{laser}$ is

$$I_{laser} = I_{max}\exp\left(\frac{-8r^2}{a^2}\right) \qquad (6)$$

where $I_{max} = \frac{2P}{\pi(a/2)^2} = \frac{8P}{\pi a^2}$

Furthermore, from Figure 2 the power density from combustion, $I_{comb}$, can be expressed as

$$I_{comb} = \frac{\rho v l(\Delta H)}{\delta} = \frac{\rho l(2\alpha t)(\Delta H)}{R\delta} s \qquad (7)$$

where $s = vR/2\alpha$

Equation (5) can be expressed as

$$T_{mp} = T_{rm} + \frac{1}{2\pi lk(1-e^{-2})}\int_0^{a/2} (\frac{8P}{\pi a^2}) \exp(\frac{-8r^2}{a^2}) rdr \int_0^{2\pi} \exp(\frac{v(-r\cos\theta)}{2\alpha}) \{K_0[\frac{v(R^2-2Rr\sin\theta+r^2)^{1/2}}{2\alpha}]\} d\theta$$
$$+ \frac{1}{2\pi lk}\int_R^{R+\frac{\delta}{2}} (\frac{\rho v l(\Delta H)}{\delta}) rdr \int_{\frac{\pi}{2}}^{\frac{3\pi}{2}} \exp(-\frac{vr\cos\theta}{2\alpha}) \{K_0[\frac{v}{2\alpha}(R^2-2Rr\sin\theta+r^2)^{1/2}]\} d\theta \quad (8)$$

The term $(1-e^{-2})$ was added to offset the difference between integrating from zero to infinity in the integral of laser power density.

By setting $r' = r/R$ and $s = vR/2\alpha$, equation (8) becomes

$$T_{mp} = T_{rm} + \frac{R^2}{2\pi lk(1-e^{-2})}\int_0^{\frac{a}{2R}} A(\frac{8P}{\pi a^2}) \exp(\frac{-8R^2r'^2}{a^2}) r'dr' \int_0^{2\pi} \exp(-sr'\cos\theta) \{K_0[s(r'^2-2r'\sin\theta+1)^{1/2}]\} d\theta$$
$$+ \frac{R^2}{2\pi lk}\int_1^{1+\frac{\delta}{2R}} \eta (\frac{2\alpha\rho l(\Delta H)s}{R\delta}) r'dr' \int_{\frac{\pi}{2}}^{\frac{3\pi}{2}} \exp(-sr'\cos\theta) \{K_0[s(r'^2-2r'\sin\theta+1)^{1/2}]\} d\theta \quad (9)$$

Here two constants (A and $\eta$) were added to equation (9) to account for laser absorptivity and incomplete combustion inside the cutting kerf.

Again equation (9) can be reduced to

$$T_{mp} = T_{rm} + \frac{AR^2}{2\pi lk(1-e^{-2})} I_{laser} + \frac{R^2}{2\pi lk} I_{comb} \qquad (10)$$

where $I_{laser}$ corresponds to the first integral on the right-hand side of equation (9) and $I_{comb}$ the second.

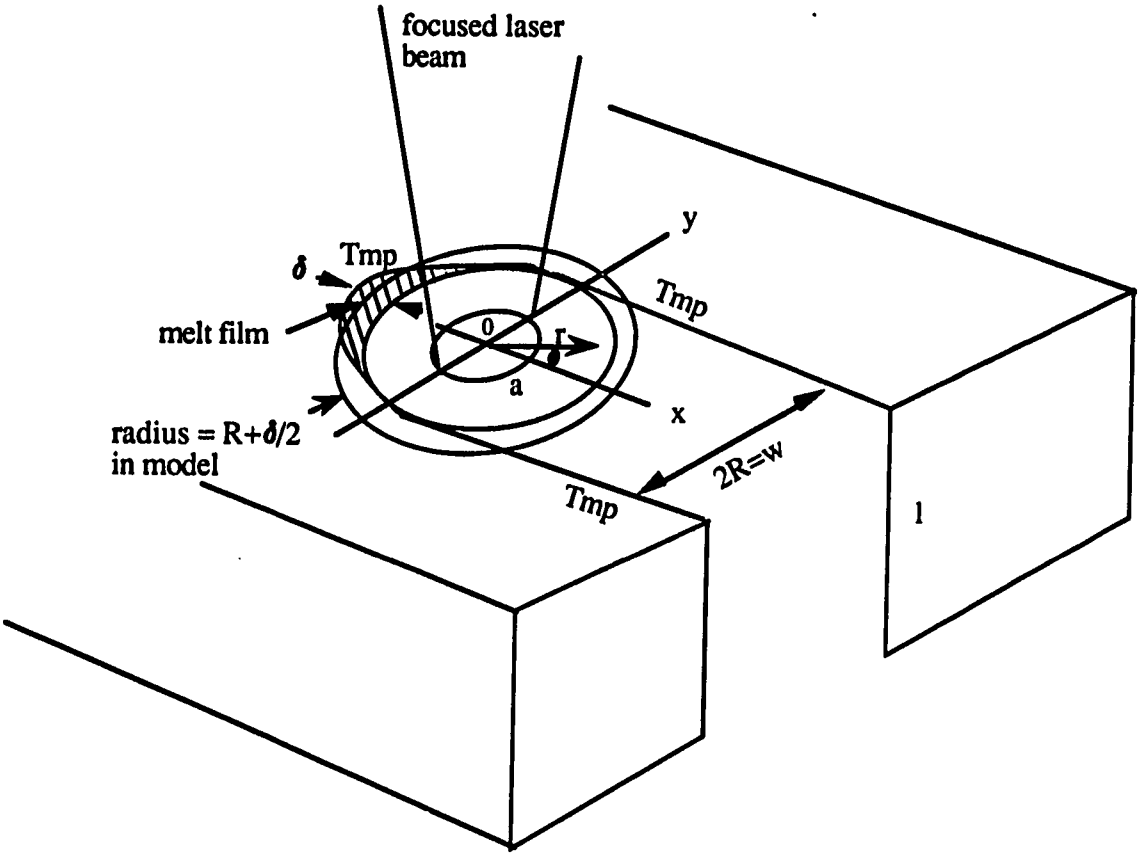


Figure 2. Laser cutting geometry

## 4. RESULTS AND DISCUSSION

The experimental cutting speed vs. workpiece thickness at two different laser power levels is plotted in Figure 3 to within 10% accuracy. Figure 4 shows a linear relationship between the kerf width and the section thickness. The reported values were taken as the average of the top and bottom kerf widths on the workpiece, both of which increased as the material thickness increased.

The thermal properties such as thermal conductivity k and diffusivity $\alpha$ change with temperature. The values of the thermal properties at the average temperature (1000 K) between ambient and the melting point of steel are used in this work (Table 1). The average thickness of the liquid melt film $\delta$ in the erosion cutting front has been studied by Schuocker (1988). $\delta$ increases with workpiece thickness and is in the vicinity of 0.1 mm. Figure 5 shows the average film thickness of liquid melt vs. material thickness in laser cutting of steel at approximately 1 kW and 80% absorptivity (Schuocker, 1988). These values were used in calculating the combustion power density in eq. (10). Roessler and Gregson (1978) reported that the reflectivity of carbon steel subjected to 10.6 $\mu$m wavelength irradiation decreased significantly when peak power intensity exceeded $10^7$ W/cm$^2$. Schuocker (1988) argued that the absorptivity of $CO_2$ laser light in cutting steel should be about 80%. Hence, a laser absorptivity A = 0.8 was used in our model. Arata et al. (1986) reported that the oxidized product in the laser cutting of steel was FeO which was confirmed by our XRD analysis of combustion droplets (Figure 6). Ivarson et al. (1991) concluded that 50% of iron in steel was oxidized to FeO in laser cutting and therefore $\eta$ = 50% was used in the present model. Thus, the following combustion reaction occurs in laser cutting of carbon steels.

$$Fe + 1/2\ O_2 \rightarrow FeO \qquad \Delta H = -63.2 \text{ Kcal/mole}$$

$I_{laser}$ and $I_{comb}$ in equation (10) were evaluated with a numerical method and were plotted as a function of s in Figures 7a and 7b at various R values. Theoretical values of v and R can be solved by using equation (10) and were plotted in Figure 8. It can be seen that the model provides good agreement with experimentally obtained maximum cutting speed values. Also, the predicted values of kerf width agree well with experimental data in the

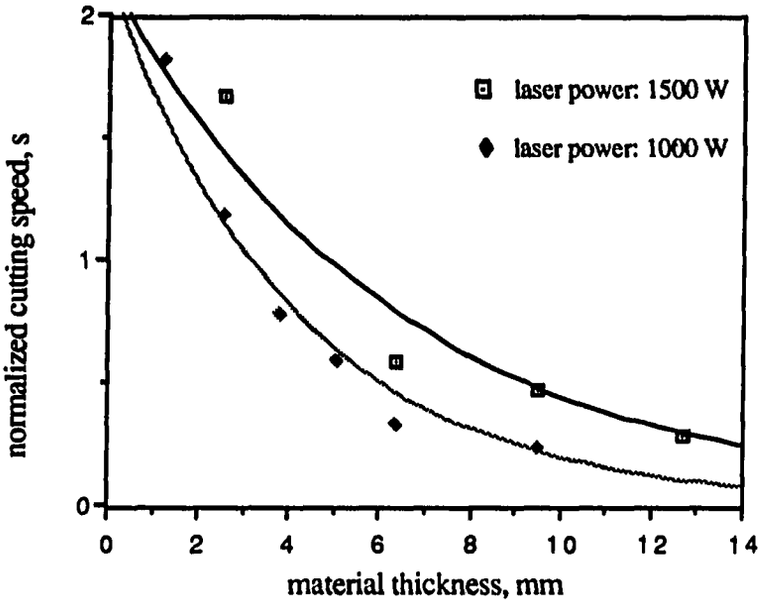


Figure 3. Cutting speed vs. material thickness at various laser powers

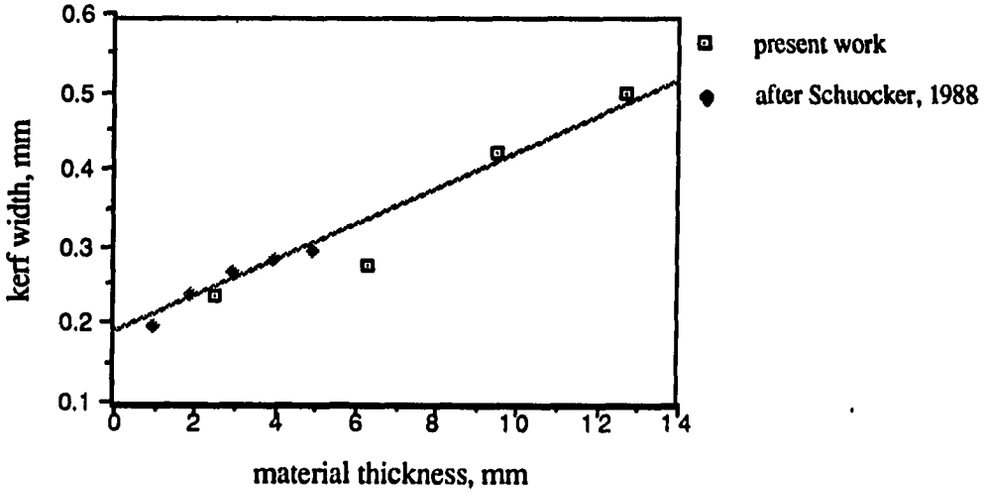


Figure 4. Kerf width vs. material thickness in laser cutting

Table 1. Thermal properties of AISI 1020 steel at 1000 K

| melting point (Tmp), K | density ($\rho$) kg / $m^3$ | thermal conductivity (k), W /m K | thermal diffusivity ($\alpha$), $m^2/s$ |
|---|---|---|---|
| 1795 | 7877 | 31.3 | $3.45 \times 10^{-6}$ |

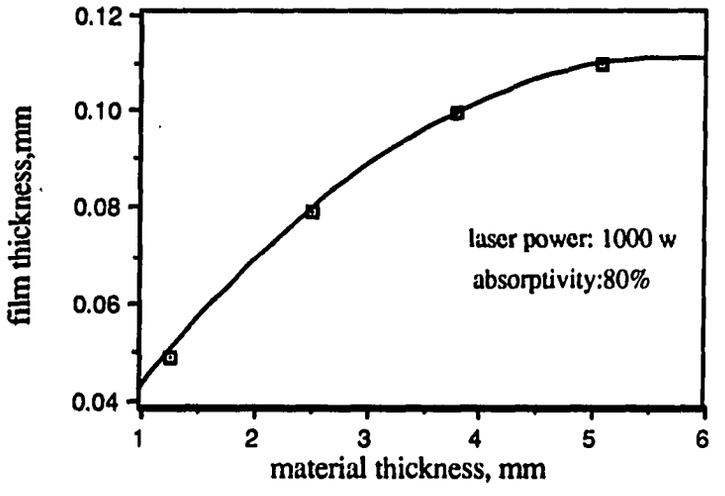


Figure 5. Relationship between average film thickness of liquid melt and material thickness in laser cutting (after Schuocker, 1988)

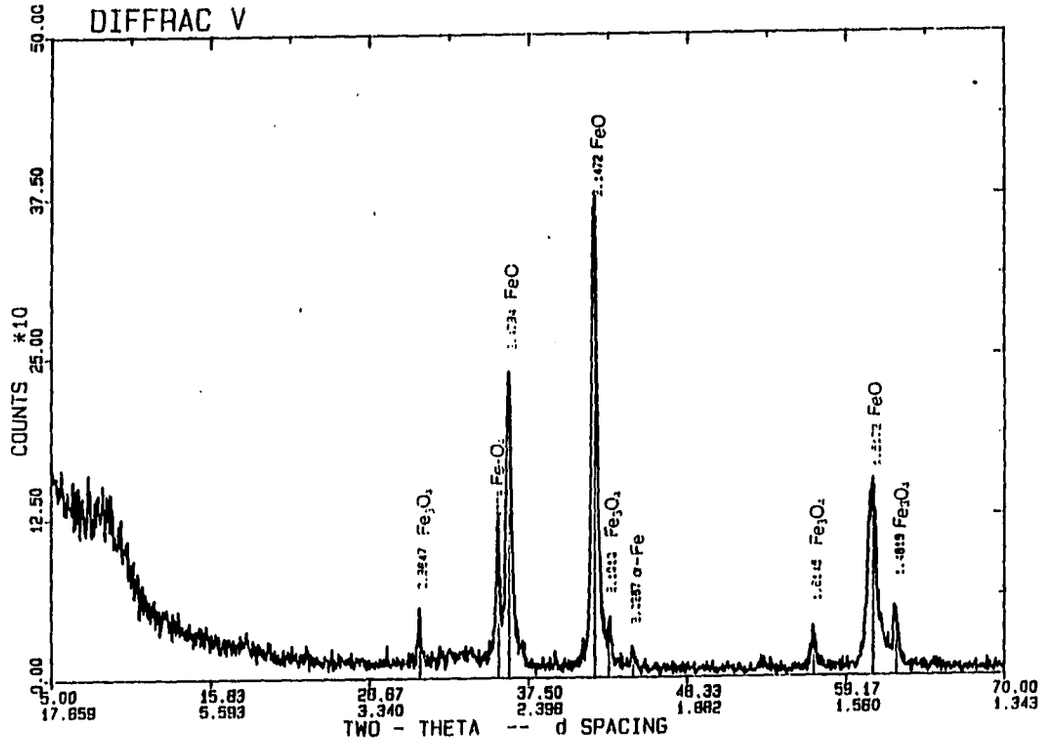


Figure 6. XRD analysis of combustion droplets
(materal: AISI 1020)

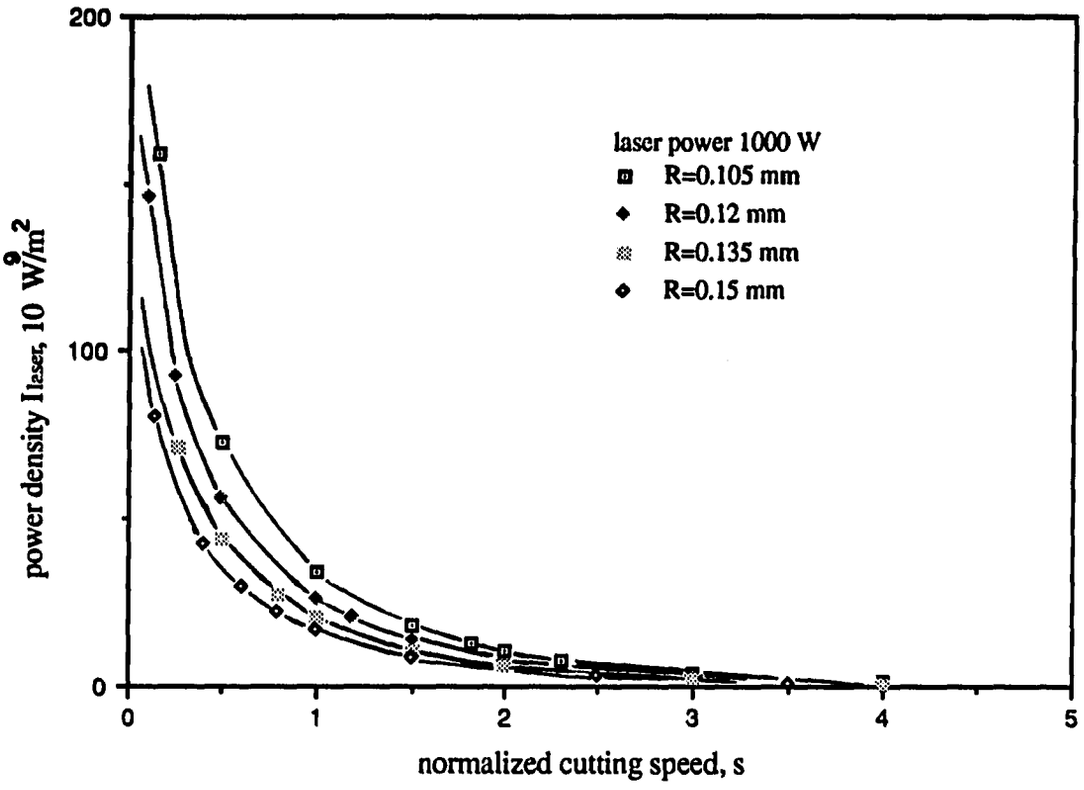


Figure 7a. $I_{laser}$ vs. s plot at various R values

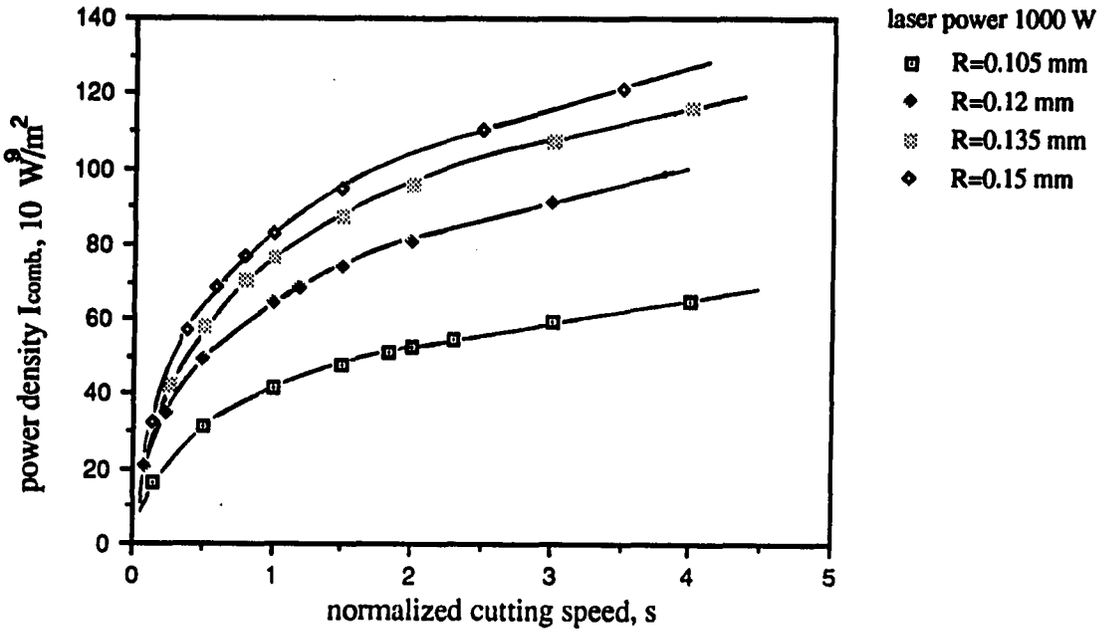


Figure 7b. $I_{comb}$ vs. s plot at various R values

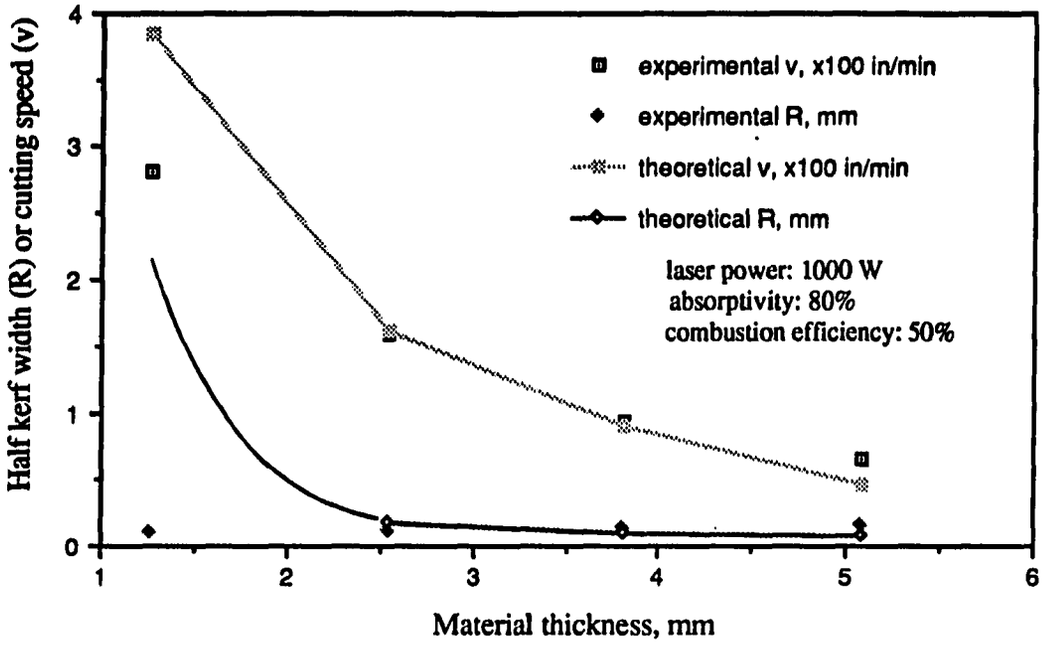


Figure 8. Theoretical and experimental maximum cutting speed (v) and half kerf width (R) vs. material thickness

medium thickness range (2-4 mm). Discrepancies between theory and experiment for the 1 mm and 5 mm cases can be related to assumptions (1) and (5). Heat loss due to evaporation in cutting thin-section material is significant and cannot be ignored. Therefore, the maximum cutting speed as well as the temperature rise in equation (4) and accordingly the kerf width will become smaller than the values observed in practice. In cutting thicker sections, the temperature along the cutting depth (Z direction) increases as the combustion reaction propagates and enlarges the kerf width. Under these circumstances, a three-dimensional model would be required to complete the analysis.

It is further found that the combustion energy (heat) is equal to approximately 55 - 70% of the total cutting energy (heat) in oxygen-assisted laser cutting of steel. This agrees with the previous reports by Kamalu and Steen (1983) and Forbes (1975) who determined experimentally that 60% - 70% of the cutting energy is supplied by combustion.

# 5. CONCLUSIONS

The following conclusions are drawn based on the experimental and analytical studies of oxygen-assisted $CO_2$ laser cutting of carbon steel.

1. Experimental and theoretical correlations between laser beam characteristics (power, absorptivity, mode pattern, focusability), combustion reaction (combustion efficiency, combustion heat) and material properties (thermal properties, density, thickness, liquid film thickness) were developed to accurately predict the processing parameters such as the maximum cutting speed and kerf width for laser cutting of steel.
2. The cutting energy was supplied by the absorbed laser irradiation and the chemical reaction between steel and oxygen. The combustion effect was found to play a very important role in laser cutting. This energy can amount to about 55-70% of the total cutting energy as predicted and verified by our model.

## REFERENCES

Abakians, H., and Modest, M. F., "Evaporative Cutting of a Semitransparent Body with a Moving CW Laser," ASME Journal of Heat Transfer, Vol. 100, 1988, pp. 924-930.

Arata, Y., "New Laser-Gas-Cutting Technique for Stainless Steel," Plasma, Electron & Laser Beam Technology, American Society for Metals, 1986, pp. 526-536.

Arata, Y., and Miyamoto, I., "Some Fundamental Properties of High Power $CO_2$ Laser Beam as a Heat Source," Trans. J.W.R.I., Vol. 3, No. 1, 1974, pp. 1-20.

Babenko, V. P., and Tychinskii, V. P., "Gas-Jet Laser Cutting," Soviet Journal of Quantum Electronics, Vol. 2, No. 5, 1973, pp. 399-410.

Band, S. Y., and Modest, M. F., "Multiple Reflection Effects on Evaporative Cutting with a Moving CW Laser," ASME Journal of Heat Transfer, Vol. 113, 1991, pp. 663-669.

Belforte, D., "Industrial Lasers' Impact on Manufacturing Technology," Proc. of SPIE, The Laser Marketplace in 1988, Vol. 950, 1988, pp. 77-85.

Belforte, D., Industrial Laser Annual Hand Book, Pennwell Books, 1990, Tulsa, OK.

Biyikli, S., and Modest, M. F., "Beam Expansion and Focusing Effects on Evaporative Laser Cutting," ASME Journal of Heat Transfer, Vol. 110, 1988, pp. 529-532.

Bunting, K. A., and Cornfield, G., "Toward a General Theory of Cutting: A Relationship Between the Incident Power Density and the Cut Speed," Trans. of the ASME Journal of Heat Transfer, 1973, pp. 116-122.

Carslaw, H. S. and Jaeger, J. C., Conduction of Heat in Solids, Clarendon Press, 1959, Oxford, United Kingdom.

Charschan, S., Lasers in Industry, Van Norstrand Reinhold Company, 1972, New York.

Chryssolouris, G., Sheng, P., and Choi, W. C., "Three-Dimensional Laser Machining of Composite Materials," Trans. of the ASME, Journal of Engineering

Material Technology, Vol. 112, 1990, pp. 387-392.

Chryssolouris, G., Laser Machining Theory and Practice, Springer-Verlag Inc., 1991, New York.

Duley, W. W., and Gonsalves, J. N., "$CO_2$ Laser Cutting of Thin Metal Sheets with Gas Jet Assist," Canadian Journal of Physics, Vol. 50, 1972, pp. 215-218.

Forbes, N., "The Role of Gas Nozzle in Metal Cutting with $CO_2$ Lasers," Laser 1975 OptoElectronics Conference, 1975, Munich, FRG.

Ivarson, A., Powell, J., and Magnusson, C., "The Role of Oxidation in Laser Cutting Stainless and Mild Steel," Journal of Laser Applications, Vol. 3, No. 3, 1991, pp. 41-45.

Kamalu, J. N., and Steen, W. N., Laser Materials Processings, edited by M. Bass, North-Holland Publishing Company, 1983, Amsterdam.

Modest, M. F., and Abakians, H., "Heat Conduction in a Moving Semi-infinite Solid Subjected to Pulsed Laser Irradiation," ASME Journal of Heat Transfer, Vol. 108, 1986, pp. 597-601.

Ready, J. F., Effects of High Power Laser Radiation, Academic Press, 1971, New York.

Ready, J. F., "Effects Due to Absorption of Laser Radiation," J. Appl. Physics, Vol. 36, 1965, pp. 462.

Roessler, D. M.. and Gregson, V. G., "Reflectivity of Steel at 10.6 $\mu$m Wavelength" Appl. Opt., Vol. 17, No. 7, 1978, pp. 992-993.

Roy, S., and Modest, M. F., "Three-Dimensional Conduction Effects During Scribing with a CW Laser, "Journal of Thermophysics and Heat Transfer, Vol. 4, No. 2, 1990, pp. 199-203.

Schuocker, D., and Abel, W., "Material Removal Mechanism of Laser Cutting," Proc. of SPIE, 1983, pp. 88-95.

Schuocker, D., and Walter, B., "Theoretical Model of Oxygen Assisted Laser Cutting," Inst., Phys. Conf. Ser., No. 72, 1984, pp. 111-116.

Schuocker, D., "Theoretical Model of Reactive Gas Assisted Laser Cutting Including Dynamic Effects," Proc. of SPIE, Vol. 650, 1986, pp. 210-219.

Schuoker, D., "Heat Conduction and Mass Transfer in Laser Cutting," Proc. of SPIE, Vol. 952, Laser Technologies in Industry, 1988, pp. 592-599.

Vicanek, M. and Simon, G., "Momentum and Heat Transfer of an Inert Gas Jet to

the Melt in Laser Cutting," Journal of Appl. Phys., Vol. 20, 1987, pp. 1191-1196.

# PAPER II: DUAL GAS-JET LASER CUTTING OF STAINLESS STEELS AND SUPERALLOYS

## ABSTRACT

A dual gas-jet, laser cutting technique involving coaxial and off-axial oxygen gas flows was developed to cut 6.35 mm (1/4 in.) thick stainless steels (AISI 304, 410, 430, 440A and 440C) and superalloys (Haynes alloy 25, Hastelloy C and Inconel MA 754) with a 1.2 kW $CO_2$ gas transport laser at a cutting speed of 12.7 mm/sec (30 in/min). Under identical process conditions, the single coaxial gas-jet could not cut the above materials even when the cutting speed was reduced to 2.11 mm/sec (5 in/min). Thresholds of off-axial nozzle diameter, gas-impinging angle, oxygen pressure and other process parameters were determined to obtain clean-cut edge quality (average dross height 0.25 mm). Experimental data coupled with a fluid-dynamics model of gas flow were presented to show the effectiveness of the dual gas-jet laser cutting method in achieving the maximum machining rate without deteriorating the quality of cut.

# 1. INTRODUCTION

Stainless steels and superalloys are widely used in aerospace, automotive, chemical and food processing and medical industries. Most of these materials exhibit high shear strength, possess hard intermetallic structures, and undergo strain-hardening; all of which make conventional tool machining difficult to perform. They also have low thermal conductivity properties, and are therefore difficult to machine and cause rapid tool wear. Laser machining is characterized by high speed cutting, precision and absence of tool wear. The non-contact process of laser cutting also simplifies the fixturing and tooling problems associated with conventional machining methods. However, standard (coaxial, oxygen-assisted) laser cutting of stainless steel and superalloy sheets does not provide satisfactory performance because the oxide dross clings to the bottom edges of the cut and forms a hard burr (Arata et al., 1986). As a result, thicknesses smaller than 3 mm only can be cut. Laser cutting of thick plates suffers from low process speed and the finished edge is similar to an oxy-acetylene flame cut. The obstacles in laser machining of stainless steels and superalloys are partly due to the low fluidity of the melt, and the high melting point of chromium oxide which also restrains oxygen diffusion in the molten cutting front. Currently, high gas pressure laser cutting, which uses pressure as high as 1 MPa (150 psi), has been adopted to machine stainless steels and other high temperature alloys in the 2-3 mm thickness range. Dross-free and oxide-contamination-free edges have been obtained by using high gas pressure cutting. The oxide-free edge is possible with the use of inert gas (such as nitrogen) instead of oxygen and is beneficial when a secondary process such as welding is needed. The workpieces cut by oxygen assist gas are not weldable and removal of the oxide layer is required to eliminate the porosity that occurs in welding (Nielsen, 1986). High gas pressure laser cutting leads to drawbacks including fracture of the focusing lens and formation of a Mach Shock Disk (MSD), which causes large variations in effective gas pressure on the workpiece (Fieret and Ward, 1986, Fieret et al., 1987). As a result, the maximum workpiece thickness in high gas pressure laser cutting is limited to a few millimeters.

In the present study, a laser cutting technique has been developed which employs dual gas-jets to remove the viscous slag in the molten cutting front and thereby allows stainless steels and superalloys to be machined faster, cleaner and thicker.

## 2. EXPERIMENTAL PROCEDURE

Different types of stainless steel and superalloy plates with a nominal thickness of 6.35 mm (1/4 in.) were cut by a Spectra-Physics Model 820 $CO_2$ laser. The compositions of the workpieces are given in Table 1. The $CO_2$ laser was operated at continuous wave mode and had a power output of 1200 watts. The beam had a nearly Gaussian ($TEM_{00}$) energy distribution. A 127 mm (5 in.) ZnSe focusing lens was used to focus the 19 mm (0.75 in.) raw laser beam to a spot size of 0.1 mm (0.004 in.) on the surface of the workpiece. The reservoir pressure of the coaxial nozzle (main jet) and off-axial nozzle (side jet) were varied from 0.13 to 0.26 MPa (20 to 40 psi) and 0.21 to 0.55 MPa (30 to 80 psi), respectively. The distance between the nozzle tips was kept at 2.3 mm (0.090 in.) and the clearance between nozzles and workpiece (stand off) was 0.7 mm (0.027 in.). Due to the configuration of the coaxial nozzle, the side jet impinging angles were employed only in the range $20^0$ to $45^0$. The workpieces were mounted on a computer numerically controlled worktable and cut in a linear movement with speeds from 12.7 mm/sec to 21.2 mm/sec (30 in/min to 50 in/min in 10 in/min increments). The off-axial nozzles were made of stainless steels with different diameters (0.3 mm to 1.5 mm) and set tandemly to the coaxial nozzle. The detailed experimental setup is illustrated in Figure. 1. The cut surfaces were examined by a profilometer (Sheffield Measurement Div., A Cross & Trecker Company, Model 3) with pilotor (Type VE) to measure the average roughness height, Ra, along the workpiece thickness. Scanning electron microscopy (SEM) was employed to study the edge quality. The clinging dross height at the bottom of cut was measured by a micrometer for various cutting conditions. The gas flow rate was measured by a wet test meter. Data concerning the material weight loss in laser cutting was obtained by weighing the sample before and after cutting using a precision scale. X-ray diffraction (XRD) was used to determine the composition of oxides of the combustion droplets.

Table 1. Nominal compositions of stainless steels and superalloys in wt.%

| element / type | Cr | Ni | Co | Mo | W | Mn | C | Fe |
|---|---|---|---|---|---|---|---|---|
| AISI 304 | 19 | 9 | | | | | 0.08 | balance |
| AISI 410 | 12.5 | | | | | | 0.15 | balance |
| AISI 430 | 17 | | | | | | 0.12 | balance |
| AISI 440A | 17 | | | | | | 0.72 | balance |
| AISI 440C | 17 | | | | | | 1.07 | balance |
| Haynes 25 | 20 | 10 | 51 | | 15 | 1.5 | | 3.0 (max.) |
| Hastelloy C | 15.5 | 58 | | 16 | 3.8 | | 0.08 | 5.5 |
| MA 754 * | 20 | 78 | | | | | 0.05 | 1.0 |

* plus 0.3 wt.% Al; 0.5 wt.% Ti and 0.6 wt.% $Y_2O_3$

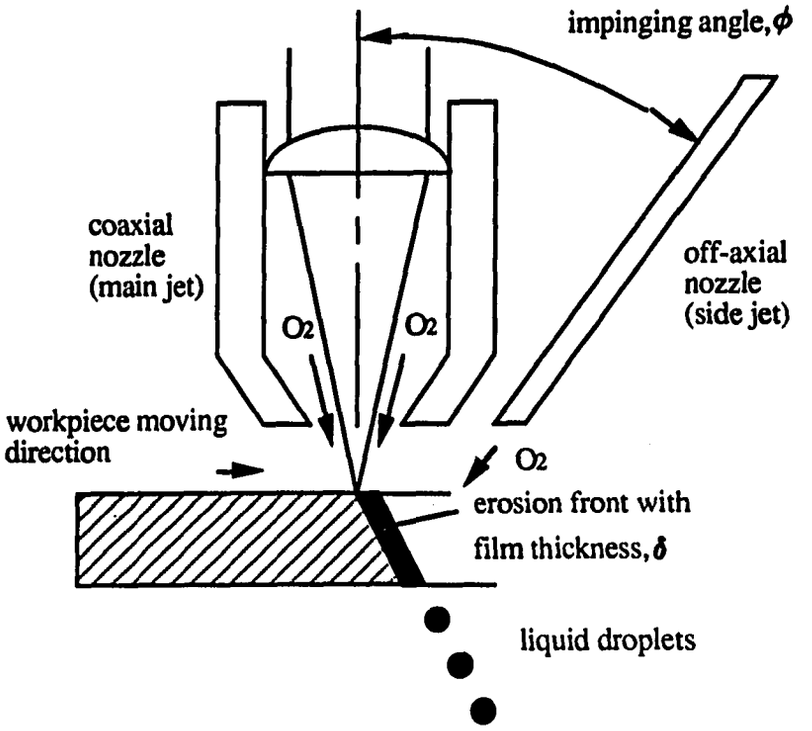


Figure 1. Schematic diagram of dual gas-jet laser cutting

## 3. RESULTS AND DISCUSSION

In industrial laser practice, a 1.2 kW $CO_2$ laser can cut 6.35 mm (1/4 in.) thick stainless steel and superalloy plates at about 0.4 to 2 mm/sec (1-5 in/min) with the assistance of a high-pressure, coaxial oxygen gas-jet. The resulting edge quality is usually poor. In the present work, laser cutting experiments with the dual gas-jet (coaxial and off-axial) provided the following significant results.

1. Cutting speed was improved to 12.7 mm/sec (30 in/min) with the added benefit of a much better edge quality. Cutting speed above 16.9 mm/sec (40 in/min) resulted in poor edge quality and excessive dross.
2. Off-axial gas-jet parameters including nozzle diameter, distance between coaxial and off-axial nozzles, gas-impinging angle and oxygen pressure were the key variables for obtaining the maximum material removal rate without sacrificing the edge quality. The threshold off-axial gas-jet nozzle diameter was determined to be 1.1 mm (0.045 in.). Below this value, satisfactory cutting performance was not possible even though the oxygen pressure was increased to 0.55 MPa (80 psi). The critical oxygen gas pressure on the off-axial reservoir was found to be a minimum of 0.31 MPa (45 psi) in order to eliminate excessive dross formation.

Figure 2 shows the experimentally obtained material removal rate of AISI 304 stainless steel as a function of the impinging angle of the side jet. The weight loss decreased as the impinging angle increased. Figures 3 to 7 show scanning electron micrographs (SEM) of cut surfaces in 304 stainless steel at 12.7 mm/sec (30 in/min) for various impinging angles.

The striations near the top surface are fine but progressively become coarse towards the bottom of cut. The formation of striations on the cut surface is due to an unsteady motion of the melt while being removed from the kerf (Schuocker, 1986, Vicanek et al., 1987). Schuocker (1986) concluded that the two striation patterns of cut surfaces in laser cutting can be explained in terms of lower temperature and turbulent gas flow at the lower melt layer. Therefore, low quality cuts at small impinging angles, as depicted in Figures 3 and 4, can be attributed to the turbulent effect.

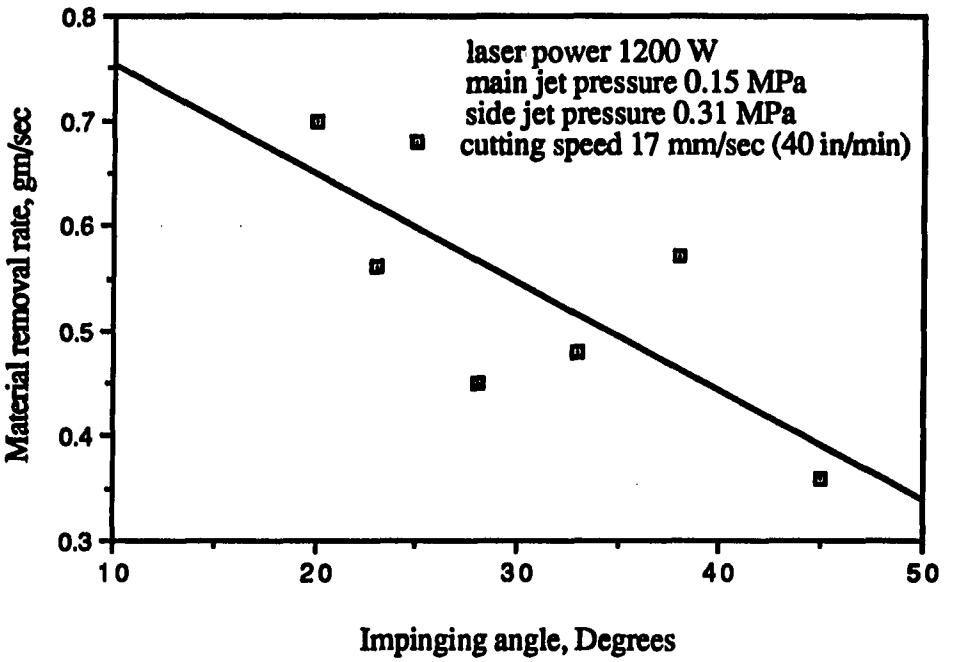


Figure 2. Weight loss vs. impinging angle

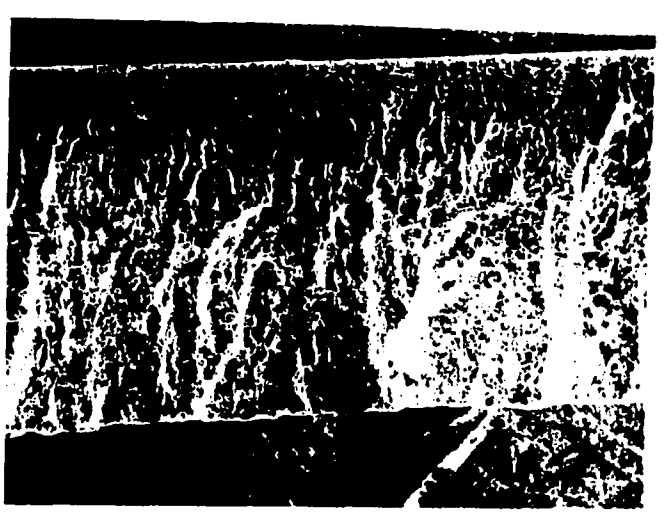

Figure 3. SEM of cut surface at $20^0$ impinging angle
(magnification = 7x)

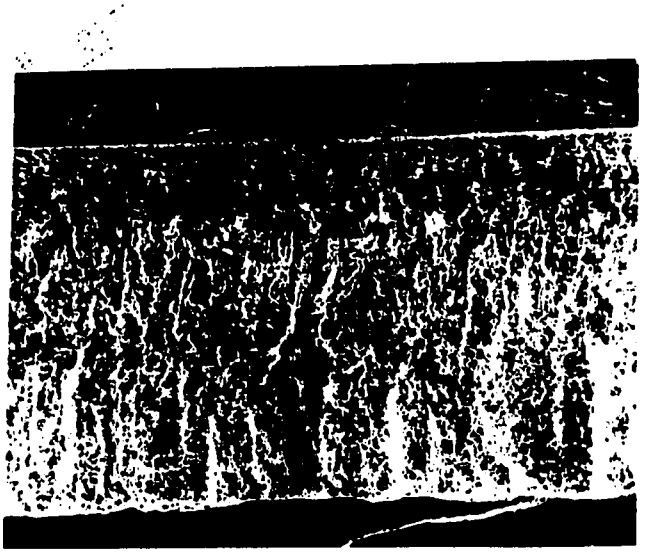

Figure 4. SEM of cut surface at $25^0$ impinging angle (magnification = 7x)

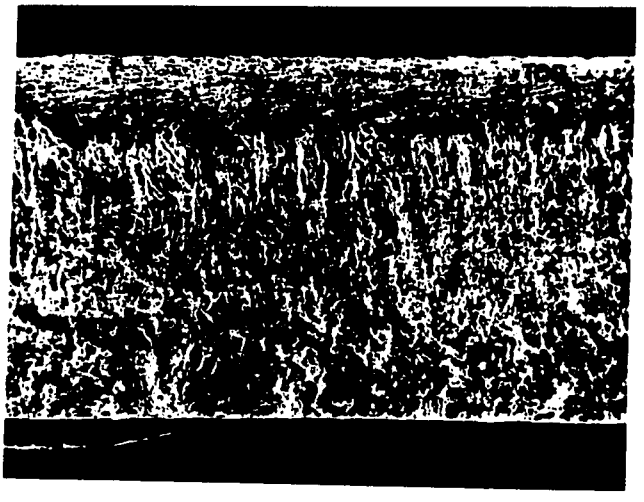

Figure 5. SEM of cut surface at $33^0$ impinging angle (magnification = 7x)

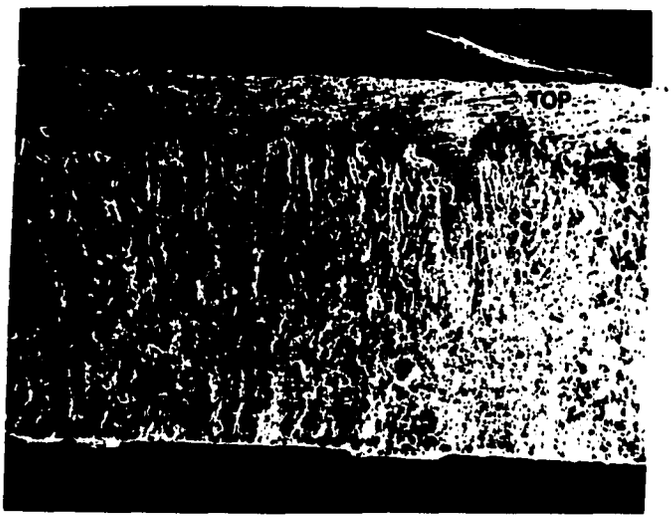


Figure 6. SEM of cut surface at $38^0$ impinging angle (magnification = 7x)

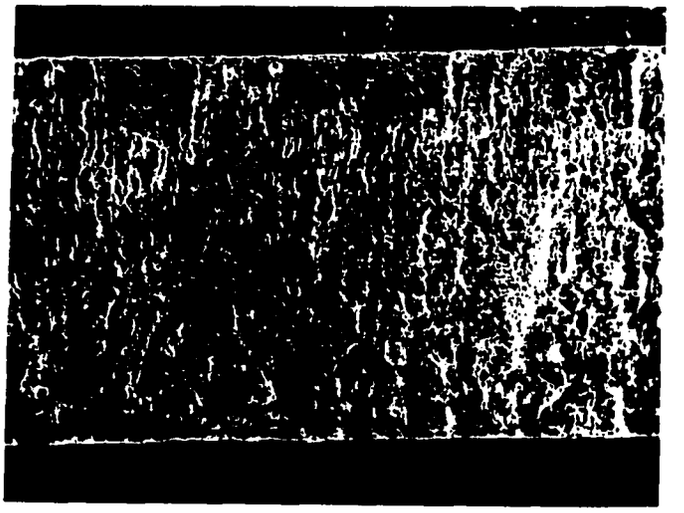

Figure 7. SEM of cut surface at $40^0$ impinging angle (magnification = 7x)

As the impinging angle decreases, the jet targeting position moves away from the top surface because the distance between coaxial and off-axial nozzles is kept constant. The extended distance from the off-axial nozzle to the erosion cutting front at small impinging angles increases the characteristic length of a free jet and promotes turbulent flows. Accordingly, the surface roughness becomes higher at small impinging angles. Table 2 lists the surface roughness (Ra) values of laser-cut AISI 304 stainless steel at different locations along the depth of cut and for various side jet impinging angles. The surface roughness measured perpendicular to the direction of striations increases along the depth of cut. As the impinging angle of the side jet increases, the surface roughness decreases except for the upper portion of the cut surface. The surface roughness within a 2 mm range below the top surface does not seem to change with impinging angles. This distinct roughness pattern along the cut depth can be explained by the development of turbulent flow inside the kerf.

Figure 8 indicates the average dross height (Dh) of AISI 304 stainless steel for various cutting conditions. In general, the Dh increases as the cutting speed increases. Since the interaction time between the gas jet and the dross is shorter at high cutting speeds, removal of dross can be expected to be incomplete.

Arata et al. (1986) reported that the laser cutting of 2 mm thick 304 stainless steel using the tandem nozzle method improved the cut quality. The optimal conditions for clean-cut quality are given in Table 3, which includes data from Arata's work and the present investigation. It can be seen in Table 3 that the material thickness in the present study is three times larger than that of the thickness in Arata's work. The optimal impinging angle is actually identical but the side jet pressure and jet targeting position in the present study are different.

Figures 9-12 show the surface finish of dual gas-jet laser-cut AISI 410, 430, 440A and 440C stainless steels at the above optimized conditions. Similar success in the production of a dross-free cutting was observed in 410 and 430 but not in 440 series stainless steels. A significant amount of dross remained at the bottom portion of the cut surface. It is believed that the high carbon content in 440 stainless steels plays an important role in excessive dross formation because a clean cut was observed on 430 stainless steel which has the same Cr content. The mechanisms associated with carbon in dross formation are discussed below.

In oxygen-assisted laser cutting of stainless steels, the following chemical reactions occurred (Arata, 1979; Nielsen, 1986) and were verified in our XRD analysis of the combustion droplets (Figures 13 and 14).

Table 2. Surface roughness vs. side jet impinging angle

| Surface roughness, Ra, mm / Distance below surface, mm / Impinging angle, degrees | 2.0 | 4.0 | 6.0 |
|---|---|---|---|
| 20.0 | 0.006-0.013 | > 0.025 | > 0.025 |
| 23.0 | 0.009-0.014 | 0.014-0.021 | > 0.025 |
| 25.0 | 0.005-0.011 | > 0.018 | > 0.025 |
| 28.0 | 0.006-0.015 | 0.014-0.024 | > 0.025 |
| 33.0 | 0.010-0.018 | 0.011-0.016 | > 0.022 |
| 38.0 | 0.005-0.014 | 0.012-0.018 | > 0.022 |
| 40.0 | 0.010-0.015 | 0.012-0.021 | > 0.014 |

When larger sign ( > ) is used, the upper value of the data is above the limit reading of the profilometer (0.025 mm).

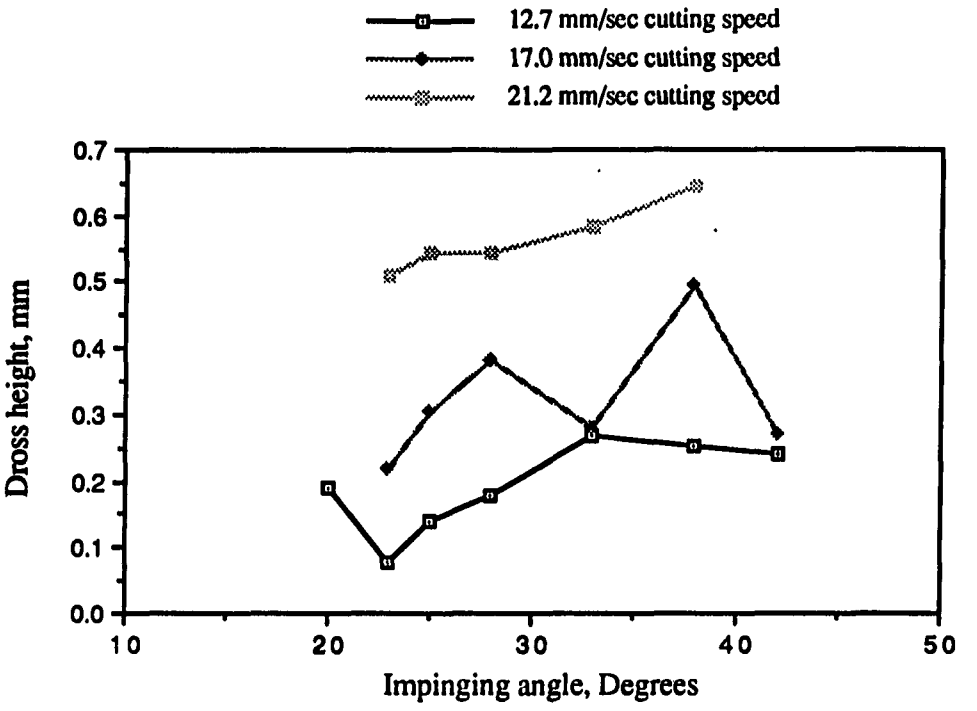


Figure 8. Dross height (Dh) vs. side jet impinging angle

Table 3. Optimal conditions for laser cutting of AISI 304 stainless steel

| | Material | Impinging angle | Main jet pressure | Side jet pressure | Jet targeting position |
|---|---|---|---|---|---|
| Arata * et al. | 304 s.s. 2 mm thick | ~ 40° | 0.15 MPa (21 psi) | >0.25 MPa (35.5 psi) | near bottom |
| Present work ** | 304 s.s. 6.35 mm thick | 38° - 40° | 0.15 MPa (21 psi) | >0.31 MPa*** (45.0 psi) | ~1/3 thickness from top |

* convergent coaxial nozzle
** stepped coaxial nozzle, orifice dia.: 1.5 mm
*** side jet tube dia.: 1.5 mm

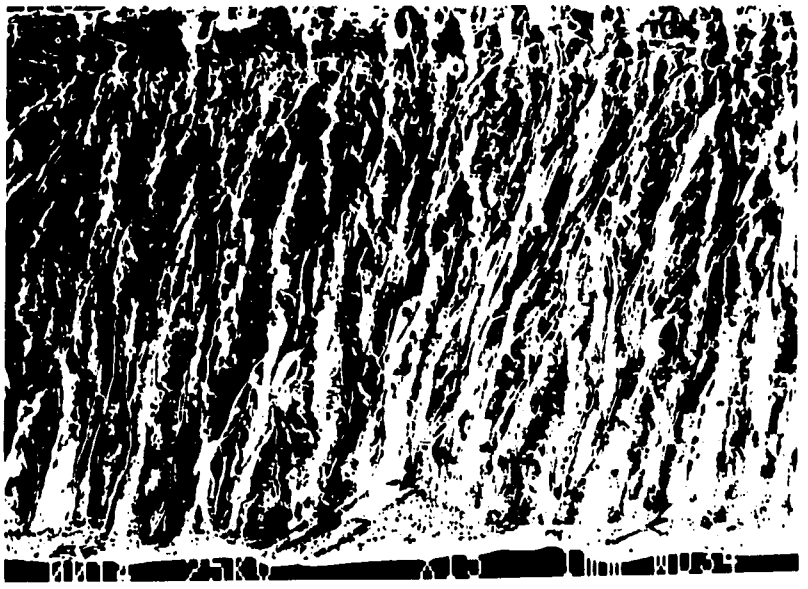

Figure 9. AISI 410 laser-cut surface
(cutting speed = 21.2 mm/sec)

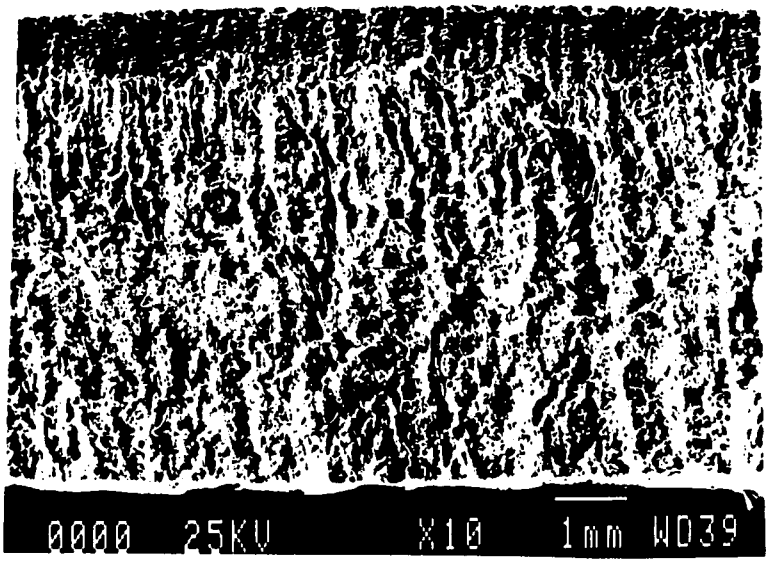


Figure 10. AISI 430 laser-cut surface
(cutting speed = 12.7 mm/sec)

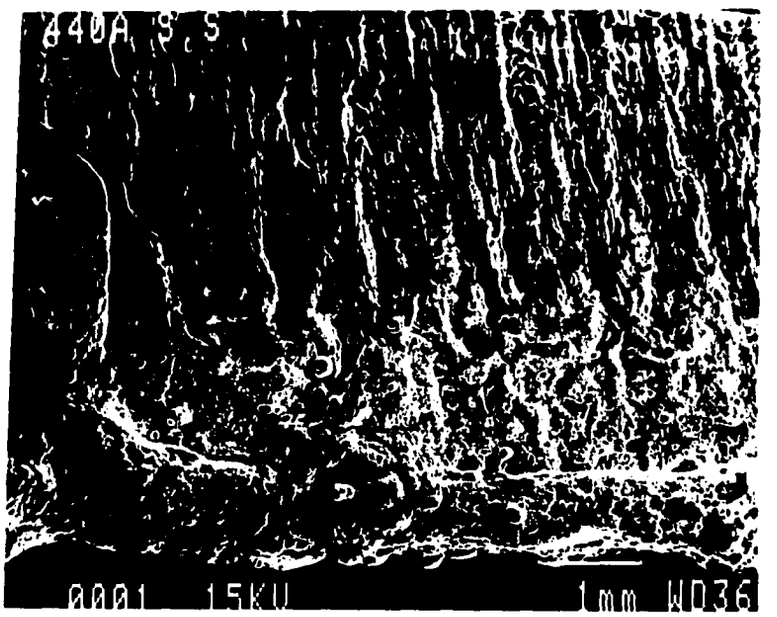


Figure 11. AISI 440A laser-cut surface
(cutting speed = 12.7 mm/sec)

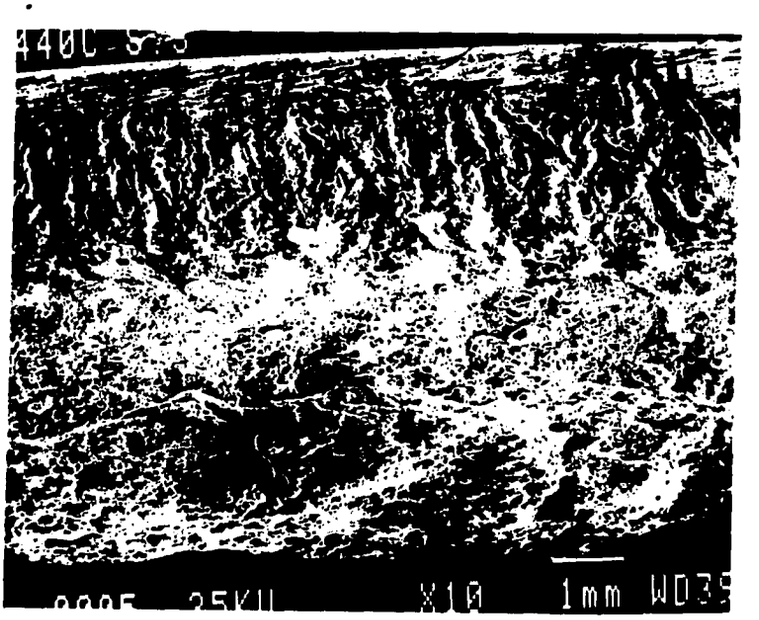


Figure 12. AISI 440C laser-cut surface
(cutting speed = 12.7 mm/sec)

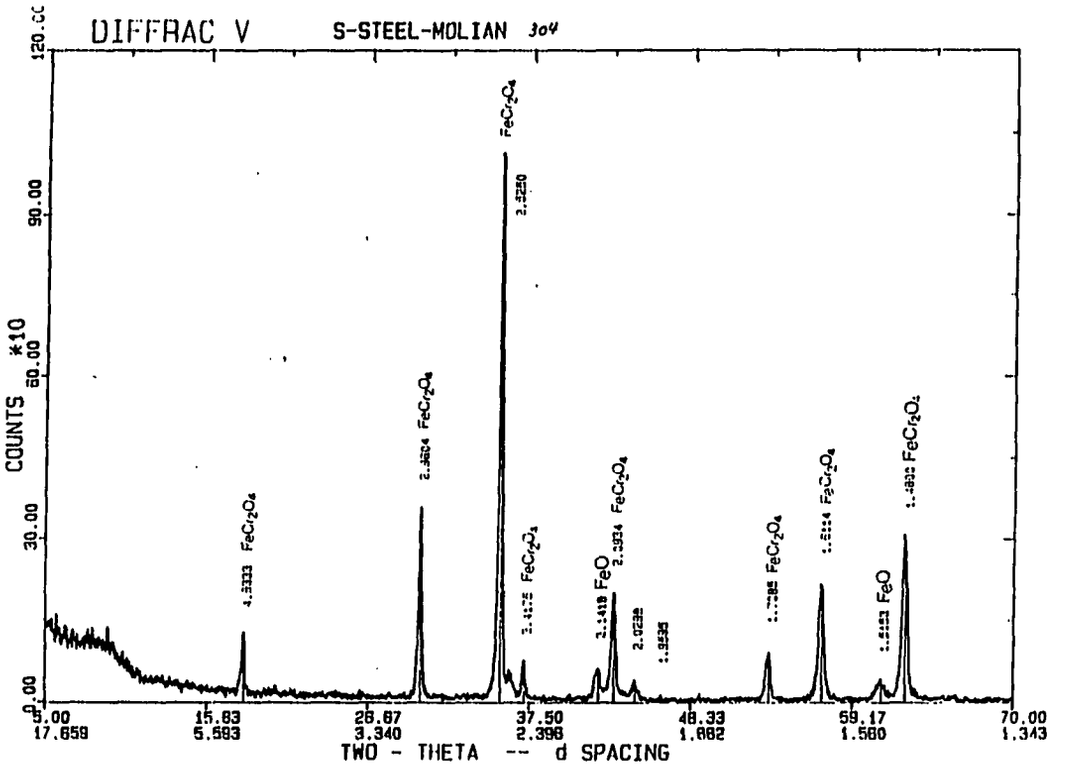


Figure 13. XRD analysis of combustion droplets
(material: AISI 304)

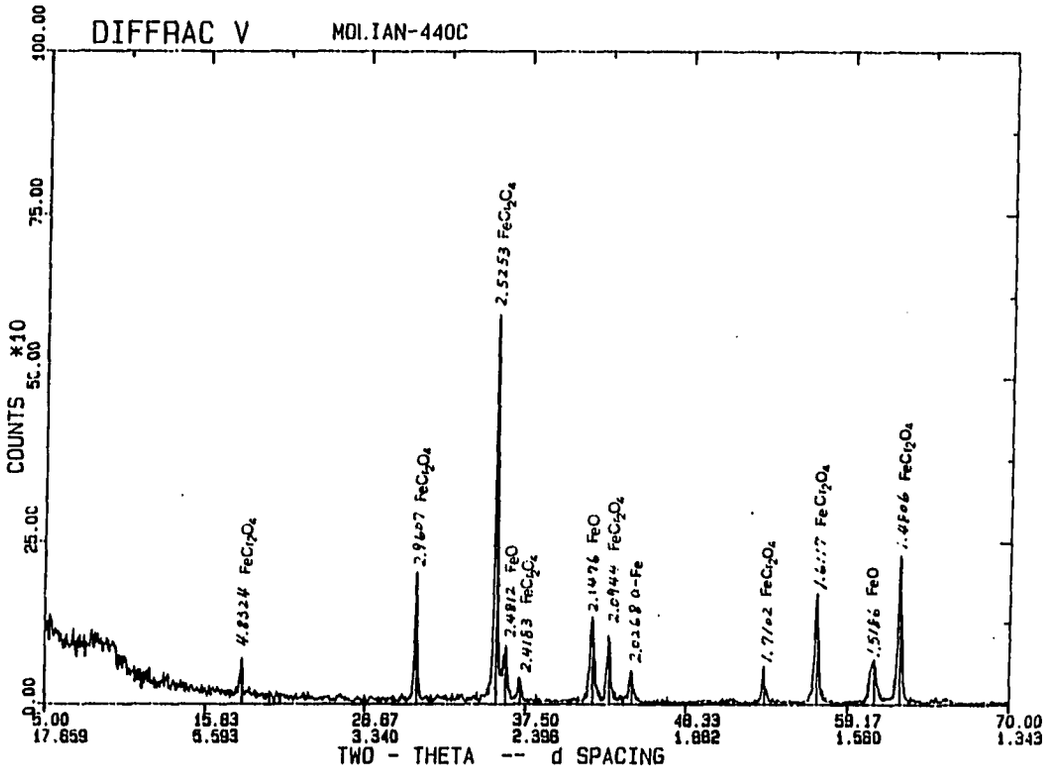


Figure 14. XRD analysis of combustion droplets
(material: AISI 440C)

$2Fe + O_2 \rightarrow 2FeO$

$4Cr + 3O_2 \rightarrow 2Cr_2O_3$

$2Ni + O_2 \rightarrow 2NiO$

$2C + O_2 \rightarrow 2CO$

$C + O_2 \rightarrow CO_2$

$2CO + O_2 \rightarrow 2CO_2$

$2Fe + O_2 + 2Cr_2O_3 \rightarrow 2FeCr_2O_4$

$FeO + Cr_2O_3 \rightarrow FeCr_2O_4$

Arata (1979) reported that the temperature inside the erosion front in the laser cutting of steel is about 2000 K. Figure 15 shows the free energy vs. temperature plots corresponding to the above chemical reactions. It is clear that carbon monoxide formation is favored at high temperature. Meyer et al. (1968) reported that decarburization in the Basic-Oxygen Furnace (BOF) steelmaking process is due to slag-metal emulsions and pure oxygen from lance reacting with liquid iron metal to form iron oxide. The iron oxide then reacts with carbon in the steel to form carbon monoxide: $FeO + C \rightarrow Fe + CO$

They also concluded that the amount of decarburization is proportional to the carbon level in the metal and is virtually independent of the rate of oxygen supply. Because of the similarity between oxygen-assisted laser cutting and the Basic-Oxygen Process (BOP) in steelmaking, the following conclusion can be made.

In dual gas-jet laser cutting of 440 stainles steels, carbon reacts violently with iron oxide to form carbon monoxide in the slag-metal emulsion phase. Since chromium oxide restrains oxygen diffusion in the molten layer, iron atoms reduced by carbon do not form oxides quickly. From the FeO and $Cr_2O_3$ phase diagrams shown in Figure 16, the absence of FeO shifts the molten layer of the erosion front away from the single liquid-phase state into the $Cr_2O_3$ + liquid region. As a result of the presence of chromium oxide, the viscosity in the molten layer increases and excessive dross is formed. Figure 17 shows the enlarged view in the bottom section of laser-cut 440 stainless steels. Many blow holes in the dross can be seen. This confirms the previous conclusion that CO formation in high carbon stainless steels is detrimental to laser cutting performance.

Figures 18, 19 and 20 show the cross sectional views of laser cut superalloys. Compared to low carbon stainless steels, it can be noted that surface finish slightly deteriorates and slags adhere to the bottom edge of the cut. Due to the small amount of iron and large

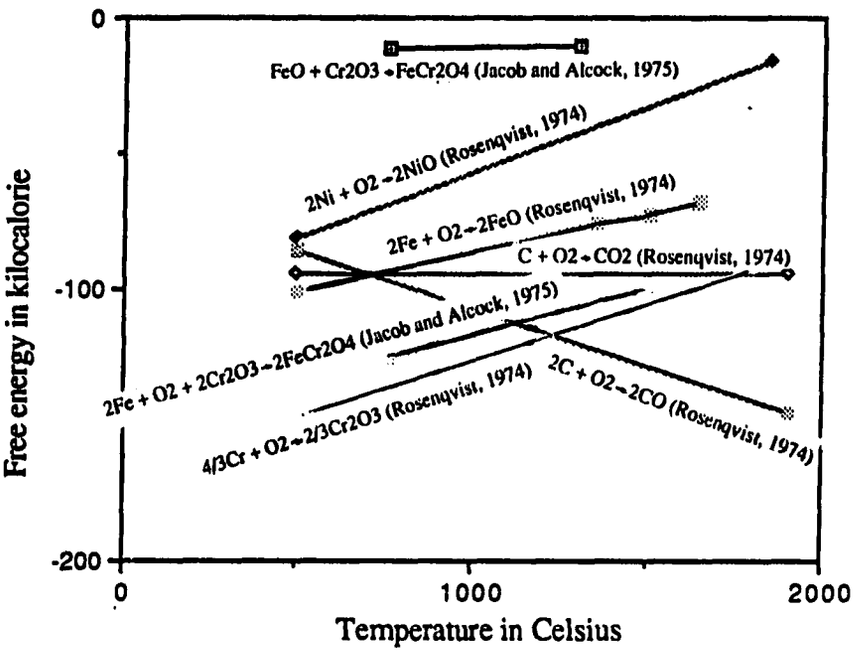


Figure 15. Free energy vs. temperature plot

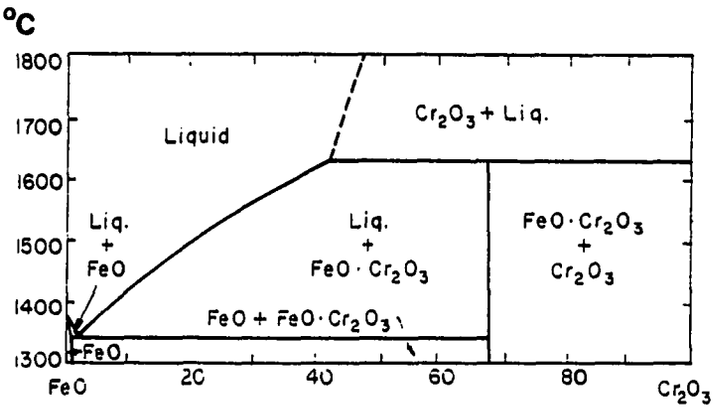


Figure 16. FeO - $Cr_2O_3$ phase diagram (Levin et al., 1969)

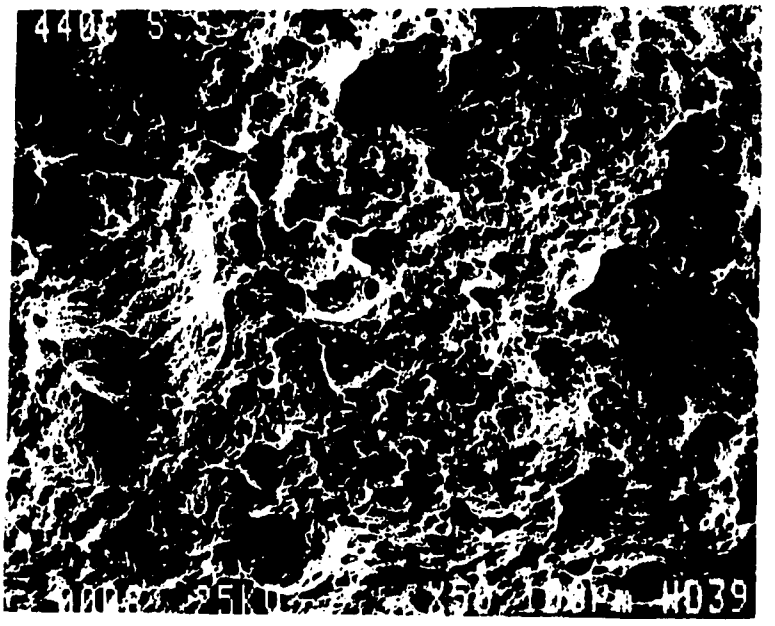

Figure 17. Blow holes in laser-cut 440C stainless steel

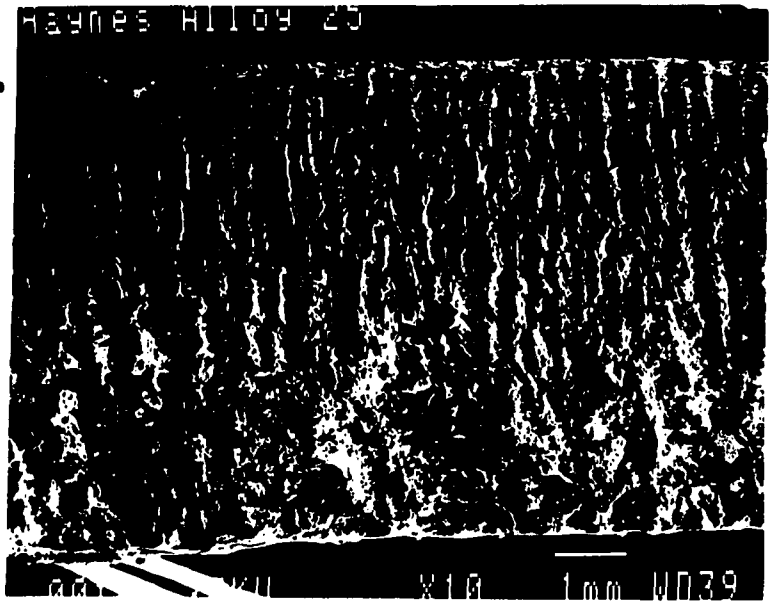


Figure 18. Haynes alloy 25 laser-cut surface
(cutting speed = 12.7 mm/sec)

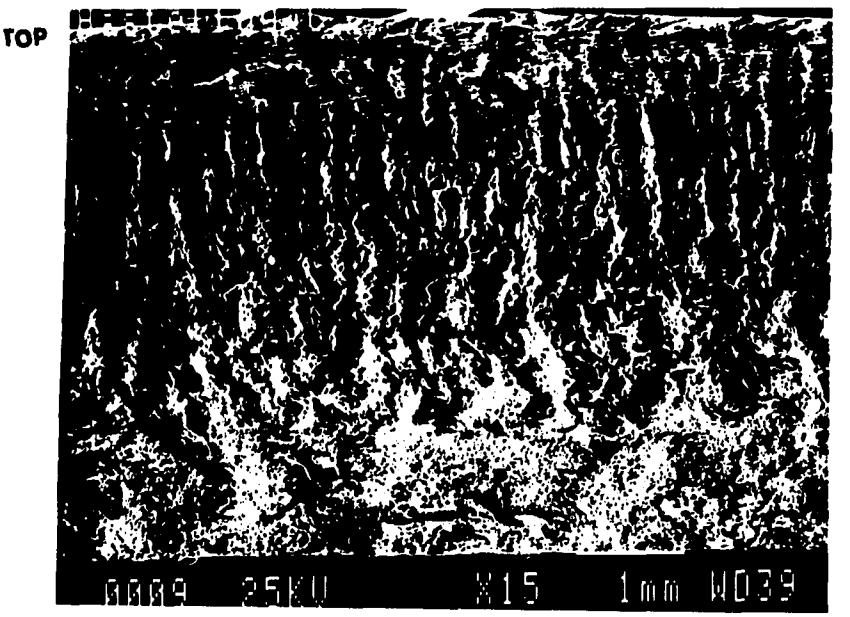


Figure 19. Hastelloy C laser-cut surface
(cutting speed = 12.7 mm/sec)

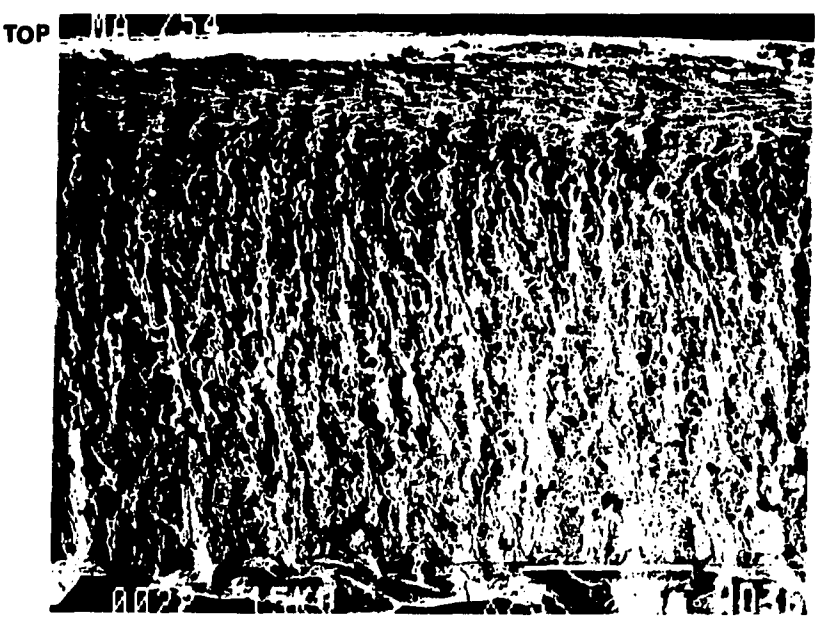


Figure 20. Inconel alloy MA 754 laser-cut surface
(cutting speed = 25.4 mm/sec)

quantity of alloying elements (such as Ni, Co, Mo and W) in superalloys, the formation of iron oxide and the increase in fluidity in the molten layer are minimized. Therefore the surface finish of superalloys is inferior to that of low carbon stainless steels in dual gas-jet laser cutting because the mechanism of dross removal occurs mainly by gas momentum transfer from the off-axial jet.

# 4. THEORETICAL MODELING

## 4.1 Coaxial gas-jet assisted laser cutting

The mechanisms involved in laser cutting are extremely complex but the models discussed by many investigators (Arata et al., 1979, Esposito and Daurelio, 1981, Chryssolouris and Choi, 1989, Schuocker, 1988, Schulz et al., 1987) are limited to heat flow aspects of laser-material interactions. The following model is based on the fluid dynamics aspects of coaxial gas-assisted laser cutting. As discussed before, the low fluidity of the melt is the main obstacle to satisfactory laser cutting of stainless steels and superalloys. The dynamic behavior of the gas jet also plays an important role in achieving clean-cut edge quality through an increase in the fluidity of the melt. To simplify the analysis, the following assumptions are made.

1. No inertia force acts on the melt film at the erosion cutting front.
2. The shear stresses at the interface between melt film and gas jet stream are equal.
3. The gas-jet is two-dimensional, incompressible, fully developed laminar flow inside the kerf.
4. The melt is a Newtonian fluid and has uniform thickness.
5. The cutting process is in steady-state.

Figure 21 shows the schematic diagram of modeling. In the x,y coordinate system the force balance of an element in the flow direction is

$$\rho_l g \sin\theta \, dx \, dy = -\left(\frac{\partial \tau}{\partial y}\right) dx \, dy \qquad (1)$$

$$\text{and } \tau = \mu_l \frac{du}{dy} \qquad (2)$$

Canceling out dx· dy in equation (1) and combining with equation (2), we get

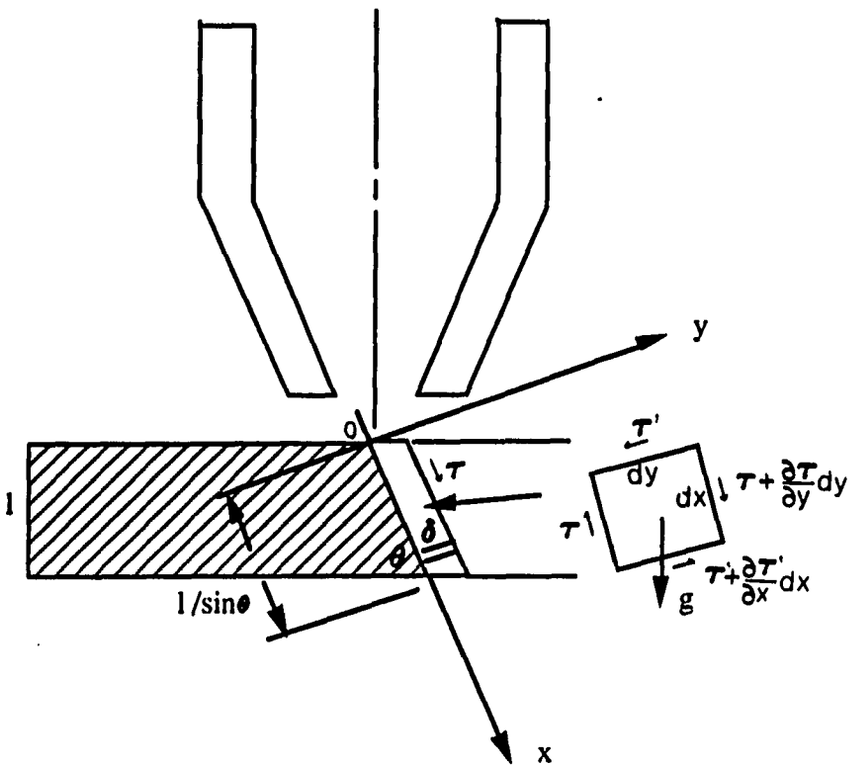


Figure 21. Schematic diagram of fluid-dynamics model

$$\rho_l g \sin\theta = -\mu_l \left(\frac{\partial^2 u}{\partial y^2}\right) \qquad (3)$$

By integration with respect to y twice, we have

$$u = -g \sin\theta \frac{\rho_l}{2\mu_l} y^2 + C_1 y + C_2 \qquad (4)$$

The boundary conditions are:

(1) $u = 0$ at $y = 0$, then $C_2 = 0$

(2) $\mu_l \left(\frac{\partial u}{\partial y}\right) = \tau$ at $y = \delta$

Where $\tau$ is the shear stress at the interface of the melt film and the gas flow and $\delta$ is the melt film thickness.

Vicanek and Simon (1987) reported that the shear stress ($\tau$) acting on the cutting front is

$$\tau = \tau_0 g(x/l, \theta) \qquad \tau_0 = (\mu_g \rho_g V^3 l^{-1})^{1/2} \qquad (5)$$

where $g(x/l, \theta)$ is a non-dimensional function of the order of unity. Then, from boundary condition (2) $C_1$ becomes

$$C_1 = \mu_l^{-1}[g(x/l,\theta)\, \mu_g^{1/2} \rho_g^{1/2} V^{3/2} l^{-1/2} + \rho_l g \sin\theta\, \delta] \qquad (6)$$

Equation (4) becomes

$$u = -\frac{1}{2} \mu_l^{-1} (\rho_l g \sin\theta) y^2 + \mu_l^{-1}[g(x/l,\theta)\, \mu_g^{1/2} \rho_g^{1/2} V^{3/2} l^{-1/2} + \rho_l g \sin\theta\, \delta] y \qquad (7)$$

The mass removal rate per unit kerf width is

$$\dot{M} = \int_0^{\delta} \rho_l u \, dy = \frac{1}{2} \mu_l^{-1}[g(x/l,\theta)\, \rho_l \mu_g^{1/2} \rho_g^{1/2} V^{3/2} l^{-1/2} \delta^2] + \frac{1}{3} \mu_l^{-1} \rho_l^2 g \sin\theta\, \delta^3 \qquad (8)$$

The material removal rate $M_{sh}$ due to shearing is,

$$\dot{M}_{sh} = w \dot{M} = \frac{1}{2} \mu_l^{-1}[g(x/l,\theta)\, \rho_l \mu_g^{1/2} \rho_g^{1/2} V^{3/2} l^{-1/2} \delta^2 w] + \frac{1}{3} \mu_l^{-1} \rho_l^2 g \sin\theta\, \delta^3 w \qquad (9)$$

## 4.2 Dual gas-jet assisted laser cutting

The theory of homogeneous jets and the characteristics of an impinging gas jet were discussed extensively by Szekely and Themelis (1971). In general, the initial flow region is confined to a length about four to six orifice diameters along the jet axis. Since the configuration and setup of the gas-jet nozzles with respect to the erosion cutting front is inside the initial flow region, it is assumed that the jet velocity on the erosion cutting front is identical to the jet velocity at the orifice and has a uniform velocity profile in the radial direction.

Figure 22 shows a schematic of the gas flows interacting with the erosion front in coaxial and off-axial laser cutting. Based on the analysis of the control volume, the momentum and energy balance in the direction parallel to the erosion front can be written as:

$$\dot{M}_{co} V_{co} + \dot{M}_{off} V_{off} \cos\phi = \dot{M}_e V_e + \dot{M}_{ex} V_{ex} \qquad (10)$$

and

$$\dot{M}_{co}(V_{co})^2 + \dot{M}_{off}(V_{off})^2 = \dot{M}_e(V_e)^2 + \dot{M}_{ex}(V_{ex})^2 \qquad (11)$$

Where $\dot{M}$ = mass flow rate of gas, kg/sec

V = gas velocity, m/sec

The effective mass flow rates on the erosion cutting front arising from coaxial and off-axial nozzles are proportional to the ratio of the melt surface area to the cross sectional area of the jet stream and can be expressed as

$$\dot{M}_{co} = \rho_{co} \dot{V}_{co} \left(\frac{4w\delta}{\pi d_{co}^2}\right) \qquad (12)$$

and

$$\dot{M}_{off} = \rho_{off} \dot{V}_{off} \left(\frac{\frac{4w d_{off}}{\cos\phi}}{\pi d_{off}^2}\right) \qquad (13)$$

In consideration of the mass balance in the melt film, the material fed into the control volume in the solid state must be equal to that of the ejected droplets in the liquid state. Then,

$$\rho_w \cdot v \cdot w \cdot l = \rho_e \cdot V_e \cdot w \cdot \delta \cdot F = \dot{M}_e \cdot F \qquad (14)$$

where $\rho_w$ and $\rho_e$ are the densities of workpiece and droplets respectively.

At this stage a parameter F is introduced which is related to the composition of droplets due to the addition of oxygen in combustion. Schuocker (1988) studied the momentum

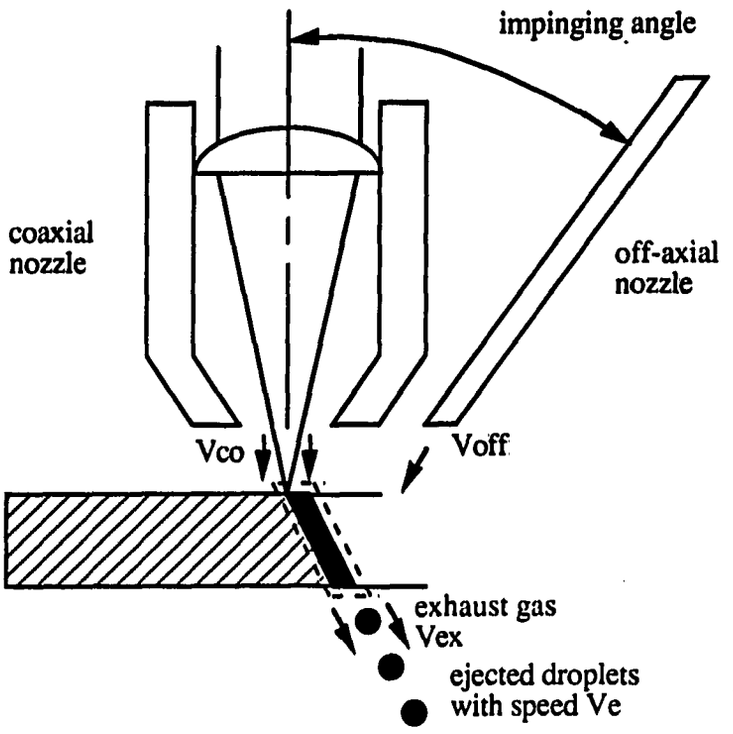


Figure 22. Schematic of gas flows interacting with erosion cutting front

transfer of gas flow in laser cutting and concluded that the velocity of ejected droplets can be expressed as:

$$V_e = \sqrt{\frac{\mu_s I V}{\rho_e \delta w}} \qquad (15)$$

By substituting equations (12), (13) and (14) into equations (10) and (11), the exhaust gas velocity ($V_{ex}$) can be obtained as:

$$V_{ex} = \frac{\rho_{co} \dot{V}_{co} (\frac{4w\delta}{\pi d_{co}^2}) V_{co}^2 + \rho_{off} \dot{V}_{off} (\frac{4w}{\pi d_{off}}) V_{off}^2 - \rho_e w \delta V_e^3}{\rho_{co} \dot{V}_{co} (\frac{4w\delta}{\pi d_{co}^2}) V_{co} + \rho_{off} \dot{V}_{off} (\frac{4w}{\pi d_{off}}) V_{off} - \rho_e w \delta V_e^2} \qquad (16)$$

In fact, the contribution of kinetic energy from the off-axial nozzle was found to be so dominant in the present experimental setup that the exhaust gas velocity can be considered to be very close to the off-axial gas velocity as calculated from equation (16). Then, from equations (14) and (15), the cutting speed in dual-jet laser cutting can be written as:

$$v = \sqrt{\frac{\rho_e \delta \mu_s V_{off} F^2}{l w \rho_w^2}} \qquad (17)$$

# 5. RESULTS OF THE MODELING

The physical properties involved in the model are difficult to determine. In coaxial gas-assisted laser cutting, the molten liquid is iron oxide (FeO) for carbon steel and a mixture of iron oxide (FeO) and chromium oxide ($Cr_2O_3$) for stainless steel (Arata, 1986). XRD analysis of droplets (Figure 23) in laser cutting of carbon steel confirms that the molten liquid is mainly iron oxide (FeO). However, in dual gas-jet laser cutting of stainless steel, the dross is composed of primarily iron chromite ($FeCr_2O_4$). $Cr_2O_3$ could not be detected (Figure 13). Arata et al. (1979) reported that the temperature at the laser cutting front increases along the cut depth and varies from 1600 $^0$C to 2100 $^0$C in 2 mm thick carbon steel. Therefore, the viscosity of the melt liquid used in the model was the value at a temperature of 2000 K. Gas density and viscosity at the surface temperature of the melt film were obtained in order to arrive at accurate results (Curle and Davis, 1971). The oxygen jet velocity at the nozzle was calculated from compressible flow and the values of $\theta$ and w were measured experimentally.

## 5.1 Coaxial gas-jet assisted laser cutting

In laser cutting of 6.35mm (1/4 in.) thick carbon steel at a power of 1 kW, the oxygen pressure is approximately 0.21 MPa (30 psi). The liquid film thickness was taken from the work by Schuocker (1988). The g(x/l, $\theta$) value was interpolated to be between 0.1 to 0.2 at $\theta = 86^0$ (Vicanek and Simon, 1987).

Material constants used in model

| | | | | | |
|---|---|---|---|---|---|
| $\mu_l$ | = | $3 \times 10^{-3}$ gm·mm$^{-1}$·s$^{-1}$ | w | = | 0.28 mm |
| $\mu_g$ | = | $7.3 \times 10^{-5}$ gm·mm$^{-1}$·s$^{-1}$ | $\delta$ | = | 0.12 mm |
| $\rho_l$ | = | 0.00604 gm·mm$^{-3}$ | l | = | 6.35 mm |
| $\rho_g$ | = | $0.2 \times 10^{-6}$ gm·mm$^{-3}$ | g | = | 9800 mm·s$^{-2}$ |
| $\theta$ | = | $86^0$ | $\dot{V}_g$ | = | $4.86 \times 10^5$ mm$^3$·s$^{-1}$ |
| V | = | $4 \times 10^5$ mm·s$^{-1}$ | dco | = | 1.15 mm |

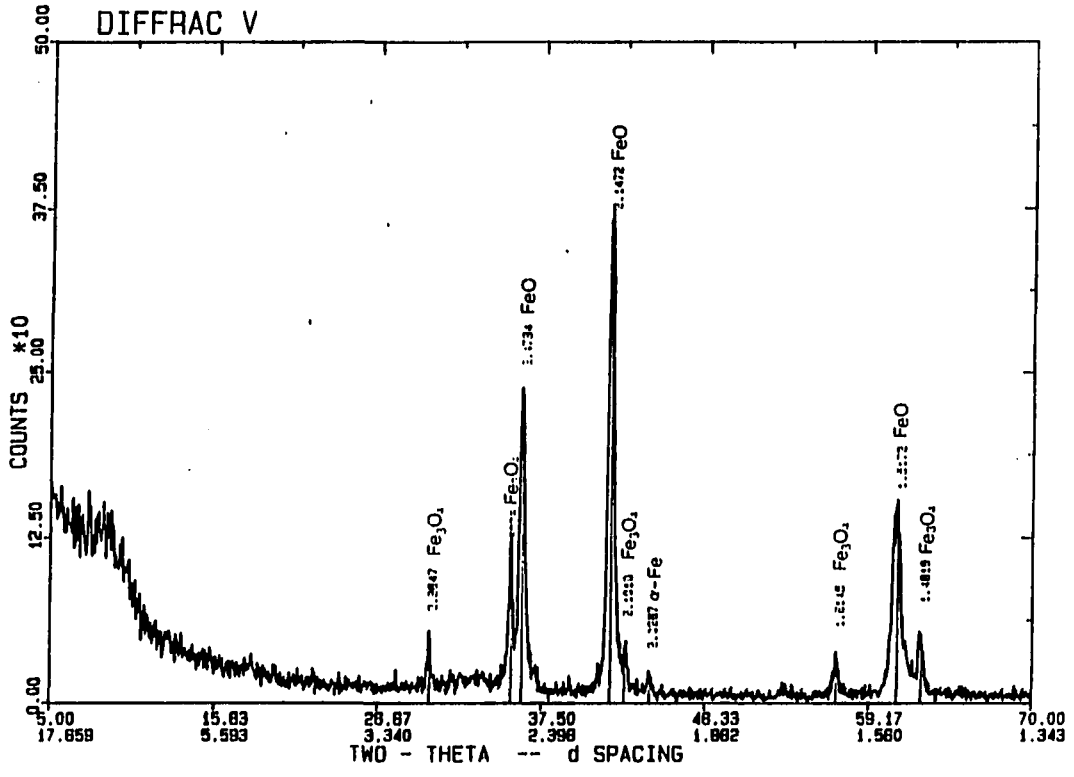


Figure 23. XRD analysis of combustion droplets
(material: AISI 1020)

From equation (9), we calculate

$$M_{sh} = 0.18 - 0.33 \text{ gm/sec}$$

If we subtract the oxygen weight in the iron oxide from the calculated weight loss, the material removal rate due to shearing is in the range 0.14 to 0.26 gm/sec. The present cutting experiment indicated that for a laser power of 1.0 kW and 6.35 mm thick carbon steel the cutting speed is approximately 29.6 mm/sec (70 in/min). The corresponding weight loss was 0.41 gm/sec. The difference in material removal rate could be compensated by considering the effect of gas momentum transfer (gas pressure gradient) which is of the same order of magnitude as gas shearing (Vicanet et al., 1986).

Schuocker (1988) reported that the velocity of ejected droplets can be formulated as:

$$V_e = \sqrt{\frac{\mu_s \tau V}{\rho_e \delta w}}$$

From mass balance (equation (14)), we calculate (F = 0.777, $\rho_w = 0.0078$ gm·mm$^{-3}$)

$$v = 10.9 \text{ mm/sec}$$

Which equals 0.15 gm/sec of weight loss. The sum of the material removal rates due to gas shearing and momentum transfer is approximately equivalent to the weight loss in laser cutting experiment.

## 5.2 Dual gas-jet assisted laser cutting

The film thickness in dual gas-jet laser cutting of stainless steel remains to be determined. For simplicity, the film thickness in the coaxial gas-jet laser cutting of carbon steel under similar process condition is used. The combustion droplets in the dual gas-jet laser cutting of stainless steel are mainly $FeCr_2O_4$, which results in a value of 0.714 for the parameter F. The following material constants are used.

| | | |
|---|---|---|
| $\rho_e$ | = | 0.005 gm·mm$^{-3}$ |
| $\delta$ | = | 0.1 mm (estimated) |
| $\mu_g$ | = | 7.3 x 10$^{-5}$ gm·mm$^{-1}$·s$^{-1}$ |
| $V_{off}$ | = | 4.4 x 10$^5$ mm·s$^{-1}$ |
| F | = | 0.714 |
| l | = | 6.35 mm |
| w | = | 0.28 mm |
| $\rho_w$ | = | 0.008 gm·mm$^{-3}$ |

From equation (17),

v = 8.5 mm/sec (20 in/min)

The experimental cutting speed is 12.7 mm/sec (30 in/min). Underestimation of machining speed using this model may be explained as follows:

1. The film may be thicker in the dual gas-jet laser cutting of stainless steel. However, this hypothesis needs further investigation.
2. The model neglected vaporization of the workpiece (equation (14)). If loss of material due to vaporization is considered, the machining speed may increase accordingly.
3. The gas shearing effect was not considered due to the unknown viscosity of iron chromite in literature. If this was included in the analysis, the machining speed could be enhanced.

# 6. CONCLUSIONS

1. The use of an off-axial nozzle combined with a coaxial gas nozzle has been demonstrated to be effective in the laser machining 6.35 mm (1/4 in.) thick low carbon stainless steel and superalloy plates. The adherent dross and the poor edge quality (problems associated with conventional laser cutting of stainless steels) are eliminated by this technique.
2. The effectiveness of dual gas-jet laser cutting of stainless steel is attributed to momentum transfer and the absence of $Cr_2O_3$ formation due to the additional off-axial oxygen-jet. These conclusions are substantiated through our model and the associated XRD analysis of dross/droplet material.
3. The poor cutting performance of high carbon stainless steels (440A and 440C) was explained by the reduction of FeO by carbon and by the shift from liquid phase to $Cr_2O_3$ + liquid phase of the melt film in the erosion cutting front.
4. The optimal process condition for the current experimental conditions with respect to surface finish was determined. It is found that a minimum of side-jet nozzle diameter (1.5 mm) and a minimum reservoir pressure (0.31 MPa) are required to effectively remove dross.
5. The fluid-dynamics model of material removal provides good correlation between theoretical and experimental data.

## REFERENCES

Arata, Y., "New Laser-Gas-Cutting Technique for Stainless Steel," Plasma, Electron & Laser Beam Technology, American Society for Metals, 1986, pp. 526-536.

Arata, Y., Maruo, H., Miyamoto, I. and Takeuchi, S., "Dynamic Behavior in Laser Gas Cutting of Mild Steel," Trans. J.W.R.I. Vol. 8, No. 2, 1979, pp. 15-26.

Chryssolouris, G. and Choi, W. C., "Gas Jet Effects on Laser Cutting," Proc. of SPIE, Vol. 1042, $CO_2$ Lasers and Applications, 1989, pp. 86-96.

Curle, N. and Davis, H. J., Modern Fluid Dynamics, Vol. 2, Van Nostrand Reinhold Company, 1971, London, pp. 259-260.

Esposito, C. and Daurelio, G., "Tuning of a Parametric Model for the Laser Cutting of Steels," Optics and Lasers in Engineering, Vol. 2, 1981, pp. 161-171.

Fieret, J., Terry, M. J., Ward, B. A., "Overview of Flow Dynamics in Gas-assisted Laser Cutting," Proc. of SPIE, Vol. 801, High Power Lasers, 1987, pp. 243-250.

Fieret, J. and Ward, B. A., "Circular and Non-circular Nozzle Exits for Supersonic Gas Jet Assist in $CO_2$ Laser Cutting," Proc. of 3rd Int. Conf. on Lasers in Manufacturing, June 1986, Paris, France.

Jacob, K. T. and Alcock, C. B., "The Oxygen Potential of the Systems Fe + $FeCr_2O_4$ + $Cr_2O_3$ and Fe + $FeCr_2O_4$ + $V_2O_3$ in the Temperature range 750 -1600 $^0C$," Metallurgical Trans. B, Vol. 6B, June 1975, PP. 215-221.

Levin, E. M., Robbins, C. R. and McMurdie, H. F., Phase Diagrams for Ceramists 1969 Supplement, Edited by Reser, M. K., The American Ceramic Society, Columbus, Ohio, 1969.

Meyer, H. W., Porter, W. F., Smith, G. C. and Szekely, J., "Slag-Metal Emulsions and Their Importance in BOF Steelmaking," Journal of Metals, Vol. 20, 1968, pp. 35-42.

Moses, A. J., The Practicing Scientist's Handbook, Van Nostrand Reinhood Company, New York, 1978, pp. 45-54.

Nielsen, S. E., "Laser Cutting with High Pressure Cutting Gases and Mixed Gases," Proc. of 3rd Int. Conf. on Lasers in Manufacturing, June 1986, Paris, France, pp. 25-

Proc. of 3rd Int. Conf. on Lasers in Manufacturing, June 1986, Paris, France, pp. 25-44.

Rosenqvist, T., Principles of Extractive Metallurgy, McGraw-Hill, Inc., New York, 1974.

Schuocker, D., "Heat Conduction and Mass Transfer in Laser Cutting," Proc. of SPIE, Vol. 952, Laser Technologies in Industry, 1988, pp. 392-599.

Schulz, W., Simon, G. Vicanek, M., "Influence of the Oxidation Process in Laser Gas Cutting," Proc. of SPIE, Vol. 801, High Power Lasers, 1987, pp. 331-336.

Vicanek, M. and Simon, G., "Momentum and Heat Transfer of an Inert Gas Jet to the Melt in Laser Cutting," Journal of Physics D: Applied Physics, Vol. 20, 1987, pp. 1991-1996.

Vicanek, M., Simon, G., Urbassek, H. M. and Decker, I., "Hydrodynamical Instability of Melt Flow in Laser Cutting," Journal of Physics D: Applied Physics, Vol. 20, 1986, pp. 140-145.

Szekely, J. and Themelis, N. J., Rate Phenomena in Process Metallurgy, Chap. 20, John Wiley & Sons, Inc., New York, 1971.

Schuocker, D., "Dynamic Phenomena in Laser Cutting and Cut Quality," Applied Physics, B40, 1986, pp. 9-14.

# PAPER III: LASER MACHINING OF EGG SHELLS

## ABSTRACT

Preparation of chicken embryo allantoic fluids for animal health requires opening the egg shell usually by a cutting, drilling or punching method. These methods are conventionally accomplished by thermal and mechanical techniques. In this study, a laser machining method is described as an alternative to these processes. Both $CO_2$ and Nd:YAG lasers were employed. A focused $CO_2$ laser beam at a power of 200 watts in conjunction with an X–Y motion table produced 25 mm diameter "clean–cuts" in egg shells for a cutting time of 0.5 sec per egg. The material removal mechanism was vaporization. When an axicon/lens combination was used with a $CO_2$ laser, the cutting time was further reduced to 0.2 sec per egg and the mechanism of material removal was changed from vaporization to decomposition of the egg shell into fine powders. Small holes, (typical diameters 0.5 mm to 1 mm), were generated on the egg shell using the pulsed Nd:YAG laser. However, the Nd:YAG laser was very inefficient compared to the $CO_2$ laser due to the poor absorption of the 1.06 micron wavelength light by the egg shell. A simple energy balance model was able to predict the experimental results successfully.

# 1. INTRODUCTION

Biological industries that produce chicken embryo allantoic fluid from eggs require drilling or punching holes on the top of egg (for inoculation) and removal of the top of the egg (for pouring the fluid into a container or removal of the embryo). Traditionally, holes are drilled on the top of the egg by a mechanical method using a dental drill. The holes may also be punched by using hard stainless steel needles. The cuts are made by a thermal process which involves two steps: punch a hole on the egg top and then place and rotate a propane torch burner over the end of the egg. During mechanical drilling and punching, the forces acting on the tool and on the egg may cause fracture of the egg if the process is not carefully controlled. In addition, the problem of sterility of the drill requires the application of antiseptic fluid. Thermal cutting with the propane torch causes strong heating of the egg shell, generates thermal stresses and, if not controlled properly, results in destruction of the egg. In fact, the rationale for punching a hole prior to propane torch cutting is to eliminate the stresses caused by gas pressure increase inside the egg due to the heating process. Both the mechanical and flame processes have several drawbacks including: sterility, long production time, poor cut quality and high scrap rate.

An alternative to mechanical drilling or punching and propane torch cutting of egg shell is laser machining. Lasers are used for conventional and exotic applications because of their unique properties — namely, high energy density, monochromaticity and directionality. In addition, the ease of interfacing lasers with computer numerical controls and/or robots allows efficient and cost effective production (Belforte, 1992). A tightly focused laser beam, due to its high intensity, is capable of melting and evaporating materials with the added benefits of low overall heat transfer, non–contact with the workpiece, high cutting speed and good cut quality. In this study, details are given of the laser–egg shell interactions, type of laser, energy intensity and material removal mechanisms for the efficient machining of egg shell.

## 2. CHOICE OF LASERS AND LASER–EGG SHELL INTERACTIONS

In order to fully understand the laser machining aspects of egg shells, it is important to describe the types of lasers used, identify the composition and structure of the egg shell and study the egg shell interaction with the laser beam.

For machining, two types of lasers are currently used: the $CO_2$ laser, an electrically pumped gas laser that radiates light with a wavelength of 10.6 microns; and the Nd:YAG laser, an optically pumped solid–state laser, that produces light with a wavelength of 1.06 micron. The key characteristics of lasers for machining are: power, wavelength, beam quality, and efficiency. $CO_2$ lasers are more powerful in a continuous wave mode than YAG lasers. However, YAG lasers can be operated at high powers in a pulsed mode and can be focused to smaller spot sizes due to their shorter wavelength. $CO_2$ lasers exhibit better beam quality, in terms of $TEM_{00}$ mode and temporal coherence, compared to YAG lasers. $CO_2$ lasers are also more efficient than YAG lasers (due to the poor thermal conductivity of YAG crystals) in converting input energy into output laser energy. An advantage of the YAG over the $CO_2$ laser is (this is relevant to automation of egg shell machining) that the YAG beam can be transmitted through the quartz fibers. In general, the YAG and $CO_2$ lasers can be used for hole drilling and cutting respectively.

According to the detailed pioneering studies of egg shell structures by Nathusius whose findings have been published by Tyler (1969), and by Simons and Wiertz (1970) who used electron microscopes for characterization, the shell consists of four distinct layers as shown in Figure 1. The outermost layer, called a cuticle, is composed of spheres of organic material with sphere sizes of up to 1 micron in diameter. The total thickness of this layer is about 10 microns. The composition of cuticle was found to be about 90% protein and 10% carbohydrate (Baker and Balch, 1962). In addition, it may contain some fat and ash up to 5% ( Wedral et al., 1974). Scanning electron microscope has been used to show that the cuticle is highly fissured, dense, and free from pores as shown in Figure 2.

The second layer, called palisade (also called the true shell), constitutes the major portion of egg shell. This layer is about 200 microns thick and consists of calcium carbonate in the form of calcite laid down on an organic matrix (2% by weight of the true shell). The crystal

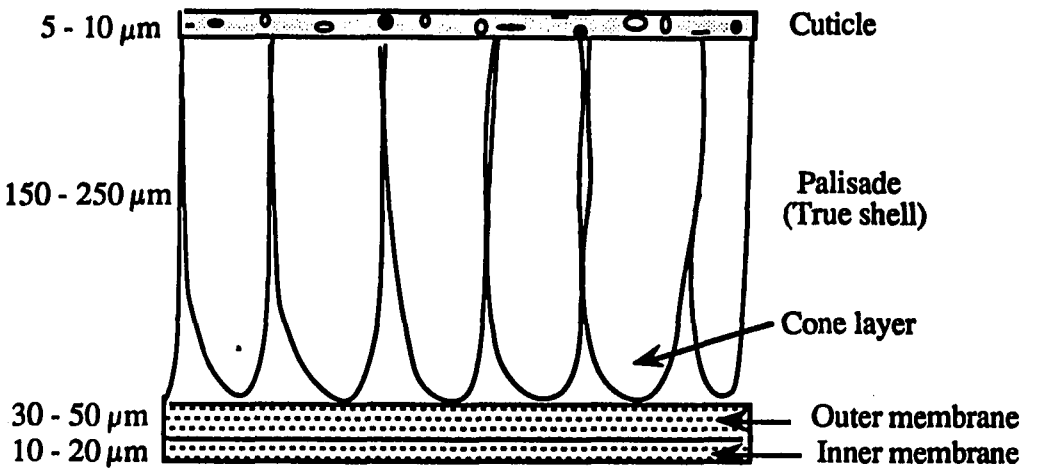


Figure 1. Schematic structure of egg shell as shown by a section through the thickness

Figure 2. Scanning electron micrograph showing the structure of cuticle

columns run perpendicular to the shell surfaces shown in Figures 1. There exists also a cone layer, called as mammillary core, which consists of organic matter and represents seeding sites on which the true shell has crystallized.

The third layer, the outer membrane, is irregular and contains the bases of the mammillary layer. This layer is typically about 40 microns thick. The fourth layer is the inner membrane which is much thinner (10–20 microns) and denser than the outer one. Both membranes consist of a network of fibers lying parallel to the shell surface and are made up of 95% protein, 2% carbohydrate and 3% fat.

The chemical and mineralogical composition of the egg shell is complex and varied. When light interacts with an egg shell, certain wavelengths are preferentially absorbed. Several different processes cause absorption of light and include: electronic, vibrational and rotational transitions in molecules and molecular ions. Figure 3, the absorption spectrum of egg shells produced in the near infrared (IR) region (Gaffey, 1990), clearly indicates that reflectance is a major problem in egg shell machining when 1 micron wavelength lasers such as Nd:YAG are used. The absorption spectra of proteins also confirms that the maximum reflectivity in an egg shell may occur near the 1 micron wavelength. In contrast, both organics and calcite exhibit an absorption of nearly 90% or better at a wavelength of 10.6 micron characteristic of $CO_2$ laser (Kodama, 1985).

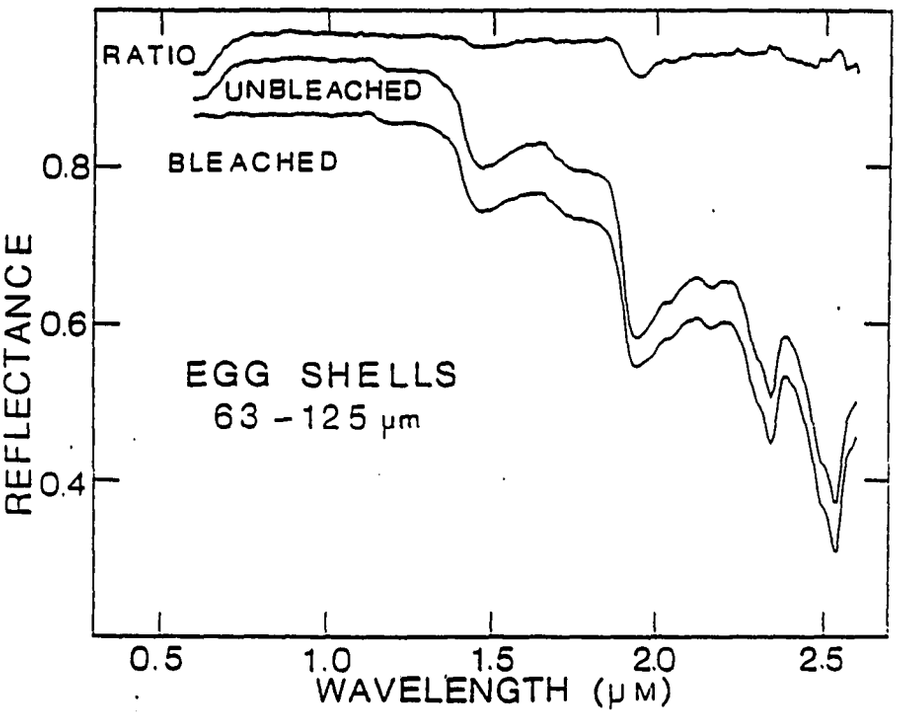


Figure 3. Absorption spectrum of egg shells in the near infrared region

## 3. EXPERIMENTAL DETAILS

Both $CO_2$ and Nd:YAG lasers were employed for machining the egg shell. The beam energy distribution for both lasers was nearly Gaussian. Table 1 provides the data concerning the laser parameters. No assist gas was used. For hole drilling, only the YAG laser was used and the beam was transmitted through quartz fibers onto the egg shell. For cutting, two different procedures were used, namely, conventional laser cutting and axicon-lens combination.

### 3.1 Conventional laser cutting

This procedure involved a stationary focused laser beam and a moving egg. The eggs were mounted on an X–Y table which in turn was moved by a computer numerical controller (CNC) at speeds from 25 mm/min (10 in/min) to 1250 mm/min (500 in/min). The laser beam was focused on the egg shell through a planoconvex lens.

### 3.2 Axicon–Lens laser cutting

This method used a stationary 12.7 mm (0.5 in.) diameter ring beam (obtained through axicon–lens combination) and a stationary egg. Axicon is an optic that is capable of bending the light rays from a point source into a continuous line of points by reflection or refraction or both. This is illustrated in Figure 4 where the rays from a collimated laser beam are bent by a divergent axicon in combination with a planoconvex lens to form a ring–shaped image. In this work, a 127 mm (5 in.) focal length ZnSe lens in conjunction with a 2° axicon ZnSe was used to generate a 12.7 mm (0.5 in.) diameter ring of a $CO_2$ laser beam. The width of the ring was estimated as 0.17 mm on the basis of the diffraction equation given by $w = 1.22\ FC/fE$ where F = focal length of lens, C = velocity of light, f = frequency of laser beam, and E = radius of laser beam. Laser power as a function of cutting time was also studied.

Table 1. Laser types and parameters used in this work

| Laser Type | $CO_2$ | Nd:YAG | Nd:YAG |
|---|---|---|---|
| Wavelength, micron | 10.6 | 1.06 | 1.06 |
| Mode | CW | CW | Pulsed |
| Power, watts | 200 | 100 | 400 (average) |
| Focused beam size, mm | 0.25 | 1 mm | 0.1 mm and 1 mm |
| Beam through optical fiber | No | Yes | Yes |

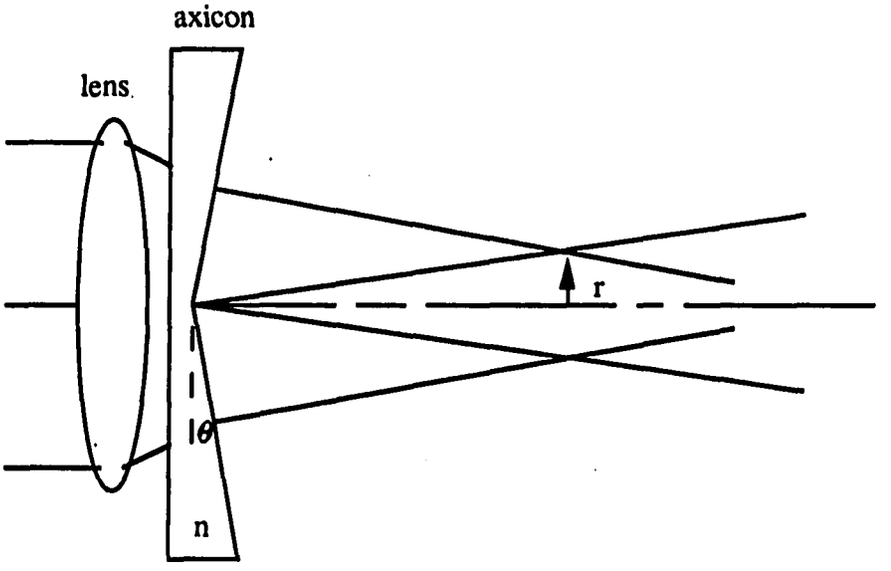


Figure 4. Ring formation produced by a combination of lens and axicon (The radius of the ring is given by: $r = (n-1)\theta F$ where n = refractive index, $\theta$ = axicon angle, and F = focal length of lens)

# 4. RESULTS AND DISCUSSION

## 4.1. Conventional laser machining

Although the Nd:YAG laser operated in a continuous wave mode at a power level of 100 watts (intensity = 80,000 W/cm$^2$), it was not capable of cutting through the egg top. When the beam was transmitted through the fiber, burning of the fiber tip was experienced and no penetration or cutting on the eggshell was observed. This confirms the poor absorptivity of the YAG laser wavelength by the egg shell. Increasing the power level to 400 watts (8 Joules, 50 pps), changing from continuous wave to pulsed mode (1 msec pulses), and focusing the beam through a 75 mm (3 in.) lens to a spot size of 0.1 mm (intensity = 5 x $10^6$ W/cm$^2$) allowed the YAG beam to cut the egg shell at a rate of 50 mm/min (20 in/min).

In contrast to the YAG laser, the $CO_2$ laser at a power of 200 watts in the continuous wave mode was able to cut through the top of egg at a speed of 1000 mm/min (400 in/min) when focused through a 127 mm (5 in.) lens for a spot size of 0.25 mm (intensity = 0.4 x $10^6$ W/cm$^2$). This demonstrates the increased absorption of $CO_2$ light by the egg shell. The time required for cutting a 25 mm (1 in.) diameter hole on the egg shell was about 0.4 sec which is much less (2.5 times less) than the propane torch cutting method currently used (1 sec/egg). Figures 5a shows the transverse section of the laser cut as compared to a mechanically fractured egg shell (Figure 5b). The high density of cracks in the laser–cut surface is attributed to thermal stresses occurring during the cutting process.

The holes required on the top of the egg for injecting the virus fluid are in the range of 1–2 mm in diameter. Since the pulsed laser is most appropriate for drilling, experiments with the pulsed YAG laser were conducted to produce holes on the egg shell. The optimum process parmeters were: 400 watts (8 J/msec, 50 pps, 1 msec pulse, 10–15 pulses, focused through 75 mm (3 in.) lens to a spot size 0.1mm and subsequently through fiberoptics). The holes were clean and free of debris as shown in Figure 6.

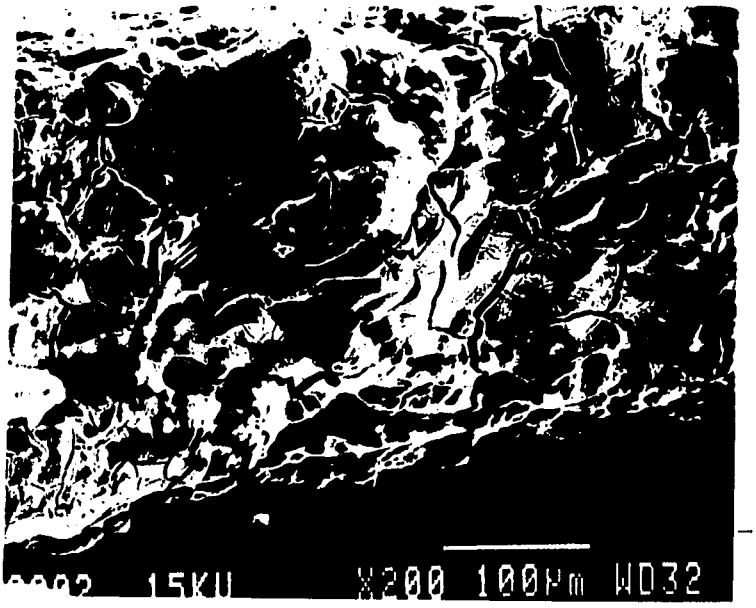


(a)


(b)

Figure 5. Transverse sections of egg shell
(a) laser-cut (b) mechanically fractured

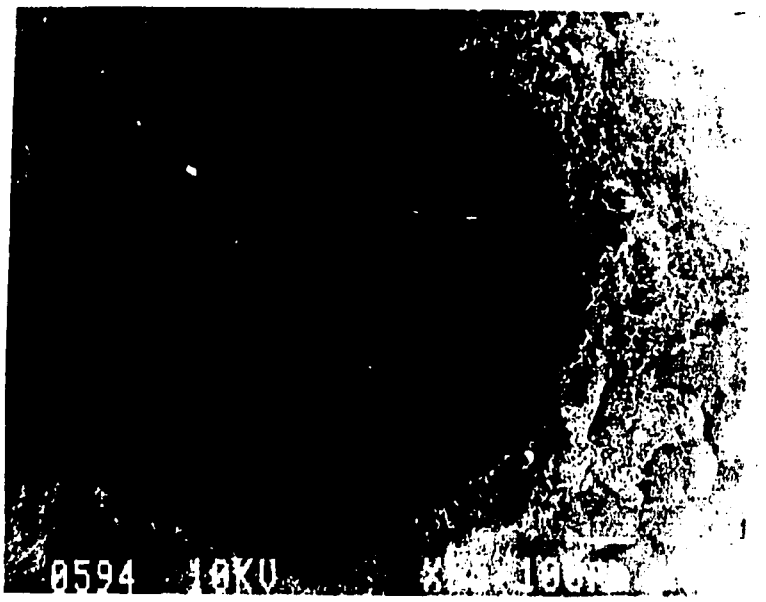


Figure 6. Photogragh showing a laser drilled hole in an egg shell

Laser cutting with a 200 watt $CO_2$ laser beam in conjunction with a X–Y motion table offer the following benefits for egg cutting:

- o Non–contact process (important from sterility point of view)
- o No need to punch a pressure relief hole prior to cutting
- o All the shell material is evaporated
- o Precise size control and hole diameter
- o Short cutting time compared to propane torch technique
- o Suitable for automation

## 4.2. Axicon–lens combination laser cutting

$CO_2$ laser cutting experiments with the lens–axicon doublet showed that a power of 200 watts was sufficient to cut a 12.7 mm diameter hole at the top of the egg (intensity = 3000 $W/cm^2$) in a time of 0.2 sec. The material removal mechanism in this method involved the decomposition of calcite into CaO powders leading to the separation of the egg top. Figure 7 shows a photograph of laser cutting while Figure 8 shows the cut appearance where CaO powders were identified as the predominant solid phase along the width of the cut hole as shown by the X–ray diffraction pattern in Figure 9. This procedure is quite different from that of conventional laser cutting where evaporation is the dominant cutting mechanism.

The benefits of axicon–lens method are:

- o Holes may be cut in the top of an egg without moving the laser beam or the egg
- o The time required is half that required when using a focused beam

Figure 7. Photograph showing laser cutting with an axicon-lens doublet

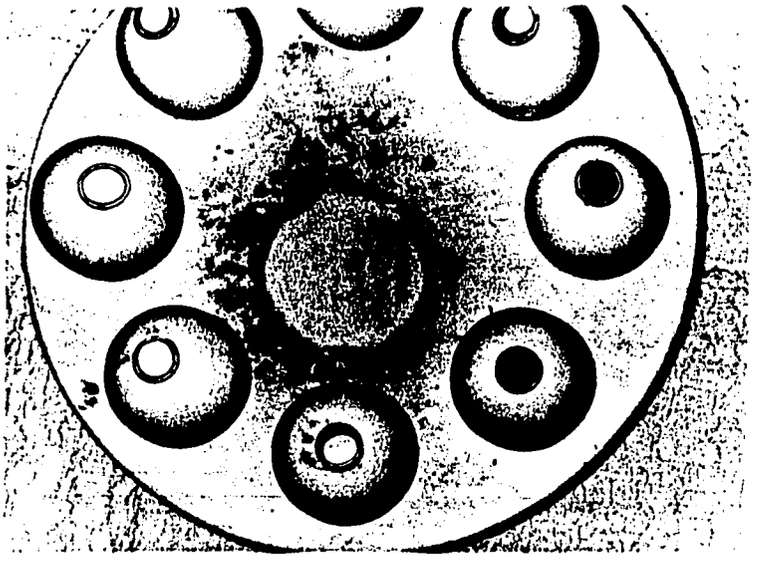

Figure 8. Photograph of laser-cut eggs showing the kerf zone

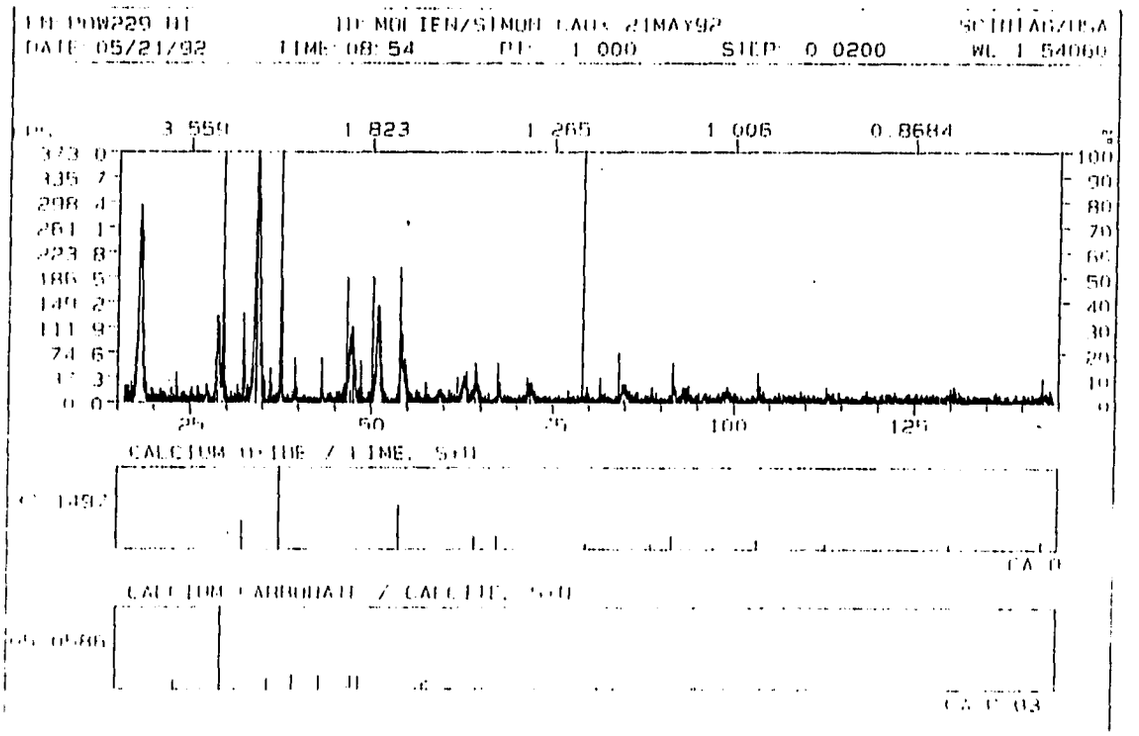


Figure 9. X-ray diffraction pattern of laser decomposed egg shell powders

## 4.3. Modeling

Several heat energy flow and energy balance models are available to predict the laser cutting process. Here we considered an energy balance model to verify the observed experimental results because the egg shell, being a mixture of ceramic and organic materials, decomposes or evaporates when irradiated with the laser beam. The following assumptions were made in this analysis:

1. The egg shell is made of 100% calcite
2. Thermal conduction, convection and radiation are negligible away from the cutting site.
3. Absorptivity of the egg shell is 0.9 for a $CO_2$ laser and 0.05 for a YAG laser
4. The energy released from the decomposition of calcite is taken into account.
   The decomposition of calcite at about 800 °C proceeds as follows,
   $CaCO_3$ ——> $CaO + CO_2$
   Heat of reaction (H) = 43.8 kcal/mole (1831.6 J/gm)
5. There is uniform heating of the egg shell without any lateral heat loss
6. The laser is a constant power source

According to the energy balance model,

Absorbed laser energy = Energy for temperature rise + Decomposition energy + Heat of fusion + Heat of vaporization of the egg shell

$$(A \cdot P \cdot w)/v = M[C_p (T_v - T_a) + H + L_f + L_v] \qquad (1)$$

The mass removed, M, is calculated as follows,

$$M = \rho ( 0.785 \cdot w^2) \, (l)$$

where $\rho$ = density of egg shell, gm/mm$^3$

$l$ = egg shell thickness, mm

The thermal properties of $CaCO_3$ and CaO are given in Table 2 (Moses, 1978, Weast, 1987, and Kulikov, 1967).

Table 2. Selected properties of CaO and $CaCO_3$

| | CaO | $CaCO_3$ |
|---|---|---|
| Density, gm/mm$^3$ | 3.3 | 2.93 |
| Specific heat, Cal/mole K | 27.8 | 12.8 |
| Melting temp., K | 2843 | – |
| Heat of fusion, J/gm | 913 | – |
| Vaporization temp., K | 3123 | – |
| Heat of vaporization, J/gm | 10,230 | – |

The results of using this simple model are given in Table 3 for individual cases. The predicted results are in excellent agreement with the experimental data. The thickness of egg shell was measured to be 0.25 mm (see Figure 5b).

Table 3. Experimental and theoretical data

| Machining Procedure | Experimental (Cutting speed or time) | Predicted |
|---|---|---|
| 1. $CO_2$ laser cutting using a focused beam (w = 0.2 mm, P = 200 watts) | 169.3 mm/s (400 in/min) | 152.4 mm/s (360 in/min) |
| 2. Nd:YAG laser cutting using a focused beam (w = 1 mm, P = 400 watts) | 8.5 mm/s (20 in/min) | 8.63 mm/s (20.4 in/min) |
| 3. Nd:YAG drilling (Hole dia. = 1mm, P = 400 watts) | 15 pulses | 14 pulses |
| 4. Axicon–lens $CO_2$ laser cutting (w = 0.4 mm, P = 200 watts) | 0.20 sec | 0.18 sec |

# 5. CONCLUSIONS

An experimental study coupled with an energy balance model of the laser machining of egg shells has demonstrated the potential of the $CO_2$ laser for obtaining high quality cuts and holes at high speeds. Laser machining provides significant benefits for egg shells over the existing thermal and mechanical methods currently used in industry.

## REFERENCES

Belforte, D and Morris, A, The Industrial Laser Annual Handbook, Pennwell Publishing, Tulsa, Oklahoma, 1992.

Tyler, C., "Avian Egg Shells: Their Structure and Characteristics," International Review of General and Experimental Zoology, Vol. 4, 1969, pp. 81–130.

Simons, P.C.M., and Wiertz, G., "Notes on the Structure of Shell and Membranes of the Hen's Egg: A Study with the Scanning Electron Microscope," Annales de Biologie Animale, Biochimie et Biophysique, Vol. 10, 1970, pp. 31–49.

Baker, J.R. and Balch, D.A., "A Study of Organic Material of Hen's Egg Shell," Biochemical Journal, Vol. 82, 1962, pp. 352–361.

Wedral E.M., Vadehra, D.V. and Baker, R.C.,"Chemical Composition of the Cuticle and Inner and Outer Membranes from Egg," Comparative Biochemistry and Physilogy, Vol. 47B, 1974, pp. 631–640.

Gaffey, S.J.,"Skeletal Versus Nonbiogenic Carbonates," Chapter 5 in Spectroscopic Characterization of Minerals and Their Surfaces, (eds.) L.M. Coyne, S. McKeever, and D.F. Blake, American Chemical Society, Washington D.C., 1990.

Kodama, H.,"Infrared Spectra of Minerals," Chemistry and Biology Research Institute, Research branch, Agriculture, Canada, 1985.

Rioux M., Tremblay, R. and Belanger, P., "Linear, Annular, and Radial Focusing with Axicons and Applications to Laser Machining," Applied Optics, Vol. 17, No.10, 1978, pp. 1532–1536.

Moses, A.J., The Practicing Scientist's Handbook, Van Nostrand Reinhold Company, New York, 1978.

Weast, R.C., CRC Handbook of Chemistry and Physics, CRC Press Inc, Florida, 67 th edition, 1987, pp. B–216.

Kulikov, I.S., Thermal dissociation of Chemical Compounds, Israel Program for Scientific Translations, Jerusalem, 1967, pp. 41.

# PAPER IV: ENHANCEMENT OF SURFACE FINISH IN LASER CUTTING OF METAL MATRIX COMPOSITES USING DUAL GAS-JETS

## ABSTRACT

An innovative laser cutting technique which employs two oxygen gas-jets (coaxis and off-axis respectively) was developed to cut 6.35 mm (1/4 in.) thick $SiC_p$/Al and $B_4C_p$/Al metal matrix composites. Under the same processing conditions, the traditional (coaxis gas-jet only) laser cutting method resulted in poor surface finish and slag adherence, which were eliminated in the dual gas-jet laser cutting technique. Correlations between volume fraction of carbide reinforcement and surface finish in terms of oxide formation and melt fluidity at the erosion cutting front were discussed. High absorptivity of the laser energy, gas momentum transfer due to the off-axial jet, and dilution effect from the oxidation of carbide reinforcement were attributed to the effectiveness of this new laser cutting technique for metal matrix composite materials.

# 1. INTRODUCTION

Current design requirements are continually driving the development of new materials which possess high strength/stiffness to weight ratio, good corrosion/wear resistance and low cost. Metal matrix composites (MMC) such as carbide-particulate-reinforced aluminum composites meet these demands and offer additional advantages like isotropic mechanical properties, superior dimensional stability, and easy fabrication (Maclean and Misra, 1983; Harrigan, 1991; Gilman, 1991). However, machining of MMC is difficult and results in rapid tool wear due to the abrasive carbide particulates. Polycrystalline diamond (PCD) was suggested as a tool material to machine these composites (Vaccari, 1991; Schreiber, 1991).

Non-traditional machining methods are becoming popular for MMCs because it is possible to machine complex-shaped parts without tool wear at high speed. Savrun and Taya (1988) reported that abrasive waterjet machining (AWM) of 6.3 mm thick 25 vol% $SiC_w$/2124 Al MMC and 7.5 vol% $SiC_w/Al_2O_3$ ceramic matrix composite yielded relatively smooth surface with minimum surface damage. Later, Hamatani and Ramulu (1990) investigated the relationships between cutting rate, abrasive particle size, kerf taper ratio, nozzle stand-off distance, and surface finish in abrasive waterjet cutting of 5.08 mm thick 30 vol% $SiC_p$/6061 Al and 6.25 mm thick 20 vol% $TiB_{2p}$/SiC composites. It was found that $SiC_p$/Al composite could be easily machined by AWM and the orthogonal accuracy (taper ratio) of the cut surface seems to be better at slow cutting conditions. Ramulu and Taya (1989) studied the machinability of 6.3 mm thick 15% vol. and 25% vol. $SiC_w$/2124 Al composites by electro-discharge machining (EDM). It was concluded that the machining time increased as the content of carbide reinforcement increased and that EDM could cause severe surface damage and softening if the cutting speed was not properly controlled. Kagawa et al. (1986, 1989) used a $CO_2$ laser to cut 0.4 - 2 mm thick graphite fiber/Al and SiC fiber/Al composites of approximate 0.5 fiber volume fraction. It was summarized that for a given composite material, a critical energy density of incident laser beam was required for the cutting action to occur. Lee (1987) investigated the laser cutting performance of graphite fiber/Al and SiC fiber/Ti composites and compared the results to those obtained by abrasive waterjet and diamond saw cutting. Laser beam cutting was found to be the fastest

cutting method, but it tended to induce thermal cracking due to the high heat flux. This drawback could be possibly overcome if a pulsed laser beam combined with an optimal level of power were used.

Due to its unique processing characteristics such as non-contact thermal process, flexibility and ease for automation, laser cutting has been accepted as a productive and cost effective method in manufacturing sheet metal parts in many industries. However, Laser machining of aluminum composites inherits the following potential difficulties which include

(1) high reflectivity and thermal conductivity of aluminum
(2) formation of passive oxide ($Al_2O_3$) and preventing surface from further oxidation
(3) high melting point of $Al_2O_3$ and consequently high viscosity of the melt film (slag formation)
(4) differences in the thermal properties between the matrix and reinforcement material

In the present study, a dual gas-jet laser cutting technique aiming at achieving superior surface finish was developed and used to cut 6.35 mm (1/4 in.) $SiC_p$/Al and $B_4C_p$/Al composites. The effectiveness of this method compared with current traditional laser cutting method was also discussed.

## 2. EXPERIMENTAL PROCEDURE

SiC particulate-reinforced aluminum and $B_4C$ particulate-reinforced aluminum composite plates with a nominal thickness of 6.35 mm (1/4 in.) were cut by a Spectra-Physics Model 820 $CO_2$ laser. The compositions of the workpieces are given in Table 1. The average size of carbide particulate is between 10 - 15 microns. The $CO_2$ laser was operated at continuous wave (CW) mode and had a power output of 1200 watts. The beam had a nearly Gaussian ($TEM_{00}$) energy distribution. A nominal 127 mm (5 in.) ZnSe focusing lens was used to focus the laser beam on the surface of the workpiece. The reservoir pressure of the coaxial nozzle and off-axial nozzle were varied from 0.13 to 0.26 MPa (20 to 40 psi) and 0.21 to 0.55 MPa (30 to 80 psi), respectively. The nozzle stand-off was maintained at 0.7 to 1.0 mm (0.027 to 0.040 in.). The impinging angles of the off-axial jet were employed in the range $30^0$ to $40^0$. The workpiece was mounted on a computer numerically controlled worktable and cut in a linear movement. The off-axial nozzle was made of stainless steels with 1.5 mm (0.060 in.) inside diameter and set tandemly to the coaxial nozzle. The detailed experimental setup is illustrated in Figure 1. The cut surfaces were examined by a profilometer with a pilotor to measure the average surface roughness (Ra) and were ion sputtered with gold to minimize charging of carbides when scanning electron microscopy (SEM) was used to study the surface quality. The combustion droplets were analyzed by X-ray diffraction (XRD) to determine the compounds and compositions.

Table 1. Compositions of metal matrix composites used in the present study

| material \ element | reinforcement | matrix |
|---|---|---|
| SiC 20% vol./ 6061 Al | SiC | 6061 Al |
| SiC 40% vol./ 6061 Al | SiC | 6061 Al |
| $B_4C$ 50% vol./ 6061 Al | $B_4C$ | 6061 Al |
| SiC 70% vol., $Al_2O_3$ 20% vol./ 6061 Al | SiC $Al_2O_3$ | 6061 Al |

6061 Al: 1.0 wt.% Mg, 0.6 wt.% Si, 0.2 wt.% Cr, 0.27 wt.% Cu and Al balance

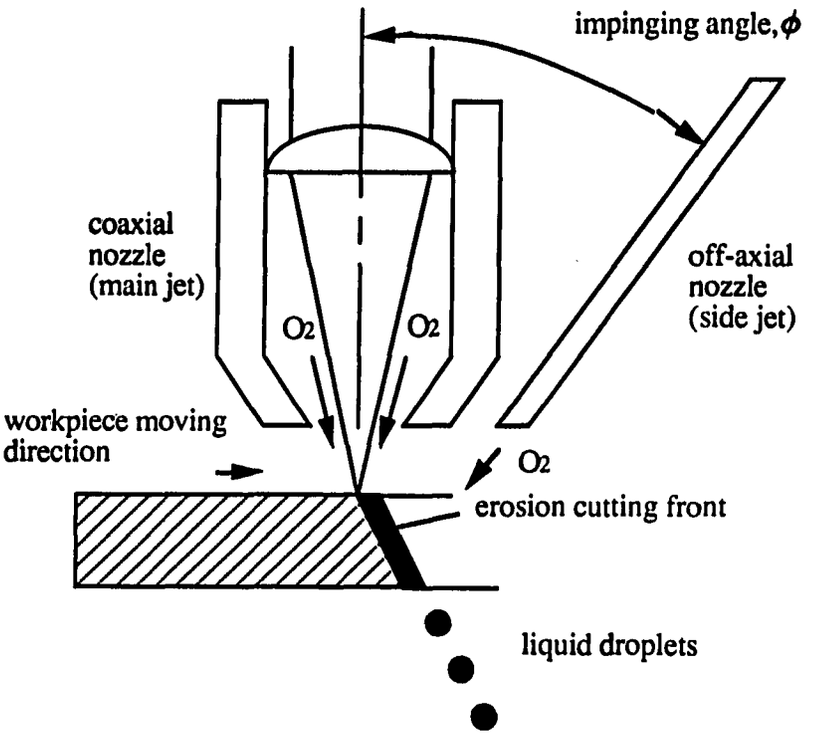


Figure 1. Schematic diagram of dual gas-jet laser cutting

## 3. RESULTS AND DISCUSSION

Due to the high relectivity and thermal conductivity of aluminum at 10.6 microns radiation wavelength, initiation of laser cutting on aluminum material could be difficult. As the surface heats up the reflectivity falls because of the change in the electronic structure of the workpiece (Ready, 1978), plasma formation of the vapor or gas breakdown (Shawlow, 1977), and surface oxidation (Duley, 1976). Figure 2 demonstrates the poor surface quality in the beginning of cutting of 6.35 mm (1/4 in.) thick 6061 Al and then to a better surface finish once the workpiece was heated up and oxidized. Compared Figure 3 with Figure 2, it can be noted that dual gas-jet laser cutting improved the surface quality especially at the bottom portion of the cut. Nevertheless, striations and significant amount of adherent dross were observed in both the traditional and dual gas-jet laser methods. Figures 4 and 5 show the laser-cut surfaces of 20% $SiC_p$/Al composite subjected to traditional and dual gas-jet cutting methods respectively. The cutting parameters were not necessarily optimized. The surface finish was improved as striations and crater-like pits were eliminated in the dual gas-jet laser technique. Figures 6 through 9 depict the drastic improvement on the surface finish of the 40% $SiC_p$/Al and 70% $SiC_p$ 20% $Al_2O_{3p}$/Al composites when the dual gas-jet laser cutting method was applied. Similar success was also obtained in dual gas-jet laser cutting of 50% $B_4C_p$/Al composite material (Figures 10 & 11). $B_4C_p$/Al composites were cut twice the speed of $SiC_p$/Al composites possibly due to the increased absorption of laser energy by $B_4C$, larger energy release during oxidation of $B_4C$, and easier volatilization of $B_2O_3$ (Vaporization temperatures for $B_2O_3$ and $SiO_2$ are 1860 °C and 2590 °C respectively). Table 2 lists the surface roughness (Ra) on the laser-cut surfaces perpendicular to the cutting direction. It can be concluded that the Ra measurements increased with the cutting depth and tended to decrease when SiC content was increased. The increasing surface roughness along the cutting depth was commonly observed in laser cutting of thick metallic materials and could be attributed to the unsteady motion of the melt (Arata,1979; Schuocker, 1986, Vicanet et al., 1986), turbulent gas flow and temperature fluctuation (Schuocker, 1986) and plasma blockage of the incoming laser beam (Shinada et al. 1980).


Figure 2. Coaxial gas-jet assisted laser cutting of 6061 Al (coaxis: 60 psi $O_2$, cutting rate: 1.7 mm/sec (4 in/min))

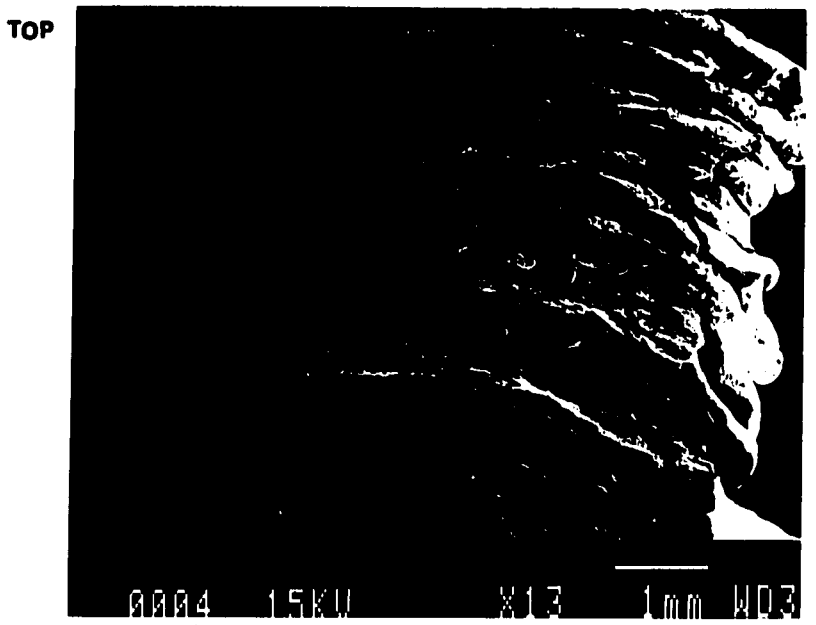


Figure 3. Dual gas-jet assisted laser cutting of 6061 Al
(coaxis: 20 psi $O_2$, off-axis: 60 psi $O_2$, cutting rate: 1.7 mm/sec (4 in/min))

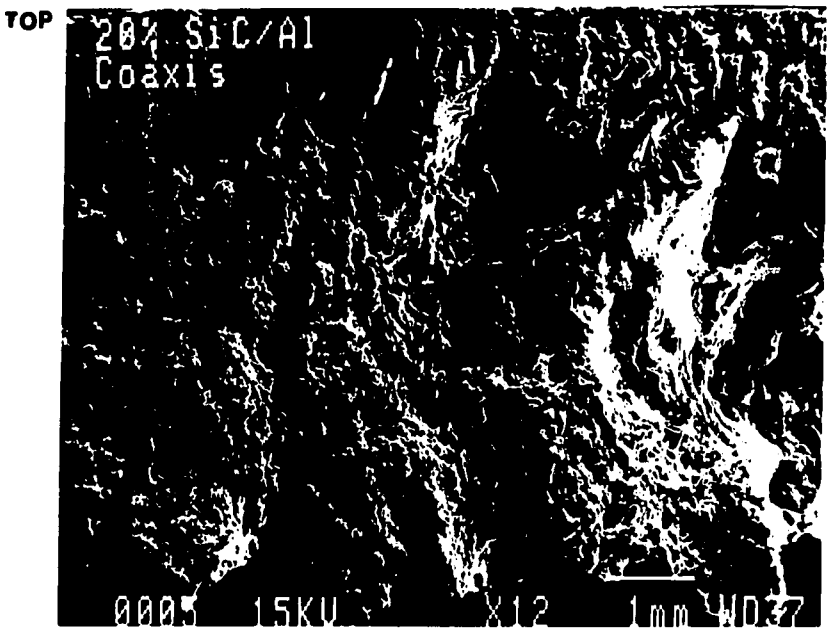


Figure 4. SEM of laser-cut surface using 60 psi coaxial gas-jet only
(material: 20% $SiC_p$/Al, cutting rate: 1.7 mm/sec (4 in/min))

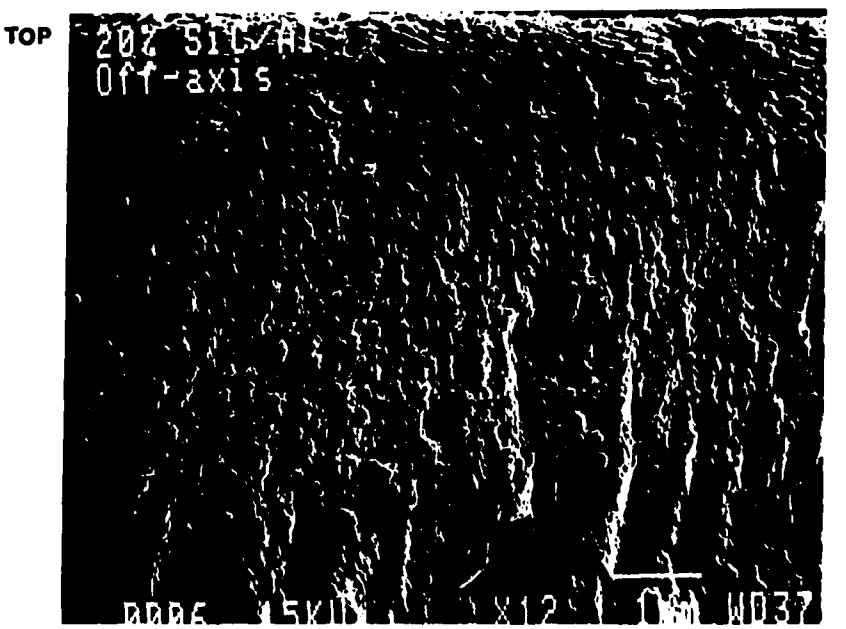


Figure 5. SEM of laser-cut surface using dual gas-jet
(coaxis: 20 psi $O_2$, off-axis: 60 psi $O_2$,
material: 20% $SiC_p$/Al, cutting rate: 1.7 mm/sec (4 in/min))

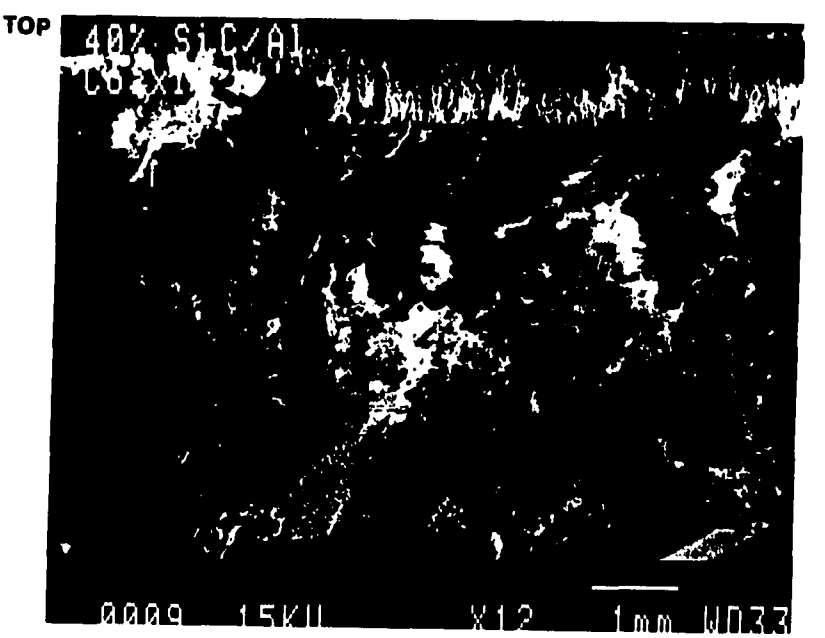


Figure 6. SEM of laser-cut surface using 60 psi coaxial gas-jet only
(material: 40% $SiC_p$/Al, cutting rate: 1.7 mm/sec (4 in/min))

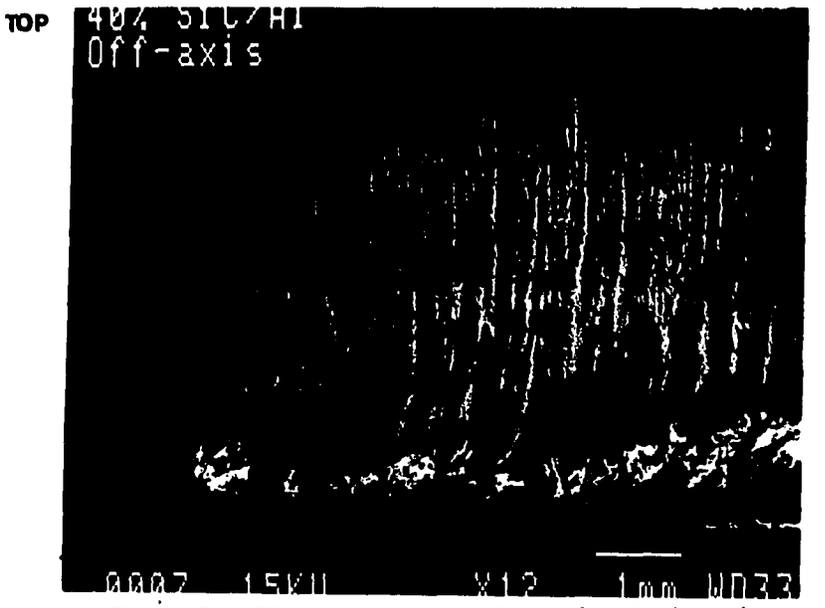


Figure 7. SEM of laser-cut surface using dual gas-jet
(coaxis: 20 psi $O_2$, off-axis: 60 psi $O_2$,
material: 40% $SiC_p$/Al, cutting rate: 1.7 mm/sec (4 in/min))

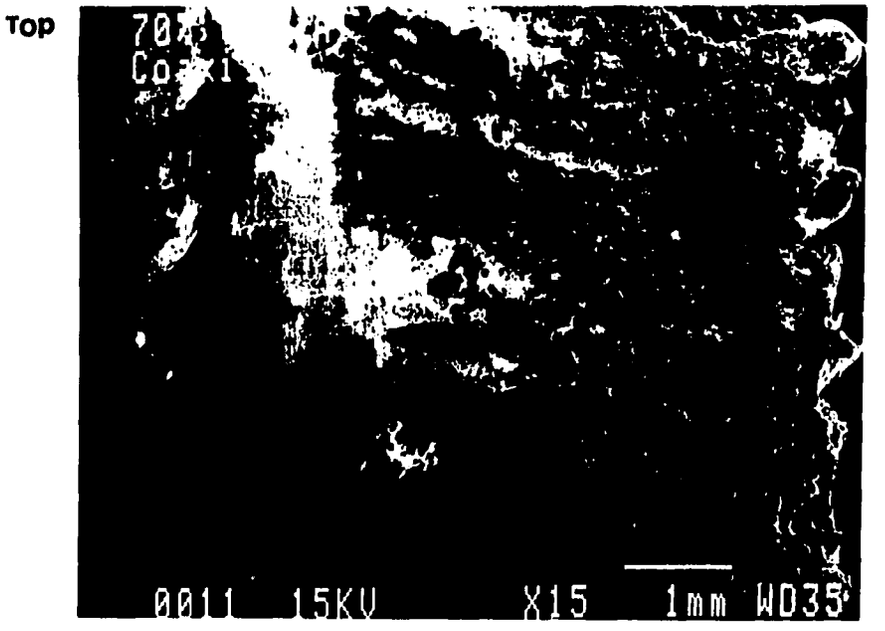


Figure 8. SEM of laser-cut surface using 60 psi coaxial gas-jet only
(material: 70% $SiC_p$/Al, cutting rate: 1.7 mm/sec (4 in/min))

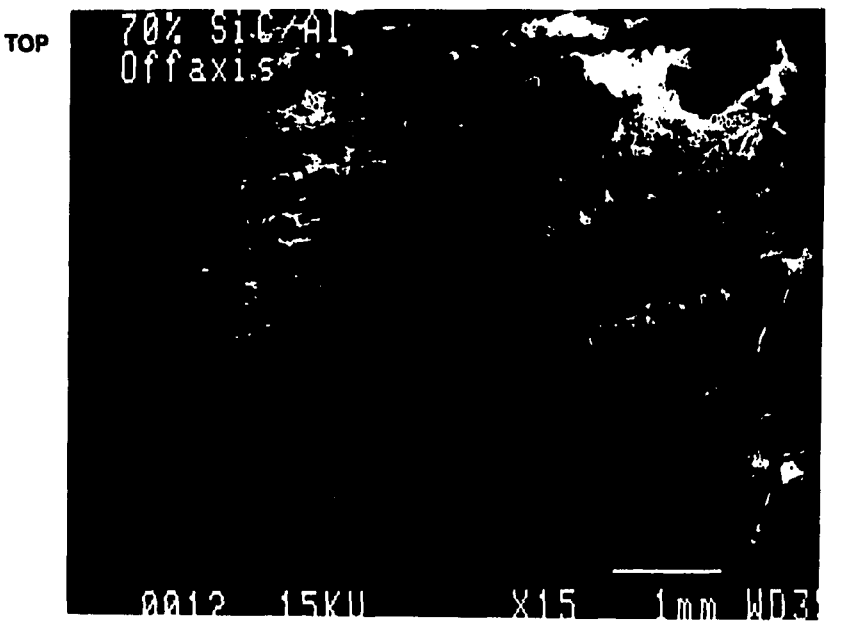


Figure 9. SEM of laser-cut surface using dual gas-jet
(coaxis: 20 psi $O_2$, off-axis: 60 psi $O_2$,
material: 70% $SiC_p$/Al, cutting rate: 1.7 mm/sec (4 in/min))

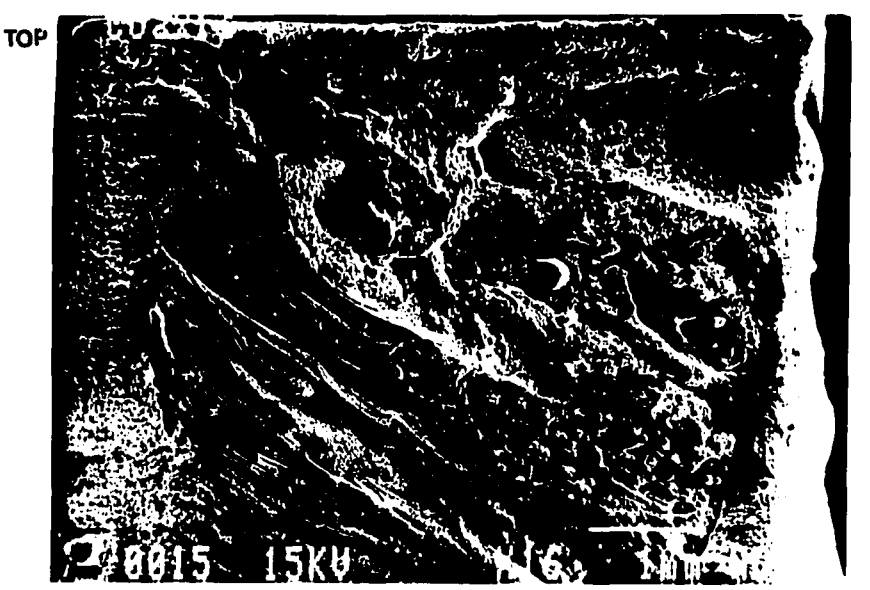


Figure 10. SEM of laser-cut surface using 60 psi coaxial gas-jet only
(material: 50% $B_4C_p$/Al, cutting rate: 3.4 mm/sec (8 in/min))

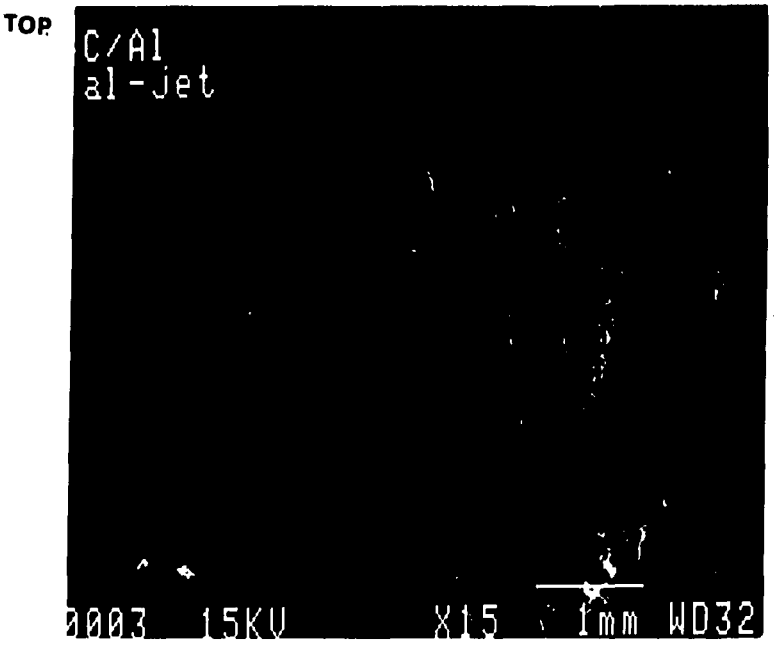


Figure 11. SEM of laser-cut surface using dual gas-jet (coaxis: 20 psi $O_2$, off-axis: 60 psi $O_2$, material: 50% $B_4C_p$/Al, cutting rate: 3.4 mm/sec (8 in/min))

Table 2. Surface finish of SiC/Al and $B_4C$/Al composites cut by a $CO_2$ laser

| Surface roughness, Ra, mm / Distance below surface, mm / Material | 1.0 | | 2.3 | | 4.0 | |
|---|---|---|---|---|---|---|
| | Coaxial-jet cutting | Dual-jet cutting | Coaxial-jet cutting | Dual-jet cutting | Coaxial-jet cutting | Dual-jet cutting |
| 6061 Al | 0.007-0.008 | 0.008-0.010 | 0.016-0.018 | 0.017-0.022 | >0.025 | >0.020 |
| 20% SiC vol./6061 Al | >0.018 | 0.012-0.013 | >0.025 | 0.015-0.023 | >0.025 | >0.025 |
| 40% SiC vol./6061 Al | 0.008-0.011 | 0.004-0.006 | 0.010-0.018 | 0.005-0.013 | >0.025 | 0.009-0.013 |
| 70% SiC 20% Al2O3 vol./6061 Al | 0.018-0.023 | 0.005-0.008 | >0.020 | 0.007-0.008 | 0.016-0.021 | 0.010-0.014 |
| 50% B4C vol./6061 Al | 0.010-0.013 | 0.007-0.012 | 0.014-0.020 | 0.007-0.010 | > 0.025 | 0.009-0.016 |

When larger sign ( > ) is used, the upper value of the data is above the limit reading of the profilometer (0.025 mm).

It is believed that both carbide reinforcement and aluminum matrix react with oxigen to form oxides in the oxygen-assisted laser cutting process. The following combustion reactions occur (Humphrey et al., 1952; Smith et al., 1955; Holley and Huber, 1951).

$SiC + 2O_2 \rightarrow SiO_2 + CO_2$ $\quad \Delta H = -290.9$ kcal/mole

$B_4C + 4O_2 \rightarrow 2B_2O_3 + CO_2$ $\quad \Delta H = -683.3$ kcal/mole

$2Al + 3/2O_2 \rightarrow Al_2O_3$ $\quad \Delta H = -400.4$ kcal/mole

The superior surface finish and dross reduction in the dual gas-jet laser cutting method on $SiC_p$/Al and $B_4C_p$/Al composites might be related to the above chemical reactions and the interaction between the gas flow and the melt film. It is well known that passive $Al_2O_3$ in oxygen-assisted laser cutting of aluminum prevents the erosion cutting front from further oxidation and consequently reduces the cutting temperature. Due to the high melting point of $Al_2O_3$ (2315 K), it was expected that the viscosity of the melt could be high. Therefore, the excessive dross formation in the traditional laser cutting of aluminum materials was a consequence of the passivity and high melting temperature of $Al_2O_3$ and that the gas flow was not able to remove the viscous melt from the kerf effectively. High pressure gas (> 150 psi) was currently employed in traditional laser cutting method to solve the dross formation problem in cutting stainless steels, superalloys, and aluminum alloys. Due to the unfavorable gas flow characteristics such as Mach Shock Disk (MSD) formation (Fieret and Ward, 1986, 1987), fracture of focusing lens, and changing focusing characteristics due to the density and pressure gradients across the flow field (Steen and Kamalu, 1983), high pressure gas laser cutting method is limited to materials of 2 - 3 mm thickness in practice. The off-axial oxygen jet in the dual gas-jet laser cutting method provides an additional dynamic force to remove the passive and viscous melt and allows the workpiece for further oxidation through the above combustion reactions. It is expected that more complete combustion reactions occur due to the off-axial gas-jet and more oxides of the carbide reinforcements are produced. Figures 12 and 13 show the phase diagrams of $Al_2O_3$ - $SiO_2$ and $Al_2O_3$ - $B_2O_3$ respectively. It can be noted that as the concentration of $SiO_2$ or $B_2O_3$ increases, the percentage of liquid increases and the melt tends to shift from the liquid + solid to liquid. Therefore, the viscosity of the melt in the dual gas-jet laser cutting of $SiC_p$/Al and $B_4C_p$/Al composites would be significantly lower as it was seen in the improvement of surface quality. Furthermore, ceramics such as oxides show a better energy coupling at 10.6 microns wavelength

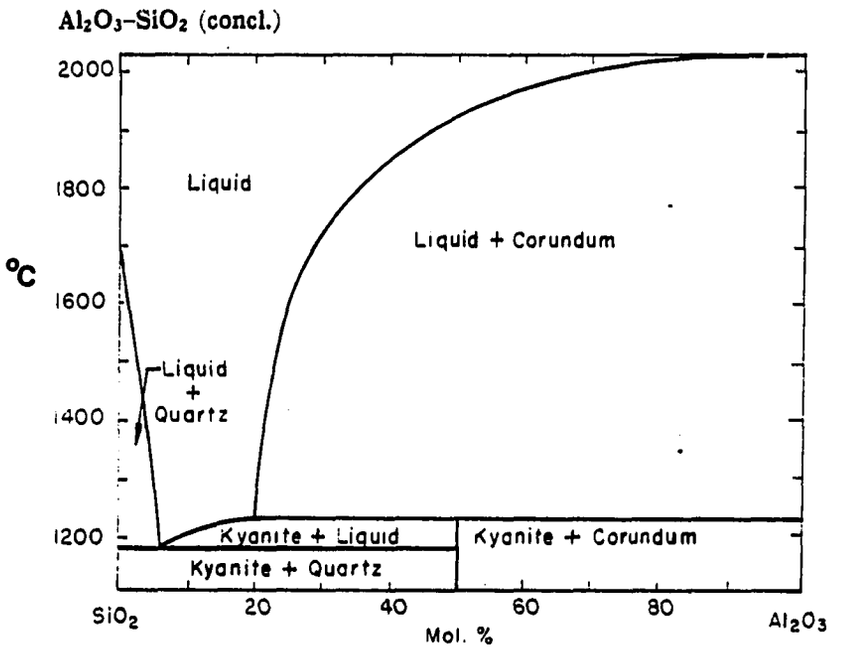


Figure 12. Phase diagram of $SiO_2$-$Al_2O_3$ (Levin, et al., 1969)

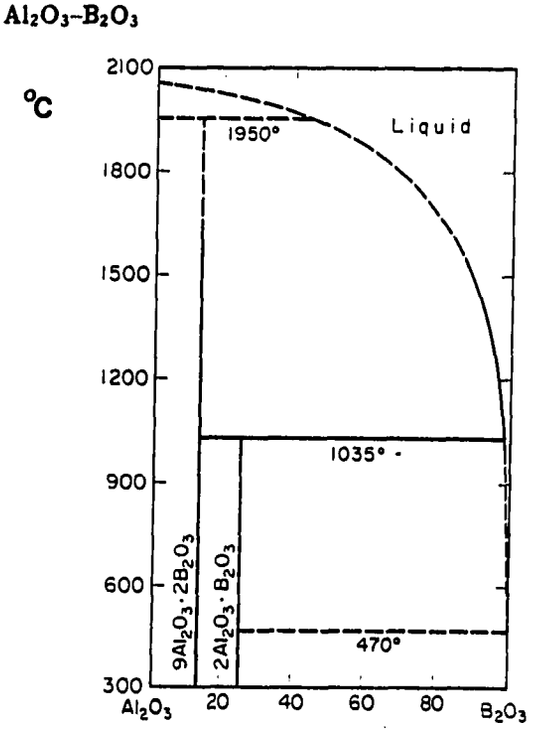


Figure 13. Phase diagram of $B_2O_3$-$Al_2O_3$ (Levin, et al., 1969)

irradiation than metals. Oxides from complete combustion reactions could also improve the laser energy absorption and thereby cutting performance. XRD analysis of droplets from $B_4C_p$/Al composite cut surfaces revealed the presence of mostly $Al_2O_3$ and some Al. No evidence of $B_2O_3$ was noted (Figure 14).

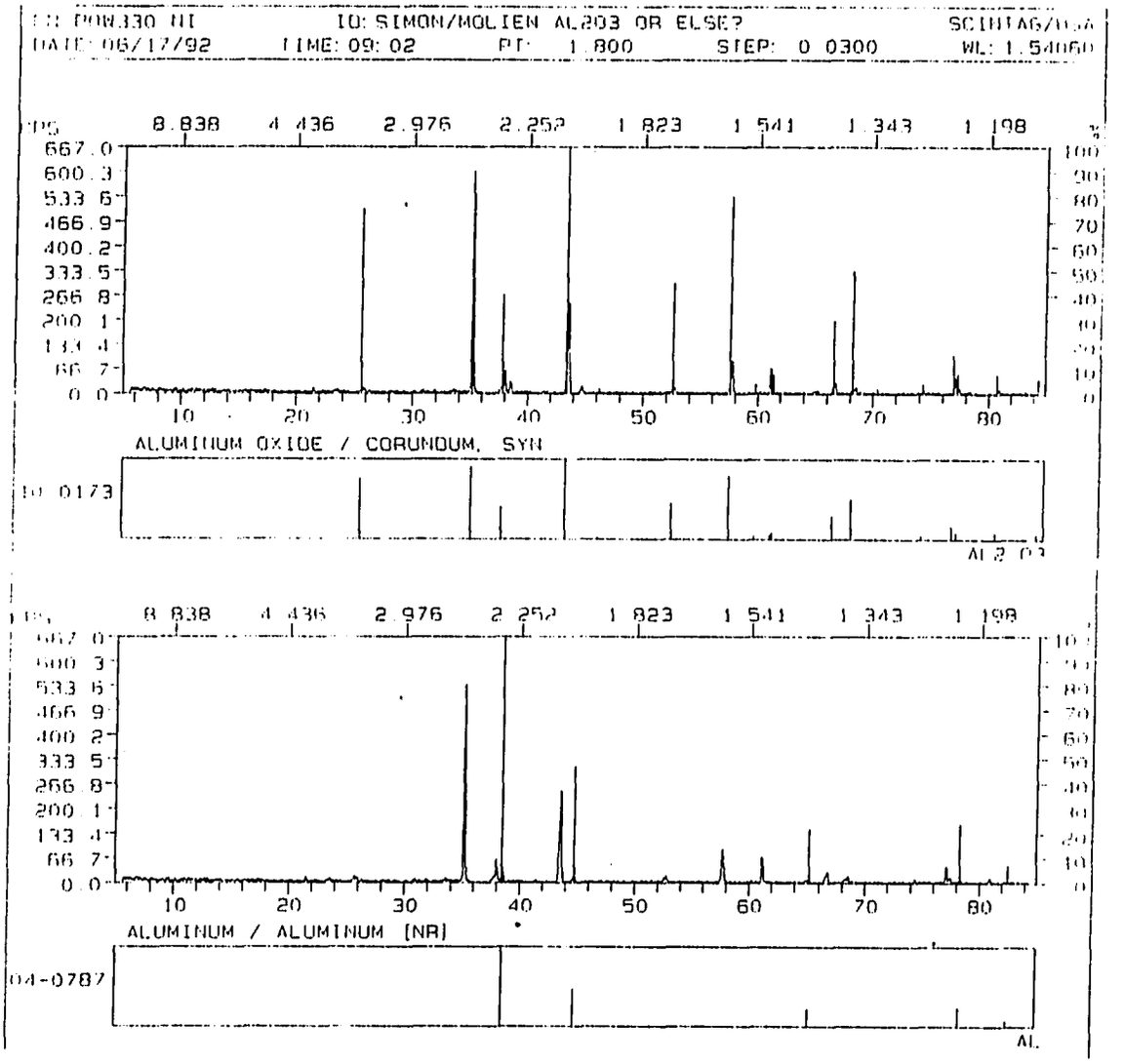


Figure 14. XRD analysis of $B_4C_p$/Al composite droplets

# 4. CONCLUSIONS

Based on the investigation of the laser cutting of $SiC_p$/Al and $B_4C_p$/Al composites, the following conclusions could be drawn.

1. The employment of an off-axial nozzle coupled with a coaxial nozzle has been shown to be effective in the laser cutting of 6.35 mm (1/4 in.) thick $SiC_p$/Al and $B_4C_p$/Al composite materials. The adherent dross and the poor surface quality occurred in the traditional laser cutting method are eliminated by this technique.
2. The effectiveness of the dual gas-jet laser cutting method is attributed to the additional dynamic force (gas momentum transfer) from the off-axial oxygen jet, complete combustions of carbide reinforcements, a better energy coupling between the laser radiation and workpiece and the dilution effect from the combustion oxides.
3. The surface finish in dual gas-jet laser cutting technique improves as the content of carbide reinforcement increases in MMC. This finding could be substantiated through conclusion (2).

## REFERENCES

Arata, Y., "Dynamic Behavior in Laser Gas Cutting of Mild Steel," Plasma, Electron & Laser Beam Technology, American Society for Metals, 1986, pp. 415-426.

Duley, W. W., $CO_2$ Laser, Effects and Applications, Academic Press, New York, 1976.

Gilman, P. S., "Discontinuously Reinforced Aluminum: Ready for the 1990s," Journal of metals, Aug., 1991, pp. 7-15.

Hamatani, G and Ramulu, M., "Machinability of High Temperature Composites by Abrasive Waterjet," Trans. of ASME, Journal of Engineering Materials and Technology, Vol.112, 1990, pp. 381-386.

Harrigan, W. C., "Scaling up Particulate-Reinforced Aluminum Composites for Commercial Production," Journal of Metals, Aug., 1991, pp. 32-35.

Holley, C. E. and Huber, E. J., "The Heats of Combustion of Magnesium and Aluminum," Journal of American Chemistry Society, Vol. 73, 1951, pp. 5577-5579.

Humphrey, G. S. et al., U.S. Bur. of Mines Rept. Invest. No. 4888, 1952.

Kagawa, Y. et al., "Laser Induced Phenomena in Metal Matrix Composites," Composites'86: Recent Advances in Japan and the United States, Tokyo, 1986, pp. 589-595.

Kagawa, Y. et al., "Laser Cutting of CVD-SiC fiber/A6061 Composite," Journal of Materials Science Letters, Vol. 8, 1989, pp. 681-683.

Lee, J. J., Boeing Aerospace Company, Internal Report, 1987.

Levin, E. M. et al., Phase Diagrams for Ceramists 1969 Supplement, Edited by Reser, M. K.,The American Ceramic Society, Columbus, OH, 1969.

Maclean, B. J. and Misra, M. S., "SiC-Reinforced-Aluminum Alloys for Aerospace Applications," Mechanical Behavior of Metal-Matrix Composites, Edited by Hack, J. E. and Amateau, M. F., The Metallurgical Society of AIME, Warrendale, PA, 1983.

Ramulu, M. and Taya, M., "EDM Machinability of $SiC_w$/Al Composites," Journal of Materials Science, Vol. 24, 1989, pp. 1103-1108.

Ready, J. F., Industrial Apllications of Lasers, Academic Press, New York, 1978.

Savrun, E. and Taya, M., "Surface Characterization of SiC Whisker/2124 Aluminum and $Al_2O_3$ Composites Machined by Abrasive Water jet," Journal of Materials Science, Vol. 23, 1988, pp. 1453-1458.

Schreiber, R. R., "Composites: a Mixed Blessing," Manufacturing Engineering, July 1992, pp. 87-92.

Schuocker, D., "Dynamic Phenomena in Laser Cutting and Cut Quality," Applied Physics B, Vol. 40, 1986, pp. 9-14.

Shawlow, A. L., Laser Interactions with Materials, Laser 77 Opto-Electronics Conf. Munich, FRG, 1977.

Shinada, K. et al. Proc. Int. Conf. on Weld. Res. in the 1980s, Osaka, Japan, 1980.

Smith, D., Dworkin, A. S., Van Artsdalen, E. R., "The Heats of Combustion and Formation of Boron Carbide," Journal of American Chemistry Society, Vol. 77, 1955, pp. 2654-2656.

Steen, W. M., Kamalu, J. N., Laser Materials Processings, Edited by Bass, M., North-Holland Publishing Company, Amsterdam, 1983.

Vaccari, J. A., "Cast Aluminum MMCs have Arrived," American Machinist, June 1991, pp. 42-46.

Vicanet, M. et al., "Hydrodynamical Instability of Melt Flow in Laser Cutting," Journal of physics D: Applied Physics, Vol. 20, 1986, pp. 140-145.

Fieret, J. and Ward, B. A., "Circular and Non-circular Nozzle Exits for Supersonic Gas Jet Assist in $CO_2$ Laser Cutting," Proc. of 3rd Int. Conf. on Lasers in Manufacturing, June 1986, Paris, France.

Fieret, J., Terry, M. J., Ward, B. A., "Overview of Flow Dynamics in Gas-assisted Laser Cutting," Proc. of SPIE, Vol. 801, High Power Lasers, 1987, pp. 243-250.

# PAPER V: PLAMA-ASSISTED LASER CUTTING OF POLYMERS

## ABSTRACT

Due to the strong absorption of laser light by sulfur hexafluoride gas ($SF_6$) at 10.6 micron wavelength, a $CO_2$ laser with $SF_6$ as assist gas was used to cut 3.18 mm (1/8 in.) thick polymers. It was believed that laser induced dissociation of $SF_6$ and the formation of gas plasma can be used to polish a cut surface and thus improve the surface finish. The experiment described in this study showed that the formation of a gas plasma was unstable and led to periodical striations on the laser-cut surface. It was concluded that the surface finish of $SF_6$-assisted laser-cut polymers shows insignificant improvement when it was compared to currenly used method such as air-assisted laser cutting.

# 1. INTRODUCTION

Polymers are widely used engineering materials due to their low cost, high strength to weight ratio and chemical inertness properties. Plastics play an important role in polymer applications and can be classified into two categories (thermoplastic and thermosetting). The cutting of plastics using mechanical methods is beset with problems such as difficulty in controling dimensional accuracy due to the low yield strength of the material, discoloration of the material by mechanical stresses and fraying caused by excessive material elongation. $CO_2$ lasers are currently used for cutting plastics because most plastics show strong absorption of irradiation in the infrared spectrum range. Furthermore, the laser cutting technique is a non-contact thermal process and the problems associated with mechanical cutting methods can be eliminated. Also, due to the flexibility of the laser cutting process, tooling costs can be reduced significantly.

The primary mechanisms involved in the laser cutting of plastics are melt shearing, vaporization, and chemical degradation (Powell, 1987). For low laser power density, melt shearing is the main mechanism for material removal for many polymers such as polypropylene, polystyrene, polyethylene, and nylon. Vaporization occurs during laser cutting of high absorptivity material such as acrylics. Chemical degradation occurs mainly when laser cutting is applied to epoxy and phenolic resins. The feasibility of laser cutting for a wide range of thermoplastic and thermoset materials was examined by Van Cleave (1980; 1981; 1983) One successful industrial application of the laser cutting of plastic is for seat belts and air bags which are made from woven nylon. It is difficult to mechanically cut woven nylon because of the toughness and fraying problems. In the laser cutting of nylon, the cut edge is sealed with no burning or charring. Surfaces of laser-cut plastics are usually smooth because of the relatively low melting temperatures of the materials. The combustion flame occurring in the cutting process can effectively polish the cut surface. This effect was demonstrated in laser cutting of acrylics where air assist gas at low pressure ($< 0.04$ MPa (5psi)) was used to allow flame polishing of the cut surface.

However, to bring the polishing effect into full play, an additional plasma flame can be used to further improve the surface finish. Dissociation of sulfur hexafluoride ($SF_6$) gas by

the $CO_2$ laser and formation of a very hot plasma have been reported (Geraedts et al., 1981; Steen, 1983; Snels, 1986; Heijmen et al., 1988; 1989). In the present study, different types of plastics of nominal 3.18 mm (1/8 in.) thickness were cut by a $CO_2$ laser with $SF_6$ as assist gas and experimental results (surface finish, cutting speed) were compared to those obtained by cutting with air.

## 2. EXPERIMENTAL PROCEDURES

Commercially available plastic sheets with nominal thickness of 3.18 mm (1/8 in.) were used in this study. Table 1 lists the material types and the repeat unit of each plastic. A continuous wave (CW) $CO_2$ laser (Spectra-physics Model 820) operating at 700 watts power level was used to cut plastic sheets with a nominal 127 mm (5 in.) zinc selenide (ZnSe) focusing lens. The laser beam showed a near $TEM_{00}$ (Gaussian energy distribution) mode pattern and was focused on the workpiece surface during the cutting process. A convergent nozzle coupled with a $SF_6$ gas tube was used for gas flow delivery. In order to protect the focusing lens from $SF_6$ plasma damage, the nozzle assembly was pressurized with air up to 0.21 MPa (30 psi). The reservoir pressure of $SF_6$ was varied from 0.04 MPa (5 psi) to 0.13 MPa (20 psi). Figure 1 shows the schematic experimental setup. The laser beam was stationary and workpieces were mounted on a computer numerically controlled worktable and cut in a linear movement with speeds up to 84.7 mm/sec (200 in/min). The lasercut surfaces were examined using a profilometer with a pilotor to measure the average roughness height (Ra). Scanning electron microscopy (SEM) was used to study the surface quality.

Table 1. Types of plastics and their chemical compositions

| Materials | Repeat Unit |
|---|---|
| PVC (Polyvinylchloride) | $(-CH_2-CHCL-)_n$ |
| Nylon 6,6 (Polyamide) | $(-NH-(CH_2)_6-NH-CO-(CH_2)_4-CO-)_n$ |
| PP (Polypropylene) | $(-CH_2-CHCH_3-)_n$ |
| HDPE (Linear Polyethylene) | $(-CH_2-CH_2-)_n$ |
| LDPE (Branched Polyethylene) | $(-CH_2-CH_2-)_n$ |

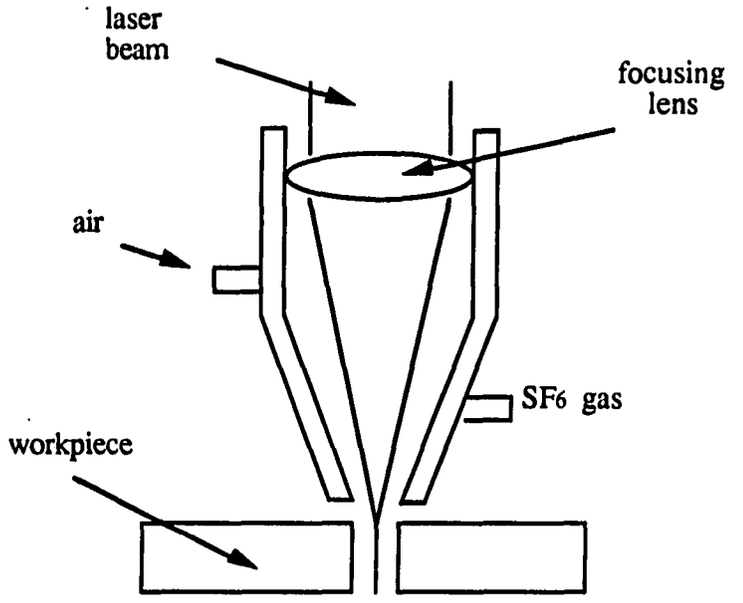


Figure 1. Schematic diagram of SF 6-assisted laser cutting process

## 3. RESULTS AND DISCUSSION

Due to the high flammability of plastics, air or nitrogen gas is currently used in the cutting of plastics in industrial laser applications. The laser cutting of thermosetting plastics produces a char layer along the kerf and this can usually be removed easily. Thermoplastic materials can generally be processed without charring and this was verified by the experimental results described in this study. The surface finish of laser-cut plastic was strongly influenced by the viscosity of the molten plastic and the flow characteristic of the assist gas. A laminar flow assist gas and the use of plastics with low melting temperature and high melt flow usually leads to good surface finish in laser cutting.

Figure 2 shows the average surface roughness in air-assisted laser cutting of plastics at a speed of 84.7 mm/sec (200 in/min). The surface roughness, measured at the middle section of the cut surface, tended to increase with the air pressure in the cutting of Nylon and LDPE. But the surface roughness obtained in air-assisted laser cutting of PVC, and HDPE decreases at first and then increases as the air pressure increases. The optimal air pressure for good edge quality in laser cutting varied with the different types of plastics and was approximately 0.04 MPa (5 psi) for Nylon and HDPE. For PVC, it ranged from 0.07 to 0.13 PMa (10 to 20 psi). A good surface finish for PP and LDPE was achieved at low air pressure (< 0.04 MPa (5 psi)). From the experiments described in this study, it is clear that to obtain a good surface finish, the air pressure should be maintained within the range of 0.04-0.07 MPa (5-10 psi). Figure 3 demonstrates the effect obtained when $SF_6$ is used as an assist gas in the laser cutting of various types of plastic materials. Figure 4 shows the relationship between air pressure and surface finish in $SF_6$-assisted laser cutting. From an examination of Figures 3 and 4, it may be seen that the surface roughness of Nylon and PP did not seem to change with alterations in $SF_6$ gas pressure. On the other hand, PVC and HDPE showed different trends in surface finish when air pressure was increased. As for LDPE, the surface roughness increased with both air and $SF_6$ gases. Comparing Figures 3 and 4 with Figure 2, it can be seen that there is no significant difference in the best surface finish condition (lowest Ra value) as between the $SF_6$ and air-assisted laser cutting of plastics.

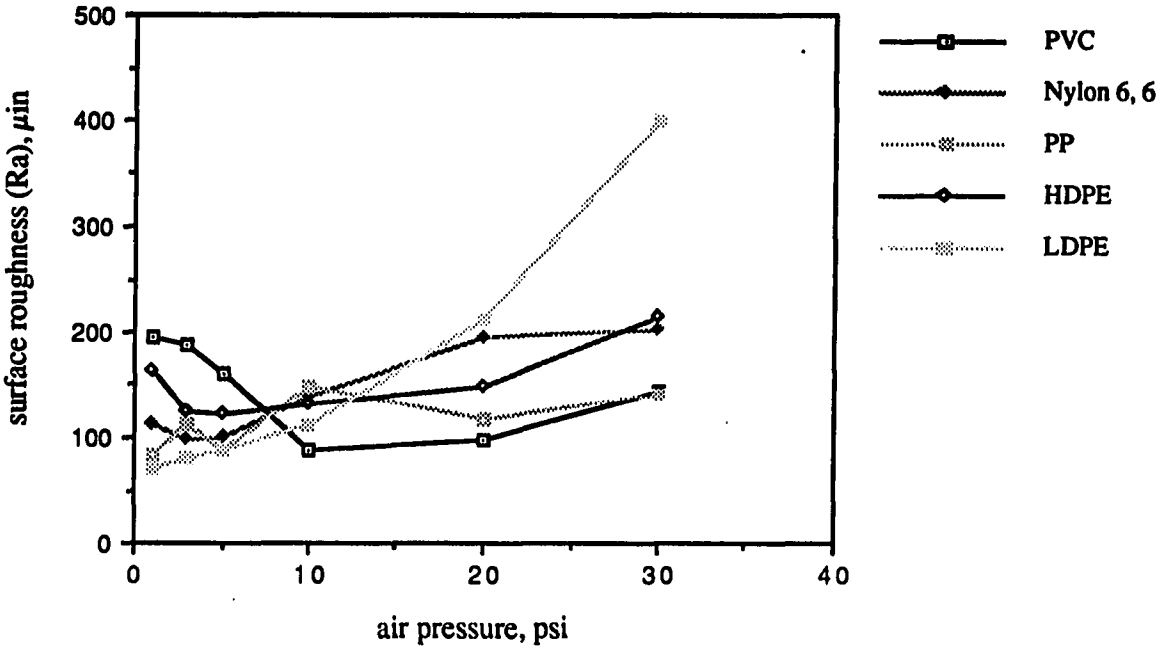


Figure 2. Surface roughness vs. air pressure in laser cutting of plastics

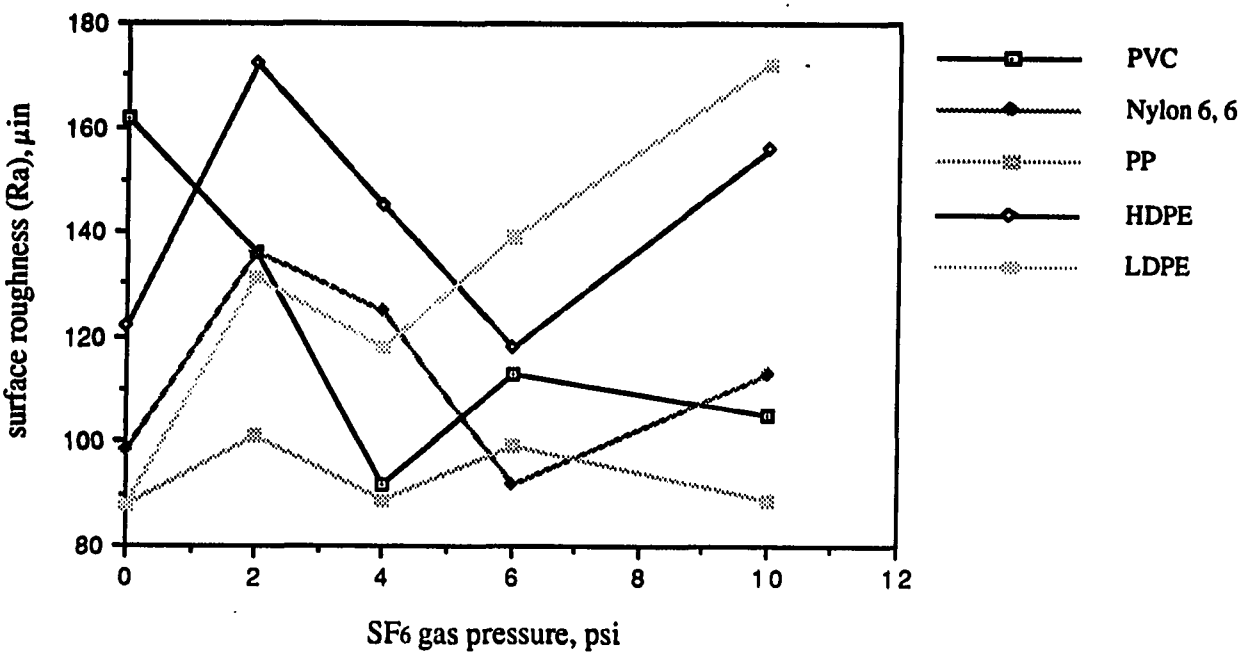


Figure 3. Surface finish vs. $SF_6$ gas pressure in laser cutting of plastics (nozzle pressurized with 5 psi air)

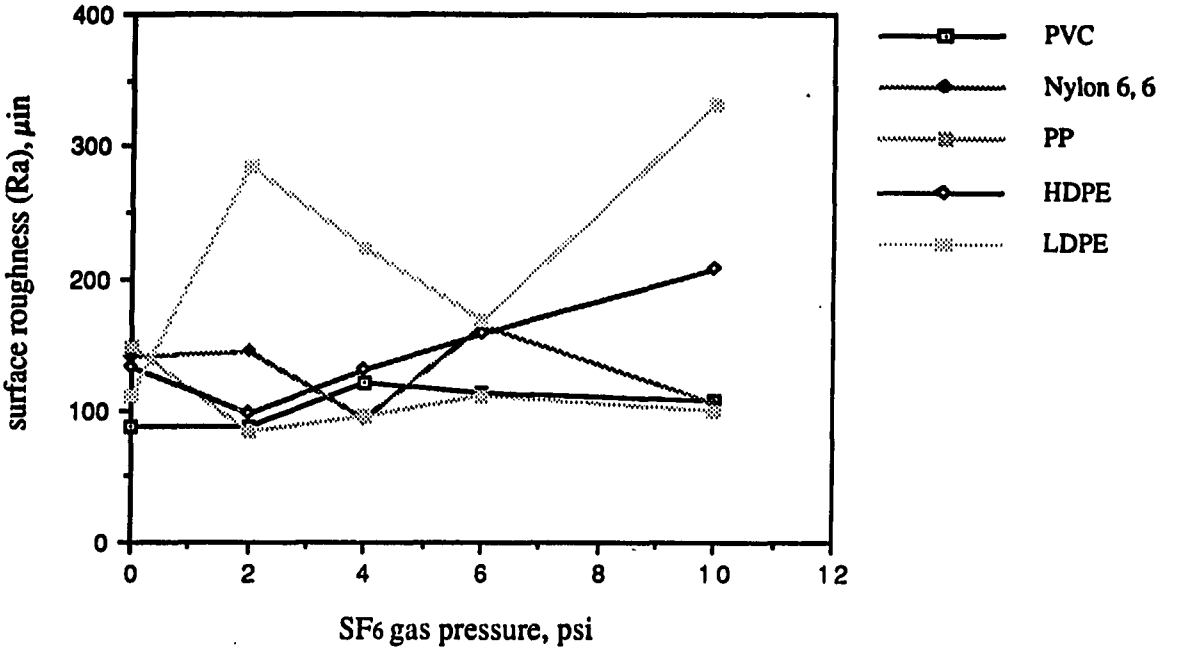


Figure 4. Surface roughness vs. $SF_6$ gas pressure in laser cutting of plastics (nozzle pressurized with 10 psi air)

Figures 5 shows the typical periodical striations on the cut surface in $SF_6$-assisted laser cutting. The spacing between each striation is approximately equal regardless of the type of plastics employed. A noisy, intermittent, buzzing sound was observed during the laser cutting process when $SF_6$ was used as assist gas. Therefore, plasma formation did occur in the $SF_6$-assisted laser cutting of plastics and caused the striations on the cut surface. However, continous dissociation of $SF_6$ gas could not be maintained in the experiment and this fact led to intermittent formation of plasma which caused the periodical striations on the cut surface. Figure 6 depicts the enlarged surface area near the bottom of the cut in Figure 5. Surface damage due to the chemical degradation of PVC by $SF_6$ plasma could be noted. Such damage was not observed in the air-assisted laser cutting of PVC (Figure 7) or $SF_6$-assisted laser cutting of the other polymers. Different laser cutting mechanisms (melt shearing in Nylon, PP, PE and chemical degradation in PVC (Powell et al. 1987)) could be used to explain the susceptibility of $SF_6$ plasma damage to plastics. The maximum cutting speed in air and $SF_6$-assisted laser cutting of plastics was also determined. The results indicated that in both cases when the cutting speed was slowly increased to 127 mm/sec (300 in/min), all samples could not be cut through except for the PVC sample. Since melt shearing is the primary mechanism in the laser cutting plastics, dissociation and plasma formation energy of $SF_6$ from the laser heat source may reduce the enegy supply available in the cutting of plastics. This may explain why the maximum cutting speed in $SF_6$-assisted laser cutting of plastics was not improved by as much as might have been expected.

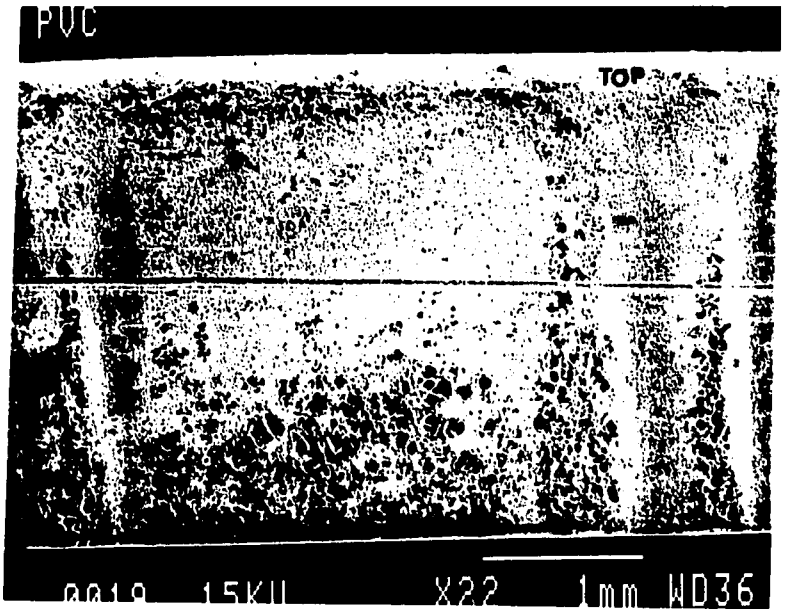


Figure 5. Periodical striation pattern on the laser-cut surface (material : PVC)

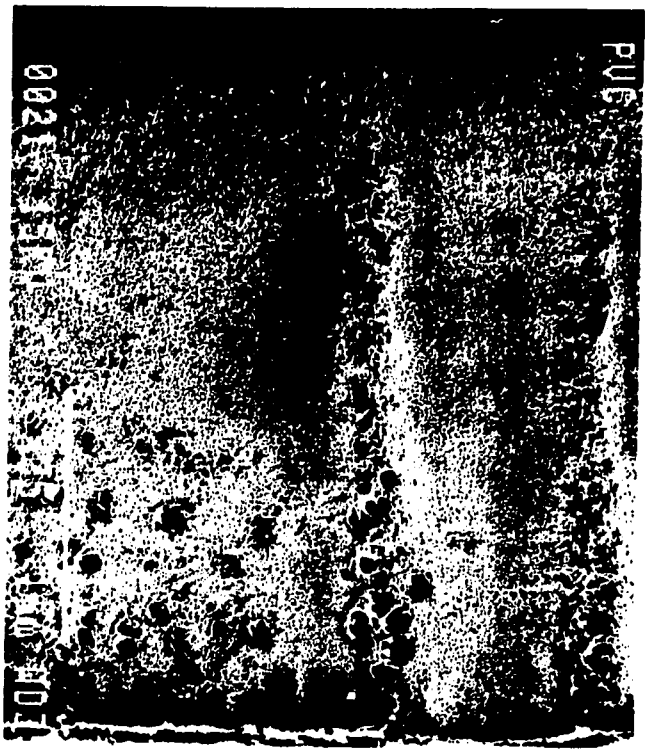


Figure 6. Enlarged view of the damaged surface

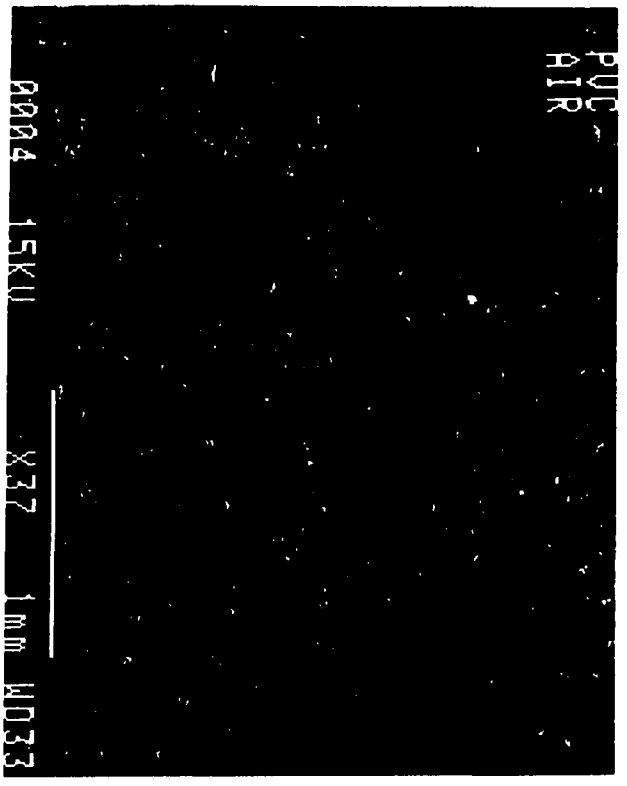


Figure 7. Air-assisted laser-cut surface of PVC

# 4. CONCLUSIONS

It was demonstrated in this study that $SF_6$ gas can be dissociated by a $CO_2$ laser beam and that evidence of $SF_6$ plasma formation was observed during the laser cutting process of plastics. However, the concept of using $SF_6$ plasma for polishing a cut surface was not substantiated and the effect was insignificant. Due to the intermittent formation of $SF_6$ plasma, the lasercut surface shows a periodical striation pattern and the surface finish deteriorates. The cutting speed in $SF_6$-assisted laser cutting of plastics was no faster than that obtained using the air assist method. This fact might be a result of the reduced laser energy available in cutting process due to the dissociation of $SF_6$ molecules.

## REFERENCES

Geraedts, J., Setiadi, S., Stolte, S. and Reuss, J., "Laser Induced Predissociation of $SF_6$ Clusters," Chemical Physics Letters, Vol.78, No. 2, 1981, pp. 277-282.

Heijmen, B., Liedenbaum, C., Stolte, S. and Reuss, J., "Hole Burning in the IR Predissociation Spectrum of $SF_6$-dimers," Laser Chem., Vol. 8, 1988, pp. 275-281.

Heijmen, B., Bizzarri, A., Stolte, S. and Reuss, J., "IR-IR Double Resonance Experiments on $SF_6$ and $SiF_4$ Clusters," Chemical Physics, Vol. 132, 1989, pp. 331-349.

Powell, J., Ellis, G., Menzies, I. A. and Scheyvaerts, P. F., "$CO_2$ Laser Cutting of Non-Metallic Materials," Proceedings, Fourth International Conference on Lasers in Manufacturing, 1987, pp. 69-82.

Powell, J., Ellis, G., Young, C. D., Menzies, I. A., "Laser Cutting of Polymeric Materials: An Experimental Investigation," Proceedings of International Conference on Laser Advanced Materials Processing, 1987, Osaka, Japan, pp. 273-278.

Steen, W. N. and Kamalu, J. N., Laser Materials Processings, edited by M. Bass, Chap. 2, North-Holland Publishing Company, Amsterdam, 1983.

Van Cleave, R. A., "Laser Cutting Plastic Materials," DOE Rept. No. BDX-613-2476, 1980.

Van Cleave, R. A., "Laser Cutting Shapes in Plastics," DOE Rept. No. BDX-613-2727, 1981.

Van Cleave, R. A., "Laser Cutting Plastics," DOE Rept. No. BDX-613-2906, 1983.

# GENERAL SUMMARY

In Paper I, a two-dimensional heat transfer model based on a moving line heat-source model was employed in combustion-assisted laser cutting process. Heat loss due to vaporization, convection, and radiation was neglected. Combustion reaction energy as well as laser energy were included in the heat source. The heat conduction equation, laser characteristics (power, absorptivity, and laser mode), combustion reaction (combustion heat and efficiency), and material properties ( thermal properties, density, thickness, and melt film thickness) were utilized to develop a model that can accurately predict the maximum cutting speed and kerf width for laser cutting of 2-5 mm thick carbon steel. Because vaporization energy was neglected in our model, the cutting speed and kerf width could not be correctly estimated for the laser cutting of thin-sectioned materials (< 2 mm). For materials thicker than 5 mm, a three-dimensional model should be used to complete the heat transfer analysis.

It was concluded that the cutting energy involved in combustion-assisted laser cutting process was composed of the absorbed laser irradiation energy and the chemical reaction energy between the material and oxygen. The model predicted that the combustion effect was very important in the laser cutting of steel and that the combustion energy can amount to 55-70 % of the total cutting energy. This conclusion was consistent with previous experimental reports by other investigators.

In Papers II and IV, an advanced laser cutting technique which employs dual gas-jets (coaxial and off-axial gas-jets ) was developed to cut difficult-to-machine materials such as stainless steels (AISI 304, 410, 430), high-temperature superalloys (Haynes 25, Hastelloy C, Inconel MA 754), and metal matrix composites (SiC and $B_4C$ particulate-reinforced aluminum composites) up to 1/4 in. thickness. The process parameters namely gas-jet configuration, tube diameter, reservoir pressure, and impinging angle of the off-axial gas-jet were optimized to achieve good laser-cut surface quality in stainless steel. Compared to the standard laser cutting method, which uses only a coaxial gas-jet, this new laser cutting method

improves the cutting speeds in addition to the providing a clean surface finish, and the ability to cut a thicker section.

The effectiveness of this innovative laser cutting technique was attributed to the oxygen supply and the momentum transfer from the off-axial gas-jet. The oxygen from the off-axial gas-jet increased the fluidity of the melt film by reducing the concentration of passivation oxides such as $Cr_2O_3$ and $Al_2O_3$ and provided a dynamic force to effectively remove dross. A theoretical model based on gas momentum transfer was developed to predict the cutting speed in off-axis gas jet laser cutting of stainless steel.

However, the application of this new laser cutting technique to some materials such as high carbon stainless steels (440A and 440C) was not satisfactory due to excessive dross formation. It was concluded that iron oxide reduced by carbon (to form CO) during the cutting process increased the $Cr_2O_3$ concentration and gave rise to the viscosity of the melt film. This theory was further supported by the CO gas blow holes observed in the dross.

In Paper III, it was demonstrated that by combining optical lenses (by using an axicon-lens doublet), the laser beam could be focused to a ring instead of a point. This new optical assembly was employed to laser-cut chicken eggs which are used to produce embryo allantoic fluid in biological industries. Compared with the propane torch cutting method currently used in production, the axicon-lens doublet laser cutting method provided additional advantages such as shortening of the cutting time by five times, sterility, and ease of automation. From our study, it was found that the $CO_2$ laser (10.6 micron wavelength) exhibited a better absorption behavior compared to Nd-YAG laser (1.06 micron wave-length) for egg shells and this method was therefore recommended for use in production.

A simple energy balance model was used to predict the cutting and drilling times on egg shells and the results showed excellent agreement with the experimental data obtained. The mechanisms associated with the cutting of egg shells were found to be vaporization and decomposition of $CaCO_3$ in conventional and axicon-lens combination laser cutting methods respectively. It was concluded from our study that a $CO_2$ laser coupled with an axicon-lens doublet can produce high quality cuts on egg shells at high speeds.

In Paper V, $SF_6$ (sulfur hexafluoride) gas was used as an assist gas in the laser cutting of polymers in order to improve the surface finish by plasma polishing. The polymers used in this study were polyvinylchloride, polyamide, polypropylene, and polyethylene. Dissociation of $SF_6$ molecules by $CO_2$ laser irradiation and formation of a hot plasma were observed in $SF_6$-assisted laser cutting of polymers. However, the induced plasma was intermittent under

the existing experimental setup and caused periodical striation patterns on the laser-cut surfaces. Compared with the air-assisted laser cutting method, the surface roughness in $SF_6$-assisted laser cutting of polymers is unaffected or marginally affected due to the striations caused by $SF_6$ plasma.

Furthermore, the cutting speeds of the $SF_6$-assisted laser cutting method were investigated and compared to those obtained by the air-assisted method. It was found that the maximum cutting speed on polymers in $SF_6$-assisted laser cutting was not improved and that the result could be attributed to the reduced laser energy caused by the dissociation of $SF_6$.

# REFERENCES

Abakians, H., and Modest, M. F., "Evaporative Cutting of a Semitransparent Body with a Moving CW Laser," ASME Journal of Heat Transfer, Vol. 100, 1988, pp. 924-930.

Adams, M. J., Metal Construction and Brit. Weld. J. Vol. 2, No. 1, 1970, pp. 1.

Affolter, P. and Schmid, H.G., "Processing of New Ceramic Materials with Solid State Laser Radiation," Proc. of SPIE, High Power Lasers and Their Industrial Applications, Vol. 801, 1987, pp. 120-129.

Sona, A., "Metallic Material Processing: Cutting and Drilling," Soares O.D.D., Perez-Amor, M. (eds.), Applied Laser Tooling, Martinus Nijhoff Publishers, 1987, Dordrecht, Netherlands.

Arata, Y., "Dynamic Behavior in Laser Gas Cutting of Mild Steel," Plasma, Electron & Laser Beam Technology, American Society for Metals, 1986, pp. 415-426.

Arata, Y., "New Laser-Gas-Cutting Technique for Stainless Steel," Plasma, Electron & Laser Beam Technology, American Society for Metals, 1986, pp. 526-536.

Babenko, V. P., and Tychinskii, V. P., "Gas-Jet Laser Cutting," Soviet Journal of Quantum Electronics, Vol. 2, No. 5, 1973, pp. 399-410.

Band, S. Y., and Modest, M. F., "Multiple Reflection Effects on Evaporative Cutting with a Moving CW Laser," ASME Journal of Heat Transfer, Vol. 113, 1991, pp. 663-669.

Belforte, D., "Industrial Lasers' Impact on Manufacturing Technology," Proc. of SPIE, Vol. 950, The Laser Marketplace in 1988, 1988, pp. 77-85.

Belforte, D., "Industrial Laser Annual Hand Book," Pennwell Books, 1990, Tulsa, OK.

Beyer, E., Herziger, G., Gasser, A., Sokolowski, W., "Plasma Fluctuations During Laser Machining with CW $CO_2$ Laser," Proc. of SPIE, High Power Lasers, Vol. 801, 1987, pp.178-184.

Biyikli, S., and Modest, M. F., "Beam Expansion and Focusing Effects on Evaporative Laser Cutting," ASME Journal of Heat Transfer, Vol. 110, 1988, pp. 529-532.

Bunkin, F.V., Kirichenko, N.A., Konov, V. I., Luk'yanchuk, B. S., "Interference Effects in Laser Heating of Metals in an Oxidizing Medium," Journal of Quantum Electron, Vol. 10, 1980, pp.891-895.

Bunting, K. A., and Cornfield, G., "Toward a General Theory of Cutting: A Relationship Between the Incident Power Density and the Cut Speed," Trans. of the ASME Journal of Heat Transfer, 1973, pp. 116-122.

Chryssolouris, G., Choi, W.C., "Gas Jet Effects on Laser Cutting," Proc. of SPIE, $CO_2$ Lasers and Applications, Vol. 1042, 1989, pp. 86-96.

Chryssolouris, G., Sheng, P., and Choi, W. C., "Three-Dimensional Laser Machining of Composite Materials," Trans. of the ASME, Journal of Engineering Material Technology, Vol. 112, 1990, pp. 387-392.

Chryssolouris, G., Sheng, P., and Von Alvensleben, F., "Process Control of Laser Grooving Using Acoustic Sensing," Trans. of the ASME, Journal of Engineering for Industry, Vol. 113, 1991, pp. 268-275.

Chryssolouris, G., Laser Machining Theory and Practice, Springer-Verlag Inc., 1991, New York.

Decker, I., Ruge, J., Atzert, U., "Physical Models and Technological Aspects of Laser Gas Cutting," Proc. of SPIE, Industrial Applications of High Power Lasers, Vol. 455, 1983, pp. 81-87.

De Iorio, I., Tagliaferri, V., Di Ilio, A. M., "Cut Edge Quality of GFRP by Pulsed Laser: Laser-Material Interaction Analysis," Proceedings of International Conference on Laser Advanced Materials Processing, 1987, Osaka, Japan, pp. 279-284.

Di Ilio, A., Tagliaferri, V., Visconti, I.C., "Laser Cutting of Aramid FRP," Proceedings of International Conference on Laser Advanced Materials Processing, 1987, Osaka, Japan, pp. 291-296.

Doyle, D. J., Kokosa, J. M., "Hazardous Byproducts of Plastics Processing with $CO_2$ Lasers," Int. Congress on Applications of Lasers and Electro Optics (ICALEO'85), 1985, San Franscisco, U.S.A.

Doyle, D. J., Kokosa, J. M., "Laser Processing Of Kevlar: Hazardous Chemical By-Products," Proceedings of International Conference on Laser Advanced Materials

Processing, 1987, Osaka, Japan, pp. 285-289.

Duley, W. W., $CO_2$ Lasers, Effects and Applications, Academic Press, 1976, New York.

Duley, W. W., Laser Processing and Analysis of Materials, Plenum Press, 1983, New York.

Duley, W. W., Gonsalves, J. N. Can. J. Phys. Vol. 50, 1972, pp.215.

Fieret, J., Terry, M. J., Ward, B. A., "Overview of Flow Dynamics in Gas-assisted Laser Cutting," Proc. of SPIE, Vol. 801, High Power Lasers, 1987, pp. 243-250.

Firestone, R. F., Vesely, E. J., "High Power Laser Beam Machining of structural Ceramics," ASME Symposium on Machining of Advanced Ceramic Materials, 1988, pp. 215-227.

Flaum, M., Karlsson, T., "Cutting of Fiber-reinforced Polymers with CW $CO_2$ Laser," Proc. of SPIE, High Power Lasers, Vol. 801, 1987, pp. 142-149.

Forbes, N., "The Role of the Gas Nozzle in Metal-cutting with CO2 Lasers," Laser 75 Optoelectronics Conference Proceedings, 1975, Munich, FRG, pp. 93-95.

Hamann, C., Rosen, H., "Laser Machining of Ceramic and Silicon," Proc. of SPIE, High Power Lasers and Their Industrial Applications, Vol. 801, 1987, pp. 130-137.

Houldcroft, p. T., Optics Tech., Vol. 1, 1968, pp. 37.

Ivarson, A., Powell, J., and Magnusson, C., "The Role of Oxidation in Laser Cutting Stainless and Mild Steel," Journal of Laser Applications, Vol. 3, No. 3, 1991, pp. 41-45.

Ketting, H. O., Olsen, F. O., "High Pressure Off-Axis Laser Cutting of Stainless Steel and Aluminum," Proceedings of International Conference on Laser Advanced Materials Processing, 1992, Nagaoka, Niigata, Japan, pp. 607-612.

Lee, C. S., Goel, A., Osada, H., "Parametric Studies of Pulsed Laser Cutting of Thin Metal Plates," Journal of Applied Physics, Vol. 58, No. 3, 1985, pp. 1339-1343.

Lee, J. J., Boeing Aerospace Company, Internal Report, 1987.

Masuda, W., Nakamura, T., "A Feasibility Study on Aerodynamic Characteristics of Underexpanded Annular Impinging Jets for Assisting Laser Cutting," Proceedings of International Conference on Laser Advanced Materials Processing, 1992, Nagaoka, Niigata, Japan, pp. 613-618.

Modest, M. F., and Abakians, H., "Heat Conduction in a Moving Semi-infinite

Solid Subjected to Pulsed Laser Irradiation," ASME Journal of Heat Transfer, Vol. 108, 1986, pp. 597-601.

Modest, M. F., and Abakians, H., "Evaporative Cutting of a Semi-infinite Body with a Moving CW Laser," ASME Journal of Heat Transfer, Vol. 108, 1986, pp. 602-607.

Molian, P. A., "Laser Cutting of Thick Metallic Solids- A Reactive Gas-Flow Approach," Proceedings of International Conference on Laser Advanced Materials Processing, 1987, Osaka, Japan, pp. 245-250.

Nielson, S.E., Laser Cutting with High Pressure Cutting Gas and Mixed Gases, Ph.D. Thesis, Technical University of Denmark, 1985.

Olsen, F. O., "Studies of Sheet Metal Cutting with Plane-polarized $CO_2$ laser," Optoelectronic in Engineering, W. Waidelich (ed.), Springer Verlag, Berlin, 1982, pp. 227-231.

Olsen, F. O., "Laser Cutting," Proc. of SPIE, Laser Technologies in Industry, Vol.952, 1988, pp. 572-582.

Petring, D., Abels, P., Beyer, E., Herziger, G., "Werkstoffbearbeitung mit Laserstrahlung," Feinwerktechnik & Messtechnik, Vol. 96, 1988, pp. 364-372.

Powell, J., "Prevention of Dross Attachment During Laser Cutting," Proc. of SPIE, Applications of High Power Laser, Vol. 527, 1985, pp. 63-66.

Powell, J., Ellis, G., Menzies, I. A., Scheyvaerts, P. F., "$CO_2$ Laser Cutting of Non-Metallic Materials," Proceedings, Fourth International Conference on Lasers in Manufacturing, 1987, pp. 69-82.

Powell, J., Ellis, G., Young, C. D., Menzies, I. A., "Laser Cutting of Polymeric Materials: An Experimental Investigation," Proceedings of International Conference on Laser Advanced Materials Processing, 1987, Osaka, Japan, pp. 273-278.

Powell, J., $CO_2$ Laser Cutting, Carl Hanser Verlag, 1990, Munich, F.R.G.

Ramanathan, S., Modest, M. F., "Effect of Variable Properties on Evaporative Cutting with a moving CW Laser," ASME HTD, Vol. 135, 1990, pp. 101-108.

Ramanathan, S., Modest, M. F.,"CW Laser Cutting of Composite Ceramics," Proceedings of International Conference on Laser Advanced Materials Processing, 1992, Nagaoka, Niigata, Japan, pp. 625-631.

Ready, J. F., Industrial Applications of Lasers, Academic Press, New York, 1978.

Roessler, D. M.. and Gregson, V. G., "Reflectivity of Steel at 10.6 $\mu$m Wavelength"

Rothe, R., Sepold, G., "Important Requirements on Laser Beam Cutting Systems for Cutting Thick Plates," Proceedings of International Conference on Laser Advanced Materials Processing, 1987, Osaka, Japan, pp. 251-253.

Roy, S., Modest, M. F., "Three-Dimensional Conduction Effects During Scribing with a CW Laser," Journal of Thermophysics and Heat Transfer, Vol. 4, No. 2, 1990, pp. 199-203.

Saunders, R. J., Conference on Industrial Applications of High Power Laser Technology, 1976, San Diego, California, pp. 32.

Schawlow, A. L., "Laser Interactions with Materials," Proc. Laser 77 Optoelectronics Conf., Munich, FRG, 1977.

Schulz, W., Simon, G., Vicanek, M., "Influence of the Oxidation Process in Laser Gas cutting," Proc. of SPIE, High Power Lasers, Vol.801, 1987, pp. 331-336.

Schuocker, D., and Abel, W., "Material Removal Mechanism of Laser Cutting," Proc. of SPIE, Vol. 455, 1983, pp. 88-95.

Schuocker, D., and Walter, B., "Theoretical Model of Oxygen Assisted Laser Cutting," Inst., Phys. Conf. Ser., No.72, 1984, pp. 111-116.

Schuocker, D., and Walter, B., "Theoretical Model for the Formation of Periodic Striations During Laser Cutting," 7th Int. Kongress Laser 85, Optoelektronik, Munchen,1985.

Schuocker, D., "Dynamic Phenomena in Laser Cutting and Cut Quality," Applied Physics, B, Vol. 40, 1986, pp. 9-14.

Schuocker, D., "Theoretical Model of Reactive Gas Assisted Laser Cutting Including Dynamic Effects," Proc. of SPIE, High Power Lasers and Their Industrial Applications, Vol. 650, 1986, pp. 210-219.

Schuocker, D., "Heat Conduction and Mass Transfer in Laser Cutting," Proc. of SPIE, Laser Technologies in Industry, Vol. 952, 1988, pp. 592-599.

Shinada, K.,et al., Proc. Int. Conf. on Weld Research in the 1980s, Osaka, Japan, 1980, pp. 27-29.

Sona, A., "Metallic Materials Processing: Cutting and Drilling," Applied Laser Tooling, Perez-Amor, M (eds), Martinus Nijhoff Publishers, 1987, Netherlands.

Steen, W. M., "Thermal History of a Spot Heated by a Laser," Heat and Mass Trans. Lett., Vol. 4, 1977, pp.167.

Steen, W. M, and Clarke, J., "Arc-Augmented Laser Cutting," Proc. Laser 78

Conf., London, 1978.

Steen, W. M., and Kamalu, J. N., Laser Materials Processings, edited by M. Bass, North-Holland Publishing Company, Amsterdam, 1983.

Tonshoff, H. K., and Gonschior, M., "Reduction of Crack Damage in Laser Cutting of Ceramics," Proceedings of International Conference on Laser Advanced Materials Processing, 1992, Nagaoka, Niigata, Japan, pp. 645-650.

Trubelja, M. F., Ramanathan, S., Modest, M. F., and Stubican, V. S., "Carbon-Dioxide Laser Cutting of a Carbon-Fiber-Silicon-Carbide-Matrix Composite," Proceedings of International Conference on Laser Advanced Materials Processing, 1992, Nagaoka, Niigata, Japan, pp. 633-638.

Utsunomiya, S., Kagawa, Y., and Kogo, Y., in Composites, '86: Recent Advances in Japan and the United States, edited by K. Kawata, 1986, pp. 589-595.

Vicanek, M., Simon, G., Urbassek, H. M. and Decker, I., "Hydrodynamical Instability of Melt Flow in Laser Cutting," Journal of Physics D: Applied Physics, Vol. 20, 1986, pp. 140-145.

Vicanek, M. and Simon, G., "Momentum and Heat Transfer of an Inert Gas Jet to the Melt in Laser Cutting," Journal of Appl. Phys., Vol. 20, 1987, pp. 1191-1196.

Van Cleave, R. A., "Laser Cutting Plastic Materials," DOE rept. No. BDX-613-2476, 1980.

Van Cleave, R. A., "Laser Cutting Shapes in Plastics," DOE rept. No. BDX-613-2727, 1981.

Van Cleave, R. A., "Laser Cutting Plastics," DOE rept. No. BDX-613-2906, 1983.

Ward, B. A., "Supersonic Gas Jet Assist Laser Cutting," Industrial Laser Review, A Laser Focus/ Pennwell Publication, Oct. 1986, pp. 1-3.

Yamamoto, J., and Yamamoto, Y., "Laser Machining of Silicon Nitride," Proceedings of International Conference on Laser Advanced Materials Processing, 1987, Osaka, Japan, pp. 297-302.

# ACKNOWLEDGEMENTS

I would like to express great gratitude to my advisor, Professor P. A. Molian, for his consistent instruction, encouragement and patience during my graduate program at Iowa State University . Many thanks also go to my committee members including Professors R. F. Scrutton, R. C. Brown, J. Verhoeven, and D. Hsu for their discussions in the study and to Mr. G. Scandrett for his technical assistance. I am especially grateful to my family for their encouragement and support at various stage of this work.

Finally I would like to acknowledge the financial support from Iowa Department of Economical Development, National Science Foundation, and Solvay Animal Health Inc. for this research.